Stony Brook University

Orientation of Cholesterol Oxidase on Model Membranes

A Dissertation Presented

by

Hui Tang

to

The Graduate School

in Partial Fulfillment of the

Requirements

for the Degree of

Doctor of Philosophy

in

Chemistry

Stony Brook University

August 2007

Stony Brook University

The Graduate School

Hui Tang

We, the dissertation committee for the above candidate for the

Doctor of Philosophy degree, hereby recommend

acceptance of this dissertation.

Professor Nicole S. Sampson, Dissertation Advisor
Department of Chemistry

Professor Erwin London, Chairperson of Defense
Department of Chemistry

Professor Robert C. Kerber, Committee Member
Department of Chemistry

Professor W. Todd Miller, External Committee Member
Department of Physiology and Biophysics
Stony Brook University

This dissertation is accepted by the Graduate School

Lawrence Martin
Dean of the Graduate School

Abstract of the Dissertation

Orientation of Cholesterol Oxidase on Model Membranes

by

Hui Tang

Doctor of Philosophy

in

Chemistry

Stony Brook University

2007

Cholesterol oxidase is a water-soluble, interfacial enzyme. It is a flavoenzyme that catalyzes two reactions in one active site: the oxidation of cholesterol to cholest-5-en-3-one followed by isomerization to cholest-4-en-3-one. Cholesterol oxidase is produced by a variety of microorganisms to utilize cholesterol as their energy source. In addition, some pathogenic bacteria might require cholesterol oxidase for host macrophage infection. The enzyme has been widely used in serum cholesterol assays; it was also one of the early tools used to probe the presence of lipid rafts in cell membranes. In boll weevils, the midgut epithelial membrane is disrupted by cholesterol oxidase activity, which led to investigation of its use as a pesticidal agent.

Since cholesterol oxidase is active at the surface of cell membranes, a detailed understanding of the structure of the enzyme-membrane complex was required. This understanding would guide optimization of the use of the enzyme, as well as help

investigate its role in pathogenicity. From a kinetic standpoint, cholesterol oxidase must associate with lipid bilayers and bind cholesterol directly from the membrane. This thesis work centered on determining the orientation of cholesterol oxidase from *Streptomyces* with respect to the membrane surface. The structure was probed using site-selective conjugation of fluorescent probes and fluorescence quenching measurements. In combination with high-resolution X-ray crystal structures of the enzyme in the absence of lipid, the experiments suggest that residues 80, 154, 274 and 333 are not in membrane contact upon binding to the lipid in the absence of the substrate. Under conditions in which the enzyme activity is negligible, these residues are not in membrane contact in the presence of cholesterol.

In addition, a mass spectrometry-based method, which involves an isotope tag, was proposed. L80C mutant ChoA was used to optimize protease digestion and thiol labeling with iodoacetamide (IAM) and N-ethylmaleimide (NEM). Peptide fragments containing IAM or NEM labeled residue 80 were detected by MALDI-TOF. A structure for anisotope-coded mass tag was proposed. This method will be usable to determine a membrane bound model for ChoA, and should be a general method for studying other interfacial proteins.

Atomic resolution structures of a double mutant of cholesterol oxidase in the presence and absence of an alcohol substrate analog, glycerol, were solved by Vrielink and her coworkers. Four distinct populations of glycerol in the active site were observed in the crystal structures of the enzyme-bound glycerol complex, including a structure with a covalent adduct between glycerol and the FAD cofactor. Two geometries of the FAD cofactor, planar and bent, were shown in the glycerol bound structures. Activity assays

with glycerol indicate that in solution glycerol is not a substrate of ChoA. Results of enzyme kinetics suggest that glycerol has a very weak affinity for the enzyme and will only bind in the absence of competitive ligands. The distortion of FAD geometry is thought to be caused by the movement of the aromatic triad of tyrosine107, phenylalanine444 and tyrosine446, upon the binding of glycerol in the active site.

To My Husband, Ye Zhao
My Parents, Jizhen Wang and Beiji Tang
with My Love!

Table of Contents

List of Figures

List of Tables

List of Schemes

List of Abbreviations

A	alanine
ABTS	2,2'-azino-bis(3-ethylbenzthiazoline-6-sulphonic acid)
Ad	acrylodan
Asn	asparagine
Arg	arginine
BSA	bovine serum albumin
C	cysteine
$CHCl_3$	chloroform
ChoA	cholesterol oxidase from *Streptomyces*
ChoE	cholesterol oxidase from *Rhodococcus equi*
Chol	cholesterol
DEAE	diethylaminoethyl
DHEA	dehydroepiandrosterone
DOPC	1,2-dioleoyl-*sn*-glycero-3-phosphocholine
DTT	dithiothreitol
[E]	concentration of enzyme
E	glutamic acid, enzyme
E^*	enzyme at interface
EPR	electron paramagnetic resonance
ePC	egg phosphatidylcholine
ESI	electrospray ionization
FAD	flavin adenine dinucleotide

FDPB	finite difference Poisson-Boltzmann
FPLC	fast protein liquid chromatography
ΔF	change in fluorescence intensity
Glu	glutamic acid
GMC	glucose-methanol-choline
H	histidine
h	hour
H_2O_2	hydrogen peroxide
His	histidine
HPAA	para-hydroxyphenyl acetic acid
HRP	horse radish peroxidase
I	isoleucine
IAM	iodoacetamide
IPTG	isopropyl β-D-thiogalactoside
K_{app}	apparent equilibrium constant
k_{cat}	Michaelis-Menten catalytic rate constant
k_{cat}^*	interfacial k_{cat}
K_d	dissociation constant
kD	kiloDalton
K_m	Michaelis-Menten constant
[L]	concentration of monomeric lipid in vesicle solution
L	liter, leucine
LB	Luria broth

l_d	liquid-disordered
l_o	liquid-ordered
M	phenylalanine
MALDI	matrix-assisted laser desorption ionization
MD	molecular dynamics
MWCO	molecular weight cut-off
MS	mass spectrometry
Mtb	*Mycobacterium tuberculosis*
MUV	medium-sized, unilamellar vesicle
N	asparagine
NEM	N-ethylmaleimide
nm	nanometer
NMR	nuclear magnetic resonance
O_2	oxygen
P	product
PC	phosphatidylcholine
PCR	polymerase chain reaction
PDB	protein data bank
PE	phosphatidylethanolamine
PLA_2	phospholipase A_2
POPC	1-palmitoyl,2-oleoyl-*sn*-glycero-3-phosphocholine
PS	phosphatidylserine
Q	glutamine

R. equi	*Rhodococcus equi*
SDS-PAGE	sodium dodecyl sulfate polyacrylamide gel electrophoresis
SM	sphingomyelin
TFA	trifluoroacetic acid
Tris	tris(hydroxymethyl)aminomethane
Trp	tryptophan
UV	ultraviolet
V	valine
V_i	initial velocity
vis	visible
W	tryptophan
Wat	water
WT	wild-type
X_{chol}	cholesterol mole fraction
X_q	mole fraction of spin-labeled quencher
ε	extinction coefficient
Tempo-PC	1-palmitoyl-2-oleoyl-*sn*-glycero-3-phospho(TEMPO)choline
5-doxyl-PC	1-palmitoyl-2-stearoyl-(5-doxyl)-*sn*-glycero-3-phosphocholine
12-doxyl-PC	1-palmitoyl-2-Stearoyl-(12-doxyl)-*sn*-glycero-3-phosphocholine

CHAPTER 1 An Introduction to the Current Status of Protein-Lipid Interface Studies and Cholesterol Oxidase

I. Analyzing the Membrane-docking Geometries of Interfacial Enzymes

Overview

Membrane surfaces are one of the primary places where living cells make decisions about turning on or off a certain signaling pathway (*1*). Many cell signaling pathways are initiated by a group of membrane-associated enzymes that transiently bind to the lipid bilayer (*2*), such as protein kinase C (*3*), and the secreted phospholipase A2 (PLA2) (*4*). Interest is growing rapidly in how membrane-binding of these proteins serves as a mechanism of signal transduction (*2*). However, protein-lipid binding mechanisms remain relatively poorly understood (*5*).

Many enzymes act at the surfaces of cell membranes. There are two fundamentally different mechanisms, interfacial and non-interfacial (*6*). For an interfacial enzyme, only the substrates in the membrane bind directly to the active site of the enzyme. In contrast, a non-interfacial enzyme at the interface can access its substrate only from the aqueous phase, i.e. water-soluble substrates (*6*). For interfacial enzymes, two types of enzymatic process may be considered: "interfacial" (IF) and "interfacial with interfacial activation" (IF + IFA) (*6*)(Figure 1.1). Since catalysis does not take place in the aqueous phase through an IF or IF + IFA mechanism, binding to the interface is crucial to enzymatic function (*5*). As a consequence, defining the interfacial binding surface of the enzyme is the first step to take in order to understand membrane-binding mechanisms.

Recently, efforts have been made to study membrane-binding sites, using different biophysical technologies. Representatives of the best studied proteins are the C2 domains of protein kinase C (PKC) and phospholipase A_2s (cPLA$_2$) (*2*). The C2 domain is "a ubiquitous signaling motif typically activated by Ca^{2+} binding that drives docking to a

specific cellular membrane" (*1*). A detailed model of C2-membrane docking has been described for phospholipase Cδ1 (*7*), showing that a concave face of the C2 structure faces the lipid bilayer. This model is supported by NMR and electron paramagnetic resonance (EPR) studies of $cPLA_2$-C2 (*8, 9*). A similar conclusion was obtained from scanning mutagenesis and surface pressure measurements on PKCα and $cPLA_2$ (*10, 11*). Moreover, NMR measurements suggested an altered environment sensed by residues on the concave face of the protein-membrane complex (*9*).

Since many cell processes are triggered by membrane-protein interactions, such as signal transduction (*2*), inflammation (*12*), and membrane trafficking (*13-16*), obtaining structural information of protein-membrane complex opens the door to understanding the mechanisms of the above cell events.

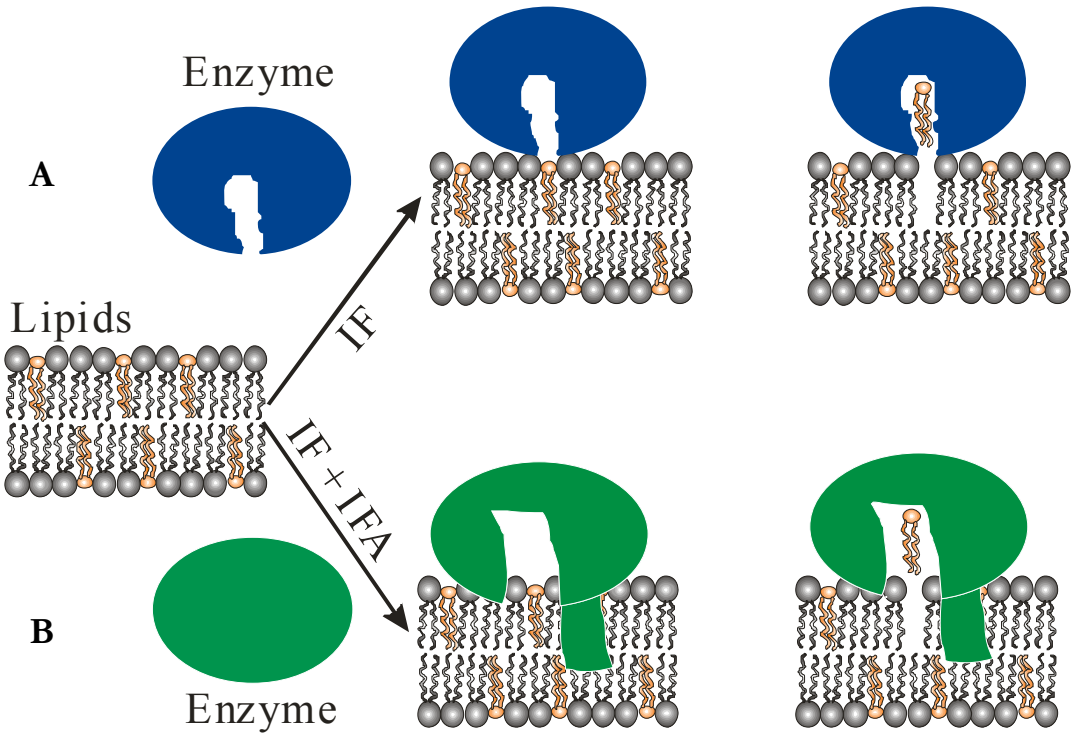

Figure 1.1. Models of interfacial enzymes acting at the membrane surfaces. The substrate at the interfaces is shown in orange. This figure was adapted from Gelb, Min and Jain (*6*), the drawings were generated by using CorelDRAW. (A) Interfacial mechanism (IF): the enzyme acts on the substrate at the interface, with no conformational change. (B) Interfacial with interfacial activation mechanism (IF + IFA): the enzyme undergoes a conformational change when it binds to the interface, then it acts on the substrate at the membrane surface with an increasing catalytic efficiency.

Current approaches for analyzing the docking of proteins of known structure to the membrane

A main challenge arises from the difficulty of acquiring a high-resolution structure of the complex of a protein bound with the membrane. It is much easier to obtain the crystal structure of the protein in the aqueous state (*1*). To date, only 3 high-resolution structures have been produced from X-ray crystallography to show the lipid environment of a membrane protein. The first structure is of bacteriorhodopsin from purple membranes of photosynthetic bacterium (*17*). The second one is determined from a protein called lens-specific aquaporin-0 (AQP0) when it is immersed in an artificial lipid bilayer (*18*). The third one is the structure of the complex of detergent-solubilized hemolysin heptamer bound to the membrane (*19*). Alternative spectroscopic and modeling approaches have been employed to characterize lipid-protein binding, including fluorescence-based measurements, solid-state NMR, electron paramagnetic resonance (EPR) power saturation, and computational methods (*1, 20-23*).

The fluorescence-based approach utilizes the sensitivity of fluorescence to environmental polarity (*24*), monitoring either the intrinsic λ_{max} of tryptophan fluorescence or a fluorescent probe attached on the protein surface, to analyze membrane depth. Parallax analysis (*24-27*) is one of the fluorescence quenching methods, which is based on measuring the quenching between tryptophan or an attached fluorophore and a quencher. Generally, the quencher is covalently connected to either the acyl chains or polar headgroup of lipid molecules (*28, 29*). More precise membrane depths can be obtained by using fluorescence quenching methods than some other fluorescence-based techniques, such as determination of membrane depths by measuring the emission λ_{max} of Trp fluorescence,

because besides membrane depth, there are other factors can influence λ_{max}(*24, 29*). A novel dual fluorescence quenching assay (*29*) has been reported and has been demonstrated to be applicable to a variable lipid structure (e.g. bilayer width). This method involves using two quenchers, acrylamide and 10-doxylnonadecane, which are not located at fixed depths (*29*). A combination of site-directed fluorophore labeling and the parallax method is the major approach described in this dissertation, which will be discussed in detail in a later chapter.

Solid state NMR can be used as a method to provide information about the conformation and dynamics of individual amino acid residues in an intact protein under physiological conditions, such as those in a complex of protein-lipid suspended in aqueous solution at room temperature (*30-32*). By metabolic introduction or chemical synthesis of carbon-13-labeled amino acid residues into a protein as NMR probes, the conformation-dependent ^{13}C chemical shift can be detected to provide information about the local environmental changes of selectively labeled amino acid residues (*33*). By using this approach, evidence for the conformational change of a protein at the membrane surface has been obtained, including the phospholipase C-δ1 pleckstrin homology (PH) domain (*33*) and bacteriorhodopsin (*31, 32*). However, this method does not provide direct evidence for membrane contact or depth of penetration into the membrane (*1*).

In recent years, a combination of site-directed spin labeling and EPR power saturation methods has been applied to define the membrane penetration depths and geometries of lipid-interacting protein domains, such as C2 domains (*34-37*). The EPR membrane depth measurement first introduces nitroxide spin probes to specific sites on the protein surface, and then the depth of the spin label in the membrane is measured by monitoring its rate of collisions with extrinsic paramagnetic probes(*1*). These probes

include a probe residing in the aqueous phase, such as the metal complex of nickel (II) ethylenediaminediacetic acid (NiEDDA), and a probe in the membrane, such as molecular oxygen (*1*). The information, including the depth of penetration of the protein into the lipid bilayer and the angle of the docked protein relative to the membrane surface, can be defined by a sufficiently large library of spin label positions scattered throughout the protein (*1*). Thus, this method "provides the most detailed molecular pictures of membrane-docked proteins currently available" (*1*).

However, this method is limited by several factors (*1*). First, the conformation and motion of the spin label can not be ignored. Second, it is not applicable for a protein whose structure changes greatly upon membrane docking. Finally, care has to be taken that concentration gradients of the paramagnetic probes are not affected by the presence of protein bound to the membrane. However, the rapid diffusion of the paramagnetic probes, which are small molecules, minimizes this perturbation.

In addition to experimental studies of lipid-protein complexes, computational approaches are another way to elucidate their structures. Two representative methods are molecular dynamics (MD) simulations (*38-41*) and the finite difference Poisson-Boltzmann (FDPB) approach (*20-22*). MD simulations have been widely used to obtain information about protein-membrane complexation at the molecular level, such as an investigation of PLA2-membrane interactions (*40, 41*). The FDPB method has been applied to analyze the electrostatic component of proteins, nucleic acids, and membranes (*20*). It has been demonstrated to be "remarkably accurate in treating electrostatic properties associated with nonspecific binding" (*20*). This method has been applied to study the membrane binding behaviors of *Agkistrodon piscivorus piscivorus* (AppD49) sPLA2 and the nonpancreatic

human group IIA (hGIIA) sPLA2(*21*), as well as membrane interactions of FYVE domains (*22*).

All the above methods have their own limitations, and new approaches need to be developed. A decade after the discovery of electrospray ionization (ESI) and matrix-assisted laser desorption ionization (MALDI), soft ionization techniques, which make it possible to ionize physiologically relevant molecules without major degradation (*42*), mass spectrometry (MS) has been increasingly applied in the field of biochemistry, and it has also "become a powerful tool in protein analysis and the key technology in the emerging field of proteomics" (*43*). Examination of the intermolecular interaction in biomolecular systems, especially noncovalent interaction, is one of the MS-based approaches to which special attention has been paid (*44*). Efforts have been made to investigate the interaction of noncovalently bound molecules, including interaction of biomolecules with solvent molecules (*45,46*), interactions between nucleic-acid molecules (*47*), and interactions in duplex and quadruplex structures (*48*). In this study, we try to develop a MS-based method for investigating the interaction between cholesterol oxidase and the lipid bilayer, starting with finding out the location where the enzyme is in contact with the membrane.

II. Introduction to Cholesterol Oxidase

Cholesterol oxidase is isolated from a variety of microorganisms. It is a flavoenzyme that catalyzes two reactions in one active site: the oxidation of cholesterol to cholest-5-en-3-one followed by isomerization of the oxidation product to cholest-4-en-3-one (Scheme 1.1). An FAD cofactor is required for the oxidation of the sterol. The reduced cofactor is oxidized by oxygen, producing hydrogen peroxide.

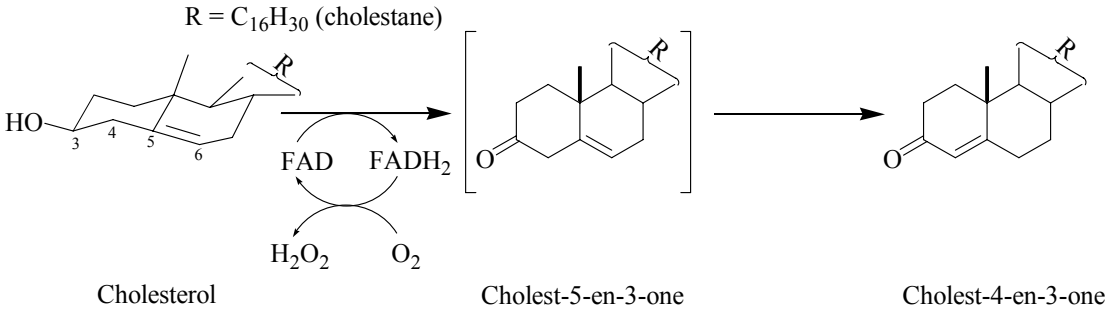

Scheme 1.1. Reaction catalyzed by cholesterol oxidase

Bacterial cholesterol oxidase was first isolated from Nocardia erythropolis in 1944 (49-51). In 1949, Schatz et al. isolated a soil Mycobacterium (52); the product 4-cholesten-3-one from incubation with a cell free extract of the enzyme (from this Mycobacterium) was first isolated by Stadtman et al. in 1954 (53). From then on, the enzyme has been found in many microorganisms.

After the suitability of cholesterol oxidase for the analysis of serum cholesterol was first illustrated by Flegg (54) and Richmond (55, 56), cholesterol oxidase rose to become the most widely used enzyme in clinical laboratories to detect the total serum cholesterol level in the diagnosis of arteriosclerosis and other lipid disorders, which are among the leading causes of death in America. A typical assay for total serum cholesterol usually utilizes cholesterol oxidase, coupled with cholesterol esterase and peroxidase. This assay

starts with the incubation of serum with cholesterol esterase, which produces free cholesterol, since ~70% of the cholesterol is esterified in serum. Cholesterol oxidase catalyzes the oxidation of cholesterol, using an FAD cofactor, which is concomitantly reduced. The FAD cofactor is regenerated by the reduction of oxygen (O2) to hydrogen peroxide (H2O2). A peroxidase enzyme reduces the hydrogen peroxide. Oxidation of an indicator molecule reactivates the peroxide and forms a stable colored complex, which can be quantitated by absorption spectrometry. Thus, the indirect detection of total serum cholesterol level is facilitated. Cholesterol oxidase has also been incorporated into nano-particles to serve as biosensors, using the colorimetric measurement of hydrogen peroxide (57, 58). The assays incorporating the enzyme are extremely simple, specific, and highly sensitive.

Although cholesterol oxidase is primarily used for the analysis of serum/lipoprotein cholesterol analysis, it was also one of the early tools used to be applied as a probe to track cell cholesterol, to determine the heterogeneity of cell membranes and the distribution of cholesterol in the plasma membrane (*59-64*). Investigating the dependence of cholesterol oxidase activity on lipid phase by varying lipid components provides a promising future for detecting microdomains in cellular membranes (*65*).

Purcell et al. discovered a highly efficacious protein that killed boll weevil larvae in *Streptomyces* culture filtrates, and this protein was identified as cholesterol oxidase. Their histological studies suggested that the primary mechanism of lethality is that cholesterol oxidase lyses the boll weevil midgut epithelium by altering the phospholipid membranes or composition of the membranes (*66*). As one of the more potent insecticidal proteins, cholesterol oxidase was proposed to be utilized in transgenic crops for pest control

strategies, and efforts were made in this direction. Murooka et al. expressed the *Streptomyces* cholesterol oxidase in tobacco cells, and about an eight-fold higher cholesterol oxidase activity in transformed callus was obtained (*67*). Expression of the cholesterol oxidase gene in plant protoplast cells also resulted in production of an enzymatically active cholesterol oxidase (*68*). Expression and chloroplast targeting of cholesterol oxidase in transgenic tobacco plants indicated that cholesterol oxidase can metabolize phytosterols *in vivo* when produced cytosolically or when targeted to chloroplasts (*69*). Because of the particularly potent effects of cholesterol oxidase on boll weevil larvae, cholesterol oxidase genes may be useful in the production of transgenic plants that are self-protected against pest infestation. However, cholesterol oxidase may alter sterol derivatives, such as steroid hormones, that influence plant growth (*69, 70*).

Evidence from diverse studies supports the role of oxidized cholesterol as a mediator of toxicity to mammals, while the precise mechanism is unknown (*71*). Studies of a relationship between cholesterol oxidation and cardiovascular pathology have been reported (*72*). Nowadays, more and more researchers are paying attention to the role of cholesterol in bacterial infections, such as those involving *Mycobacterium tuberculosis* (*Mtb*) and *Rhodococcus equi* (*R. equi*) (*B. sterolicum,* the *Brevibacterium sterolicum* species has recently been reclassified as *Rhodococcus equi (73)*). An essential role for cholesterol in the entry of mycobacteria into macrophages has been reported for *Mycobacterium bovis*, a relative of *Mtb*. The results indicate that a physical interaction between cholesterol and tryptophan aspartate-containing coat protein (TACO) is involved in the inhibition of fusion of phagosomes and lysosomes, resulting in the intracellular survival of mycobacteria (*74*).

Conversion of Δ^5-3ß-hydroxysteroids to Δ^4-3-ketosteroids is a reaction that is required for the biosynthesis of all classes of steroid hormones, which have multiple effects within the immune system. Catalysis of this conversion by 3β-hydroxysteroid dehydrogenase contributes to vaccinia virus virulence by inhibiting an effective inflammatory response to infection (*75*). Recent studies on a cholesterol catabolic pathway suggested that "cholesterol metabolism is central to *Mtb*'s unusual ability to survive in macrophages" (*76*). Cholesterol oxidases or 3β-hydroxysteroid dehydrogenase may alter in steroid hormone synthesis so as to suppress the inflammatory response to infection by *Mycobacteria* (personal communication with N. S. Sampson).

An opportunistic pathogen, which infects people with compromised immune function, *R. equi* secretes high levels of cholesterol oxidase, ChoE. It has been proposed to play a role in maintenance of the infection in the host macrophage (*71*). Data collected from site-directed mutagenesis demonstrated that ChoE is an important cytolytic factor for *R. equi (77)*, although it seems not to be important in the early stages of infection (*78*).

Although cholesterol oxidase has been widely used in both basic scientific research and clinical applications, a detailed understanding of this enzyme, including chemistry (oxidation and isomerization of cholesterol), structure and molecular mode of action, needs to be pursued to guide optimization of the uses of the enzyme, as well as investigation of its role in pathogenicity.

Cholesterol oxidase is a monomeric, 57 kDa protein. The three-dimensional structures of both the oxidase from *Streptomyces sp. SA-COO* (*79, 80*) and the oxidase from *R. equi.* have been solved (*81, 82*). They are type I oxidases (Figure 1.2a). Each contains the FAD cofactor noncovalently bound to the enzyme. These two oxidases are

nearly identical in sequence and structure. The structure of a type II oxidase obtained from a different *Brevibacterium* strain has also been solved (Figure 1.2b). It has a covalently bound FAD. Its sequence and structure are completely different from the type I oxidase. Despite the identical reactions carried out by the covalent and noncovalent FAD enzymes, there is a large difference in their redox potential and kinetic properties (*83, 84*).

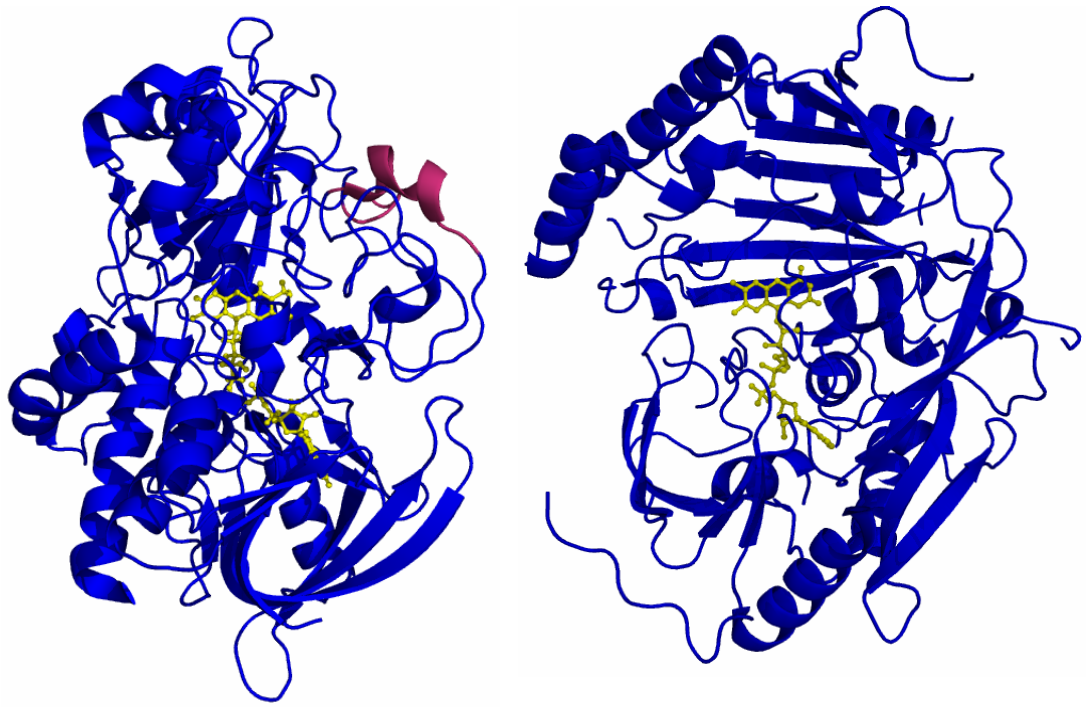

(a) (b)

Figure1.2. Secondary structure representations of (a) Type I cholesterol oxidase (PDB entry 1MXT) and (b) type II cholesterol oxidase (PDB entry 1I19). The substrate cavity is deeply buried. The substrate binding loop of type I cholesterol oxidase is colored in pink, the FAD cofactor is shown in yellow. The figures were made with PyMOL (*85*).

The noncovalent FAD forms of the enzyme are members of the GMC (glucose-methanol-choline) oxidoreductase family. The complete conservation of His447 within the GMC oxidoreductase family is revealed by sequence and structure alignments of the active site(*82*). Two residues, His447 and Asn485, thought to be involved in substrate oxidation, are semiconserved (*86*). A combination of site-directed mutagenesis, kinetics, and X-ray crystallography indicate that His447, Glu361 and Asn485 are the key active site residues playing important mechanistic roles in substrate positioning, oxidation, and isomerization (Figure 1.3).

Glu361 acts as general base catalyst for isomerization (*82, 87-89*). The atomic resolution structure has revealed the location of hydrogen atoms on His447, which is proposed to orient the substrate with respect to the FAD cofactor. The NE2 atom of His447, which is critical to the redox activity of this flavin oxidase, acts as a hydrogen bond donor rather than as a hydrogen acceptor (*90*). Asn485 plays an important role in substrate oxidation; it is crucial for creating an electrostatic potential around the FAD cofactor, enhancing the oxidation reaction through an N-H…π electrostatic interaction (*83*). A structure of the complex of the reduced enzyme with dehydroepiandrosterone showed that a bound water molecule (Wat541) is close to the hydroxyl group of the steroid and bound in a deeply buried active site (*82*). Instead of acting as a mediator in a hydrogen-bond network at the active site, Wat541 has been reinterpreted as a mimic of the substrate hydroxyl group by viewing the sub-angstrom resolution (0.95 Å) crystal structure of the *Streptomyces* enzyme (*90*).

Despite the identical reactions carried out by the type I and type II cholesterol oxidase, the covalent FAD forms of the enzyme are structurally distinct from the

noncovalent FAD enzymes (*79, 91*). Large differences have been found in redox potential and kinetic properties, suggesting diverse catalytic mechanisms. Compared to type I oxidase, which has a midpoint reduction potential of -278 mV (*83*), type II oxidase, which has a midpoint reduction potential of -101 mV (*84*), is a better oxidizing agent. More hydrophilic residues are seen at the active site of the type II enzyme, while the active site of the type I enzyme contains more hydrophobic residues. In the type II enzyme Arg477 replaces His447 in the type I reaction, and Glu475 is analogous to Glu361 in the type I enzyme.

A "hydrophobic channel" that extends from the exterior surface of the molecule to the buried active site cavity, has been identified in both type I and type II enzymes. This channel has been proposed to act as an access route for molecular oxygen during the oxidative half-reaction and an exit route for hydrogen peroxide. In the type II oxidase, this tunnel is situated between the FAD-binding domain and the substrate-binding domain. From the 1.7 Å crystal structure, the tunnel is directly visible (*79*), while in the type I oxidase, it only becomes visible at 0.95 Å resolution (*90*). The residues lining the tunnel are all hydrophobic in nature. The tunnel is only wide enough to accommodate a single water molecule. A conformational rearrangement is observed in the WT crystal structure in which conformation A corresponds to the "closed" channel, and conformation B corresponds to the "open" channel. The tunnel is transient and thought to be gated by the redox state of the cofactor. For type I enzymes, the tunnel is gated primarily by Asn485; for type II enzymes, it is gated primarily by Arg477.

A structure of the complex of the reduced enzyme with dehydroepiandrosterone showed the substrate bound in a deeply buried active site (*82*) (Figure 1.4). Compared to

wild-type cholesterol oxidase, a mutant enzyme with a truncation of the tip of an active site loop (79-83) shows a 6-fold improvement in k_{cat}/K_m with dehydroepiandrosterone as substrate and a 170-fold reduction with micellar cholesterol, indicating that the tip of the loop is necessary for packing with the "tail" of cholesterol and is responsible for substrate specificity at C_{17} (*92*). The UV/vis and CD spectra of the mutant reveal that the mutant enzyme, with FAD bound, is properly folded with FAD bound, and only a small change was observed in the binding affinity of the mutant for vesicles relative to wild type. This suggests that the loop is crucial for movement of the substrate from the lipid bilayer, not membrane binding (*92*).

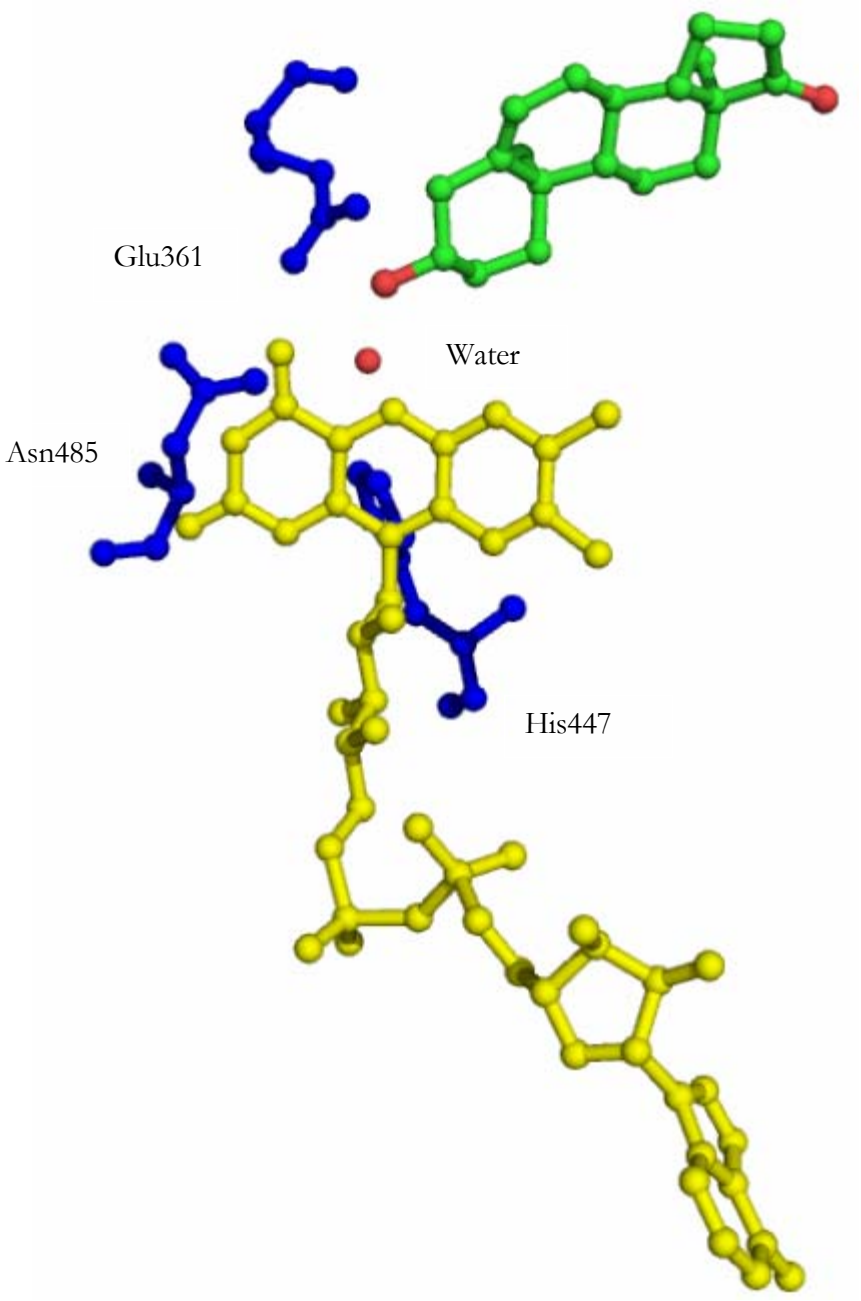

Figure 1.3. Active site region of the complex of type I *R. equi* cholesterol oxidase with dehydroepiandrosterone (DHEA) (PDB entry 1COY). FAD is shown in yellow, DHEA is colored in green (oxygen atom of DHEA is in red). The drawing was generated using PyMOL (*85*).

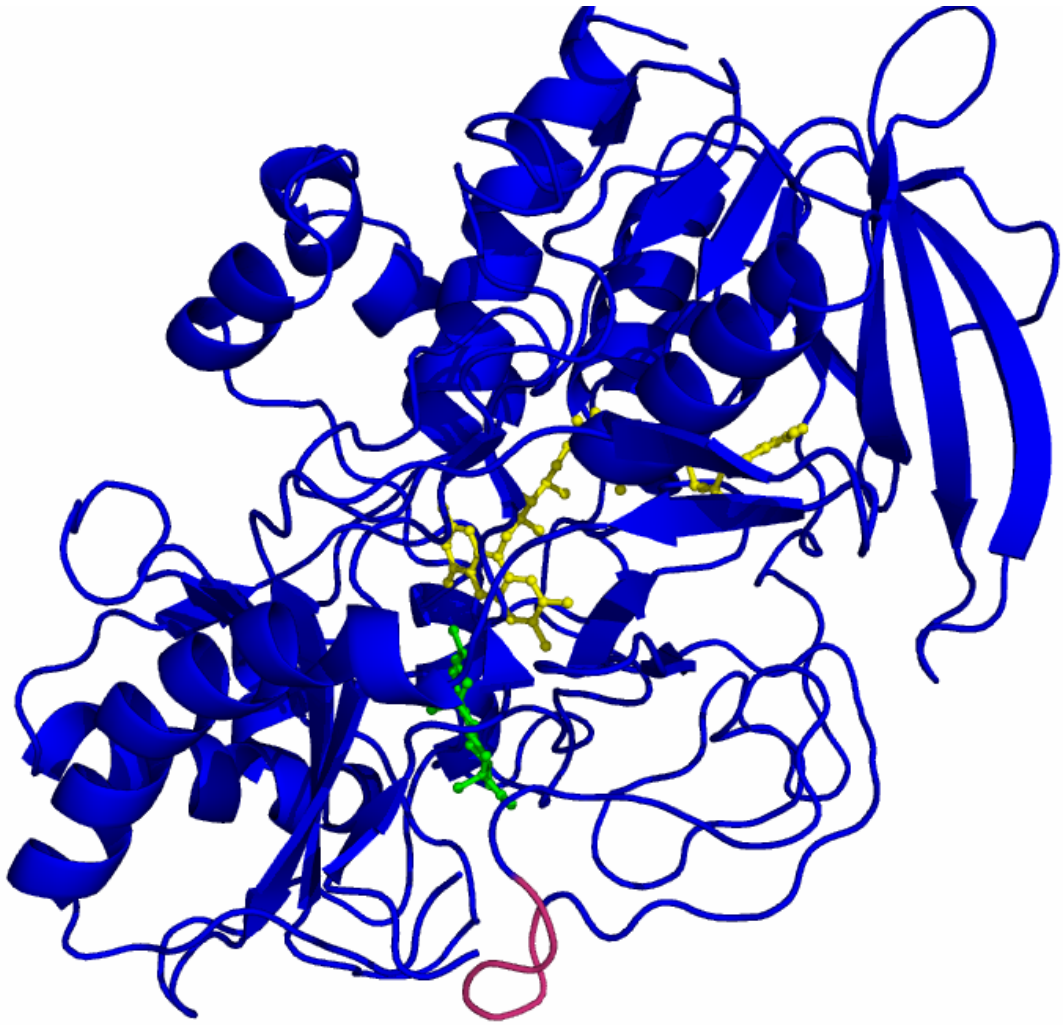

Figure 1.4. The overall structure of the complex of the type I *R. equi* cholesterol oxidase with dehydroepiandrosterone (DHEA) (PDB entry 1COY). The substrate binding loop is shown in pink, FAD cofactor is colored in yellow, the substrate DHEA is in green. This figure was made using PyMOL (*85*).

Cholesterol oxidase is an interfacial enzyme. Previous studies provided direct evidence that cholesterol oxidase binds to the membranes, weakly and shallowly (*27*). However, this result did not distinguish orientations on the lipid bilayer in which the large face or the smaller face are in membrane contact According to the crystal structure, the entrance to the active site is situated on a large face, and that face could potentially contact the membrane. Alternatively, the protein could be oriented such that the smaller face is in membrane contact.

The current study of cholesterol oxidase binding is based on this model of the DHEA-bound cholesterol oxidase structure (*82*), because a crystal structure of cholesterol oxidase bound with cholesterol and a structure of the enzyme interacting with the lipid bilayer is not available. We postulated a working model for cholesterol oxidase associated with lipid bilayers (Figure 1.5). In our proposed model, during the binding process, the enzyme first undergoes a conformational change to form a pathway to allow active site access to the cholesterol in the membrane. Next, the substrate is oxidized and isomerized at the active site, and the resulting product is returned to the lipid bilayer or released to the bulk solution. Last, the enzyme resumes its original form when it leaves the lipid bilayer, and starts over again.

This thesis describes studies of the orientation of cholesterol oxidase on model membranes through a combination of high-resolution X-ray crystallography, mutagenesis, steady-state kinetic analysis, fluorescence quenching measurements and a mass spectrometry-based method.

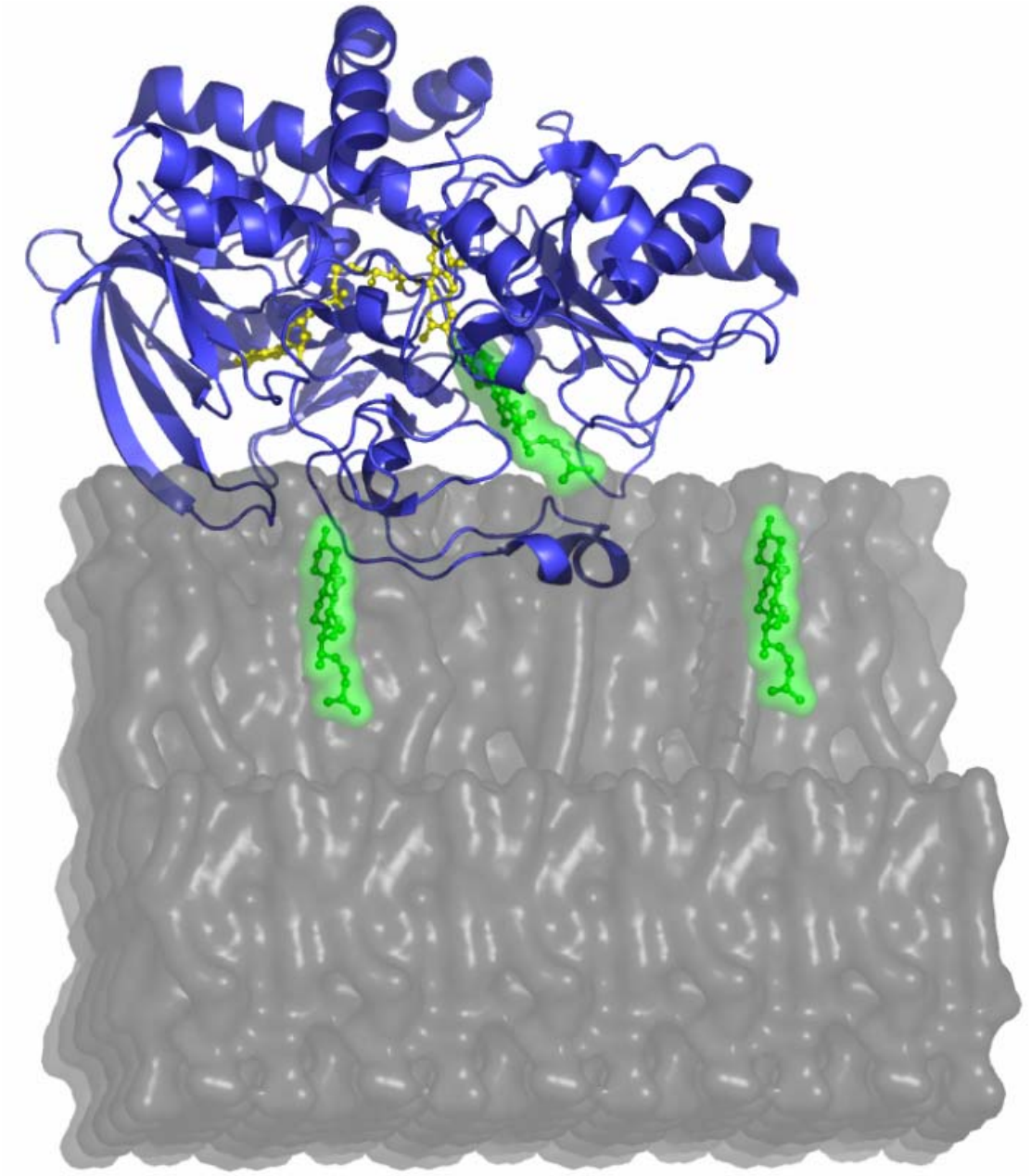

Figure 1.5. Working model of how cholesterol oxidase (PDB entry 1MXT) interacts with the lipid bilayer (*93*). Cholesterol oxidase is shown in blue, FAD cofactor is in yellow, cholesterol is in green, and lipids are in grey. The figure was made with PyMOL (*85*).

CHAPTER 2 Construction of Cysteine Cholesterol Oxidase Mutants for Membrane Docking Studies

- The pCO242 plasmid described in this chapter was constructed by Dr. David Wolfgang who is a former postdoc in Sampson's laboratory.

I. Introduction

Cholesterol oxidase is water soluble. Both its substrate and product are neutral and hydrophobic molecules. It is known that cholesterol prefers a hydrophobic environment, such as the lipid bilayer, it also spontaneously transfers between membranes through the aqueous milieu (*94*). The rate of inter-membrane exchange is much slower than the rate of cholesterol oxidation catalyzed by cholesterol oxidase (*95*). Thus, cholesterol oxidase must bind to the membranes during catalysis to allow the substrate to access directly to the active site of the enzyme via an interfacial binding surface (*95*).

Examination of the X-ray crystal structures of native enzyme from both *Rhodococcus equi* and *Streptomyces* revealed a deeply buried hydrophobic active site cavity that is sequestered from the aqueous environment by one or more protein loops, the loops seem to cover the entrance to the active site in the free enzyme state (Figure 2.1, Figure 2.2). Cholesterol resides in the hydrophobic part of the lipid bilayer. In a dehydroepiandrosterone-bound structure of *Rhodococcus equi* cholesterol oxidase, the substrate analog, which lacks an 8-carbon "tail" compared to cholesterol, completely fills the steroid binding site. Clearly, conformational changes of the protein must occur during the binding process to help cholesterol to bind in the oxidase's active site from the membrane. It is not clear what the structure of the enzyme will be with cholesterol bound and what the structure of the complex of the enzyme and lipid membrane looks like.

The substrate binding site appears to be capped by two surface loops (73-86, 432-438) (Figure 2.1). These loops are composed of hydrophilic residues on the outside faces and hydrophobic residues on the inside faces. Although it is unknown what the conformation of the "open" enzyme will be, we postulate that one of both these loops open to form a

hydrophobic pathway between the membrane and the steroid binding site to facilitate cholesterol movement out of the lipid bilayer. Upon binding, the loops can close over the substrate analog and bury it. The four rings of the sterol are completely buried in the active site. When cholesterol is bound, the 8-carbon "tail" might stick out of the active site and packs with the open loops.

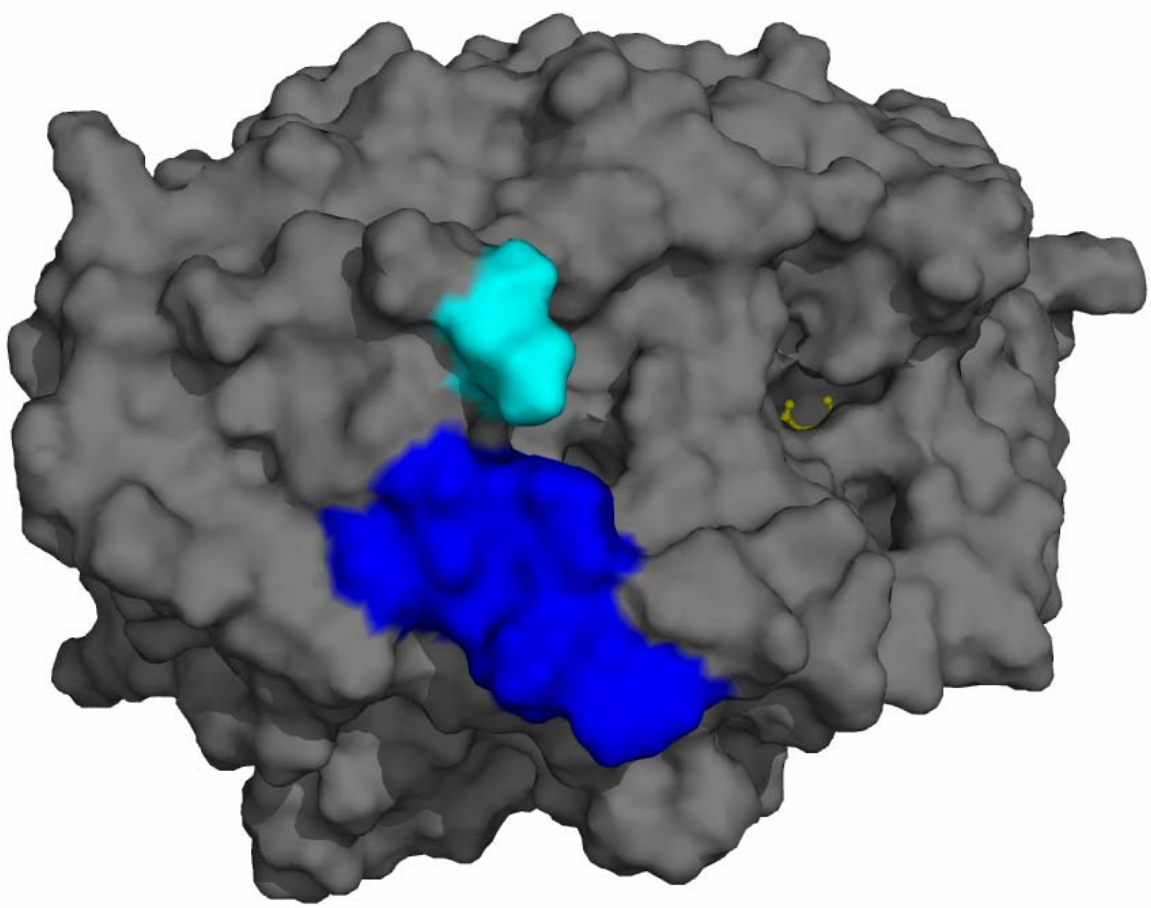

Figure 2.1. Molecular surface of *Streptomyces* wild-type cholesterol oxidase (PDB entry 1MXT). Loop 73-86 is colored in blue, loop 432-438 is shown in cyan and FAD cofactor is in yellow. The figure was made with PyMol (*85*).

Deletion mutagenesis studies proved loop 79-83 residues to be essential for packing with the "tail" of cholesterol (*92*), suggesting that the loop is responsible for the movement of cholesterol from the lipid bilayer. Type I Rhodococcus equi cholesterol oxidase was specifically labeled with fluorophore on the tip of the loop and this construct was used to probe explicitly the loop-lipid bilayer interactions (*27*). The depth of the loop in the

membrane was determined to be 8.1 Å from the center of the lipid bilayer, using the fluorescence parallax method of Chattopadhyay and London (*25*). The depth suggests that the protein sits on the surface of the membrane, with only minimal insertion. Thus, in the protein-membrane complex, the enzyme is on the surface of the membrane, and the amino acid side chains of the loop insert into the membrane to shield the cholesterol from the polar head groups as it moves from the bilayer into the active site. Mutagenesis experiments suggested that the contact surface is composed of more than the loop itself (*27*). However, the extent of the enzyme surface that is in contact with the membrane is not known. Further studies were required to determine the orientation of the protein with respect to the membrane and the magnitude of the surface area that is in contact with the membrane. The initial fluorescence experiments (*27*) were performed with a cysteine mutant of the *Rhodococcus equi* cholesterol oxidase since wild-type enzyme contains only one cysteine. Examination of X-ray crystal structures of *Rhodococcus equi* and *Streptomyces* cholesterol oxidases reveals that these two oxidases are nearly identical in sequence and structure. In this thesis, the *Streptomyces* cholesterol oxidase was used due to the higher protein expression level, and because ultra-high ChoA structures were available as well as many mutants.

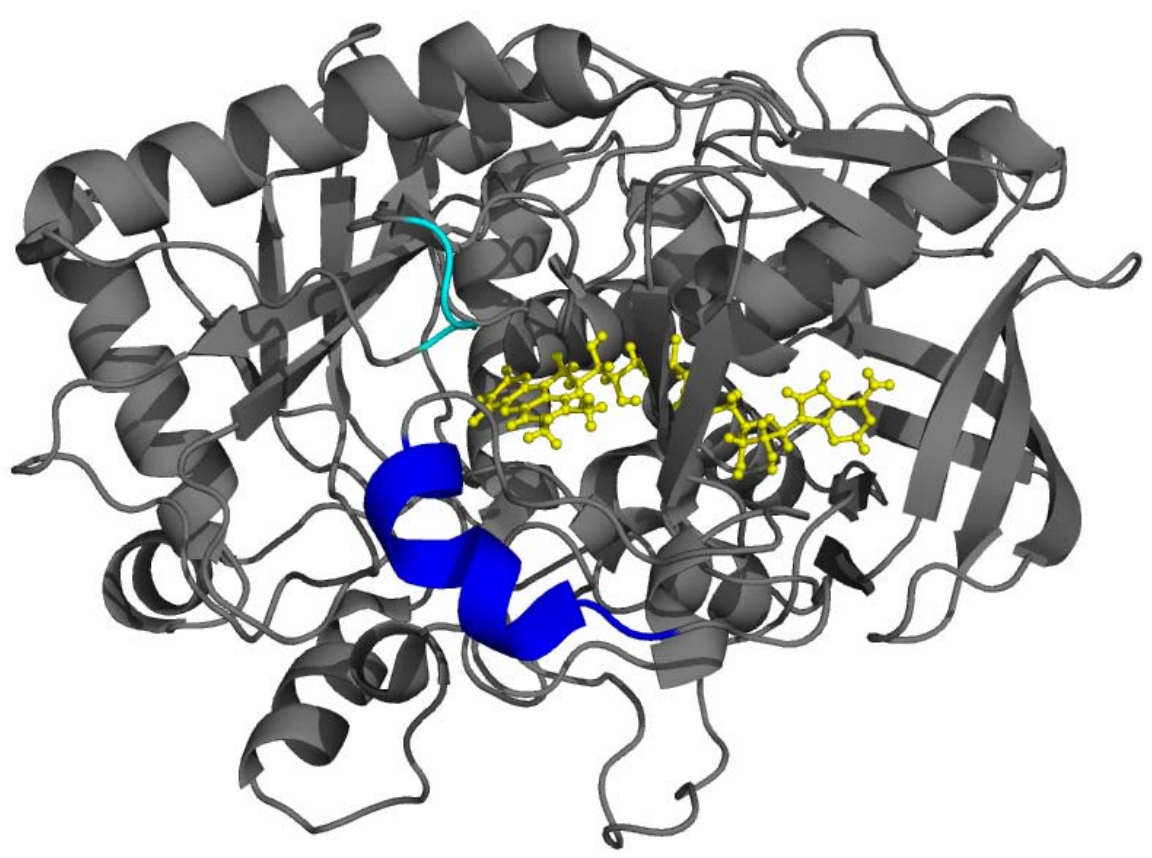

Figure 2.2. Secondary structure representation of *Streptomyces* wild-type cholesterol oxidase (PDB entry 1MXT). This figure shows that protein loops cover the entrance to the active site cavity. Loop 76-86 is colored in blue, loop 431-435 is shown in cyan, FAD cofactor is in yellow. The figure was made with PyMol (*85*).

The crystal structure shows that the loop is situated on a large surface of 3920 $Å^2$ that could potentially contact the membrane (Figure 2.3). This face has very little secondary structure except for the two turns of helix in the loop. It may be possible that the structure rearranges upon binding. ~40% of the residues on this face are hydrophobic. Alternatively, the enzyme could be oriented such that a smaller face is in membrane contact (Figure 2.3).

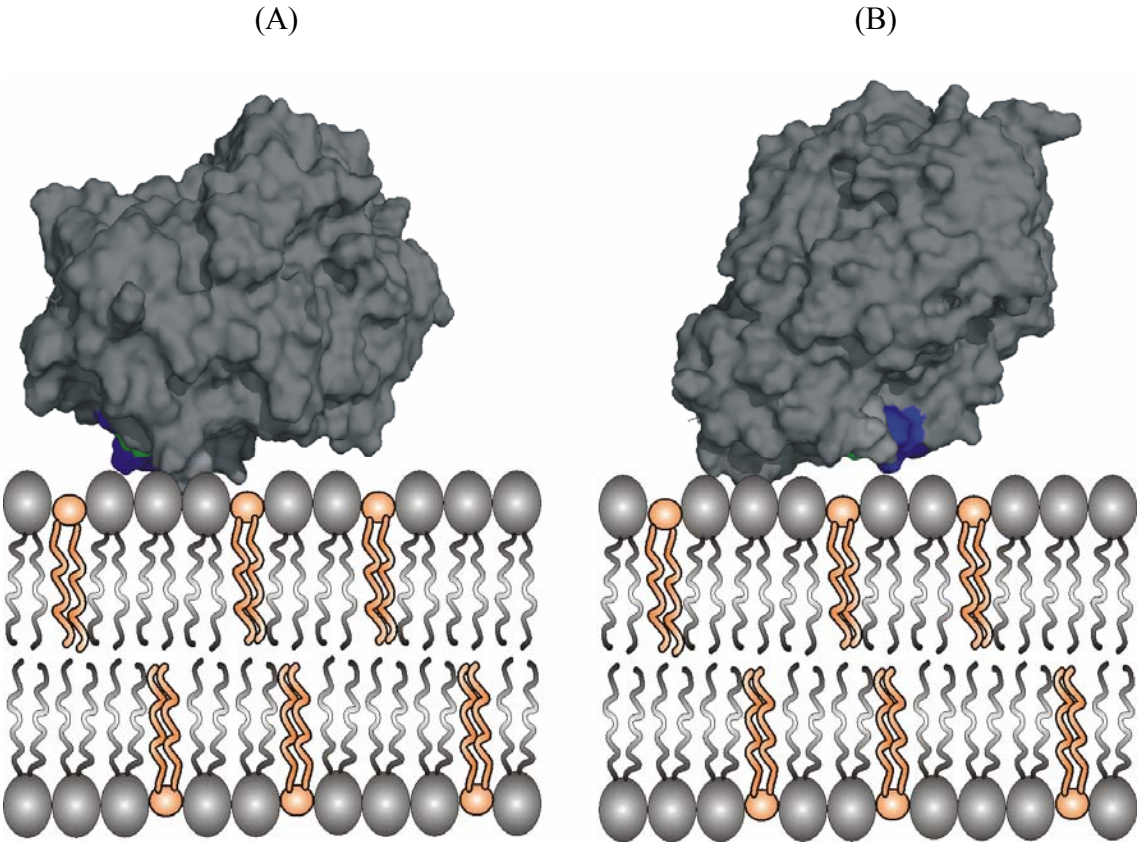

Figure 2.3. Models of cholesterol oxidase binding to the membrane. (A) The enzyme binds to the lipid bilayer via a large protein surface; (B) the enzyme binds to the model membrane via a small protein surface. Lipids and the substrate are shown in gray and orange, respectively. Loop 77-83 is colored in blue, residue 80 is in green, the overall structure of cholesterol oxidase is shown in dark gray. This figure was made with CorelDRAW.

We have site-selectively mutated cysteine into sites across these two protein faces one at a time (Figure 2.4). To do a negative control experiment, two residues located on the opposite site of these two faces, the “back face”, were mutated into cysteines. The “back face” has been assumed not to be in contact with the membrane. The targeted residues are

primarily hydrophobic residues and their side chains are all surface exposed despite their hydrophobicity. The selected residues are L274, A393, on the large face, W333, I427, on the smaller face, L80, N88, on the loop, and M154, V34, on the "back face". Fluorophore e.g., 6-acryloyl-2-dimethylaminonaphthalene (acrylodan), was placed at selected sites (Scheme 2.1) and binding measurements were performed to determine which face is in contact with the membrane, and which residue(s) is (are) in contact with the membrane. To eliminate the possibility of fluorophore reacting at multiple sites, the 4 intrinsic cysteines (C56, C282, C445, and C452) were removed and replaced with alanines to generate a 4CA mutant, this work was done by Dr. David Wolfgang. All of the mutants described in this work are derived from the 4CA mutant.

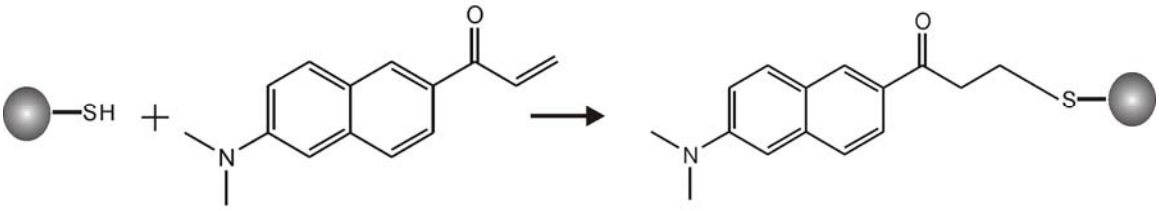

Cysteine mutant Acrylodan Cysteine mutant-acrylodan adduct

Scheme 2.1. Reaction scheme of cysteine and acrylodan.

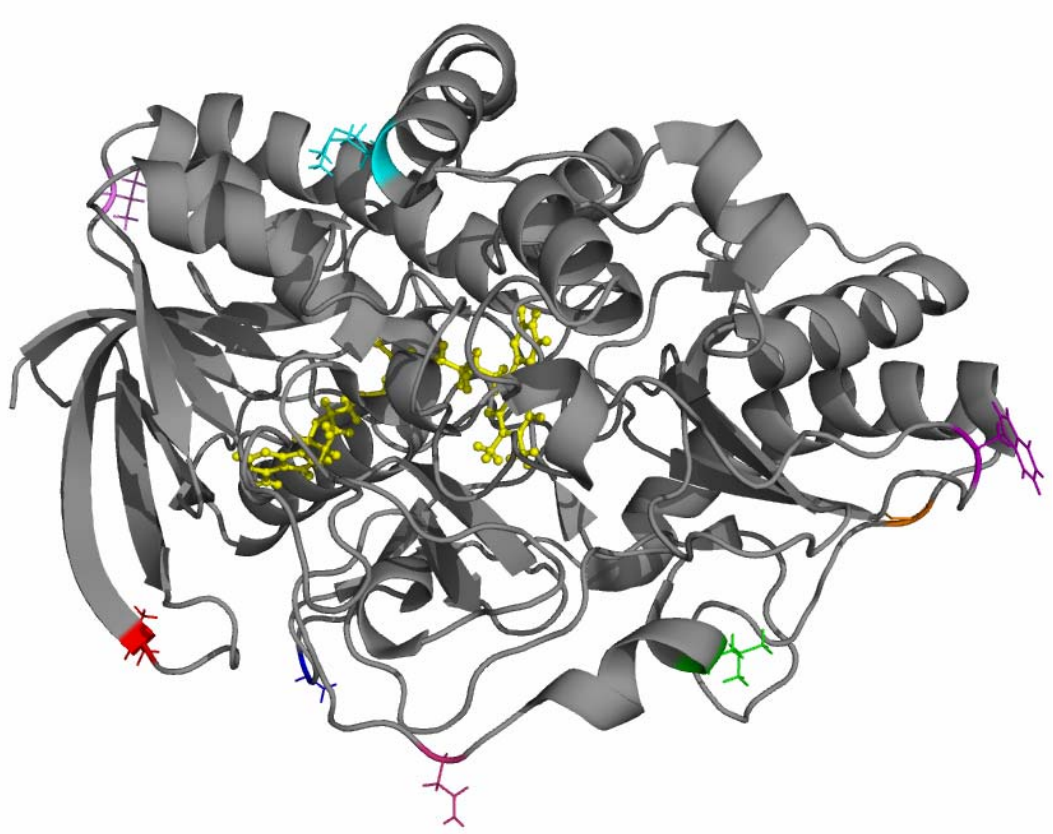

Figure 2.4. Acrylodan labeling sites across the surface of the Streptomyces wild-type cholesterol oxidase (PDB entry 1MXT) with residue L80 (green), N88 (pink), L274 (red), A393 (blue), W333 (purple), I427 (orange), M154 (cyan), and V34 (violet). FAD is shown in yellow. This figure is made with PyMol (*85*).

II. Materials and Methods

Materials. Cholesterol and BSA were purchased from Sigma Chemical Co. (St. Louis, MO). Triton X-100 was from Aldrich Fine Chemical Co., (Milwaukee, WI). The plasmid for heterologous expression of *Streptomyces* cholesterol oxidase, pCO202 has been described previously (*92*), and is a derivative of pCO117, a generous gift from Y. Murooka (*96*). Restriction endonucleases, T4 DNA ligase were purchased from New England Biolabs (Beverly, MA). Oligonucleotides were purchased from IDT, Inc. (Coralville, IA). Cloned Pfu DNA polymerase was purchased from Stratagene (La Jolla, CA), iProof DNA polymerase was purchased from Bio-Rad (Hercules, CA). Acrylodan was purchased from Molecular Probes (Eugene, OR). Unless otherwise specified, all chemicals, solvents and other materials, were supplied by Fisher Scientific (Pittsburgh, PA). Water for assays and chromatography was distilled, followed by passage through a Barnstead NANOpure filtration system (Barnstead International, Dubuque, IA) to give a resistivity better than 18 MΩ.

General Methods. A Shimadzu UV2550 UV-Vis Spectrophotometer (Kyoto, Japan) was used for assays and acquisition of UV spectra. Fluorescence measurements were taken on a PTI Spectrofluorimeter QM-4/2005-SE with double monochromators (Photon Technology International, Lawrenceceville, NJ), using a 150 watt Xenon lamp (Ushio Inc., Japan). Restriction digests and ligations were performed according to procedures described in Sambrook et al. (*97*). Big dye sequencing (Applied Biosystems, Foster City, CA; performed by the Stony Brook University Sequencing Facility) was applied to all mutated regions, and the plasmids were purified with the Wizard Plus DNA Purification System (Promega, Madison, WI) with water elution. DEAE-52 cellulose was from

Whatman (Maidstone, UK). The following buffers were used A: 50 mM sodium phosphate, pH 7.0; B: buffer A + 2.0 M $(NH_4)_2SO_4$; C: 50 mM sodium phosphate, pH 7.0 + 0.025% triton X-100 (w/v).

Plasmid Construction of Cholesterol Oxidase Mutants. Methods for plasmid preparation were standard unless otherwise described (*97*). Mutations were introduced by PCR mutagenesis using mutagenic primers (Table 2.1). Restriction enzyme digested DNA fragments with the targeted mutation sites was ligated into purified vector, which was digested by the same restriction enzymes, with T4 DNA ligase. The *Streptomyces* cholesterol oxidase gene, containing four mutations, C56A/C282A/C445A/C452A, is referred to as the 4CA mutant. The plasmid constructed to express the 4CA cholesterol oxidase mutant is called pCO242, and is a derivative of the pUC19 vector. This work was performed by Dr. David Wolfgang. The detailed construction strategies, except for pCO242, are enclosed in supplement I. All of the resulting mutant genes were verified by dideoxy DNA sequencing.

Table 2.1. Primers and restriction sites used for construction of cholesterol oxidase

Primer	Lab code	Mutation site[a]	Restriction maker[b]	Restriction sites used	Plasmid	Sequence (5'-3')[c]
1	KA-25II-2	A282	+EcoRV	HindIII BglII	pCO256	CCAAGGAGATCTCCGCCCGATATCTGTTCCTCGGC
2	NSS118					GCAGCAAGCTTACGACGCCGTGACGTC
3	KA-25II-3a	A56	+SspI	Sph I Bsm I	pCO257	CCGGGTTGAGCATGCCGGCGAAAATATTACCATCTGGACC TGG
4	XC11					ATGACTGCACAACAGCATCT
5	KA-25 II-1	A445 A452	+AvrII	StuI HindIII	pCO242	CCCAGCTGAAGGCCTTCGCCGACGACTTCGCCTACCACCCG CTCGGCGGCGCCGTCCTAGGCAAGGCGACGGAC
6	HT-10	NdeI HindIII		NdeI HindIII	pCO270	GGTCCACATATGACTGCACAACAGCATCTGTCC

7	HT-8					GGACCTGAAGCTTTACGACGCCGTGACGTC
8	I427C-ISLE	C427	+KpnI	BglII	pCO251	CGGCGAAGGCCTTCAGCTGGGTACCGAAGAGGTCGTACCG
	E			StuI		GTAGCACGTGCCGT TCGCCT-
9	TH-L274C-	C274	-BalI	BglII	pCO250	GCAGGAGATCTCCTTGGTAGCCAG
	antisense			Sal I		GCACTTGCCGTCGGTGTCCTTC
10	DW61-1A	C80	-AatII	XhoI	pCO247	CGGTTGACAACGTCGAGCCAGCAGAAGCTGCCG
				IthIII		
11	HT-13	C154	+ HpaI	SalI	pCO274	CGCGGGTCGACTCCTCCGAGATGTACGACCGCTACTTCCCC
				StuI		CGCGCCAACTCCTGCCTCCGCGTTAACCACATCG
12	HT-14	C393	-NruI	HpaI	pCO275	GCGCGGTCCGTGCAGGCGTCGTACACGAAGGTGCCGCGCT
				Rsr II		GGGGGTTCTTGGTGATGGCGAGGTAGAGGC
13	HT-12					GGCAGCTTCCTCTGGCTCGACGTCGTTAACCG
14	HT-23	C34	-XhoI	KpnI	pCO276	GGGGGTACCGGTTACGGTGCTGCAGTTTCCGCTCTGCGTCT
				Stu I		GGGTGAAGCTGGTTGCCAGACTCTGATGCTG GAG
15	HT-24	C88	-SnaBI	HpaI	pCO277	GGGCGTTAACCGGTGCATCGATCCCTACGCGGGGGTCCTG

				StuI		GACCGTGTGAACTATGATCAGATGTCGGTATACGTTGGC
16	HT-17	C333	-SmaI	ApaI	pCO278	GGCTGGGGCCCCAACGGCAACATCATGACCGCCCGCGCCA
				Stu I		ACCACATGTGCA ACCCC

[a]Denotes amino acid codon mutated. [b]Silent mutation used for screening the ligation product, + refers creating a restriction site, - refers removing a restriction site. [c]Mutated bases for plasmid construction (bold-print underlined bases) and restriction markers (normal-print underlined bases).

Plasmid pCO270 (4CA in pET20b vector) was constructed in the following way. First, primers 1 and 2 were used to change cysteine282 to alanine, the mutant gene was subcloned into pCO240 (*98*) using Hind III and Bgl II restriction sites to produce pCO256. Second, primers 3 and 4 were used to change cysteine56 to alanine, the resulting mutant gene was ligated into the Sph I and Bsm I fragment of pCO256 to generate pCO257. Third, to change cysteine445 and cysteine452 to alanines, primers 5 and 2 were used. The mutant fragment was subcloned into the pCO257 using Stu I and Hind III restriction sites to yield pCO242. Finally, to put the 4CA gene into pET20b vector, which contains a T7 promoter, an NdeI site was introduced into pCO242 by using primers 6 and 7. The resulting gene was ligated into the NdeI to HindIII fragment of pET20b to generate pCO270.

Plasmid pCO271 (I427C/4CA in pET20b vector) has a cysteine at position 427, which was originally isoleucine. To change isoleucine427 to cysteine, primers 8 and 4 were used to produce a mutant fragment, which was subcloned into pCO242 using BglII and StuI restriction sites to generate pCO251. An NdeI site was introduced into pCO251 using primers 6 and 7, the resulting gene was subcloned into an NdeI to HindIII fragment of pET20b to generate plasmid pCO271.

Plasmid pCO272 (L274C/4CA in pET20b vector) is the mutant gene containing cysteine274, which was originally leucine. To change leucine274 to cysteine, primers 9 and 4 were used to produce a mutant fragment, which was subcloned into pCO240 using BglII and SalI restriction sites to generate pCO250. pCO250 was digested with BglII and SpeI, followed by ligation into pCO242 to yield pCO252. An NdeI site was introduced into pCO252 using primers 6 and 7, the resulting gene was subcloned into an NdeI to HindIII fragment of pET20b to generate pCO272.

Plasmid pCO273 (L80C/4CA in pET20b vector) was derived from two plasmids, pCO247 and pCO253. The L80C mutation was introduced using primers 10 and 4, and the mutant fragment was subcloned into pCO202 using XhoI and IthIII restriction sites to generate pCO247 (this work was performed by Dr. David Wolfgang). The XhoI and BglII fragment obtained from pCO247 was subcloned into pCO242 to yield pCO253. An NdeI site was introduced into pCO253 using primers 6 and 7, the resulting gene was subcloned into an NdeI to HindIII fragment of pET20b to generate pCO273.

Plasmid pCO274 (M154C/4CA in pET20b vector), pCO275 (A393C/4CA in pET20b vector), pCO276 (V34C/4CA in pET20b vector), pCO277 (N88C/4CA in pET20b vector), and pCO278 (W33C/4CA in pET20b vector), were constructed in the same way. pCO274 was constructed with primers 11 and 7 to change methionine154 to cysteine, the mutant fragment was subcloned into pCO270 using Sal I and Stu I restriction sites. Primers 12 and 13 were used to change alanine 393 to cysteine, and the mutant fragment was subcloned into pCO270 using Hpa I and Rsr II restriction sites to generate pCO275. pCO276 contains cysteine 34, which was originally valine. To construct pCO276, primers 14 and 7 were used, and the mutant fragment was subcloned into a KpnI to StuI fragment of pCO270 to yield pCO276. pCO277 was constructed with primers 15 and 7 to change asparagine154 to cysteine, the mutant fragment was subcloned into pCO270 using Hpa I and Stu I restriction sites. Primers 16 and 7 were used to change tryptophan333 to cysteine, and the mutant fragment was ligated into pCO270, using ApaI and StuI restriction sites, to yield pCO278.

Purification of L274C/4CA Mutant. Cell paste of *E. coli* BL21(DE3)plysS transformed with pCO272 was obtained from 12 L of 2 x YT-ampicillin (100 μg/mL)

-chloramphenicol (34 μg/mL) medium grown at 18 ºC for 20 h after addition of IPTG (100 μg/mL) at A_{600} = 1.0 by centrifugation at 4 000 g for 30 min. The pellet was resuspended in 50 mL of buffer A and lysed by French press at 11 000 psi. All subsequent steps were conducted at 4 °C. Cell debris was removed by centrifugation at 135 000 g for 90 min. The supernatant was precipitated by 1.0 M $(NH_4)_2SO_4$ and the pellet was discarded. $(NH_4)_2SO_4$ was added to the supernatant to a final concentration of 2 M. The pellet was obtained by centrifugation at 4 000g. This pellet was resuspended in buffer A (30 mL) and desalted using dialysis (NMWCO 6,000-8,000) against buffer A. The dialysate was loaded onto a column of DEAE52[1] cellulose preequilibrated with buffer A. Fractions were collected by elution with buffer A (200 mL). Typically, 10-mL fractions were collected. Fractions containing cholesterol oxidase (as determined by SDS-PAGE[1]) were combined and concentrated by $(NH_4)_2SO_4$ precipitation (2.5 M). The pellet was redissolved in buffer A to give a final concentration between 10 to 20 mg/mL of protein. Protein concentrations were determined by UV absorbance using ε_{280} = 81,924 $M^{-1}cm^{-1}$ (calculated from the molar extinction coefficients of tryptophan and tyrosine (*99*)).

Purification of I427C/4CA, L80C/4CA, M154C/4CA, A393C/4CA, W333C/4CA, N88C/4CA, and V34C/4CA. These mutant cholesterol oxidases were prepared as described above for L274C/4CA.

Fluorophore Labeling of Cholesterol Oxidase Mutants. Acrylodan was first dissolved in acetonitrile to make a stock solution with a concentration of 10 mM. Protein (10 μM) was incubated in dark at 4 °C overnight in the presence of 100 μM acrylodan in buffer A, 10 molar equivalents of DTT (versus acrylodan) was added to react with the excess fluorophore. The mixture (50 mL) was ultrafiltered (YM30 membrane, Spectrum

Laboratories Inc., Rancho Dominguez, CA) into buffer A (50 mL), 8 times, to get a final volume of 5 mL.

Further Purification of Fluorophore Llabeled L274C/4CA. The acrylodan labeled protein was further purified on an alkyl Superose column (30 mL alkyl superose HR 10/10 column, Pharmacia Biotech, Upsala, Sweden), preequilibrated with 1.5 M $(NH_4)_2SO_4$ in buffer A. The protein was loaded on the column and eluted by running a linear gradient from 1.5 M $(NH_4)_2SO_4$ in buffer A to buffer A without $(NH_4)_2SO_4$ (100 mL). The flow rate was 0.5 mL/ min. Fractions (5 mL) were collected and the elution profile was monitored at A_{280}. Fractions were assayed for content and purity by SDS-PAGE. Fractions containing cholesterol oxidase were combined and concentrated by $(NH_4)_2SO_4$ precipitation (2.5 M) to get typically 2 mL of protein with a final concentration of 10-20 μM. The precipitate formed was pelleted by centrifugation. The pellet was redissolved in 2 mL buffer A, desalted using dialysis (NMWCO 6,000-8,000) against buffer A (2 L), 3 times. A 0.22 μm syringe filter was used to sterilize the protein solution for long-term storage.

Further Purification of I427C/4CA, L80C/4CA, M154C/4CA, A393C/4CA, W333C/4CA, N88C/4CA, and V34C/4CA. These mutant cholesterol oxidases were prepared as described above for L274C/4CA.

Activity Assay of Wild-type and Variant Cholesterol Oxidases. The activities of mutant cholesterol oxidases were measured by following the appearance of conjugated enone as a function of time at 240 nm (ε_{240} = 12 100 M^{-1} cm^{-1} (*100*)). When cholesterol was used as a substrate, it was added as a propan-2-ol solution to buffer C at 37 °C. When propan-2-ol was used, the final assay mixtures were 2% propan-2-ol. Independent sets of data were fit to hyperbolic form of the Michaelis-Menten equation using KaleidaGraph

(Synergy Software, Reading, PA).

III. Results and Discussion

Preparation of Cholesterol Oxidase Mutants. Point mutations were prepared by PCR cassette mutagenesis. The mutant cholesterol oxidases were heterologously expressed in *E. coli.* The purity of each mutant was confirmed by SDS-PAGE analysis (Figure 2.5) and by UV/Vis spectroscopy (Figure 2.6) (UV spectra from 4 cysteine mutants were shown, these mutants were the major ones used in the fluorescence quenching measurements, which is described in a later chapter.). The yield was improved by using a T7 promoter in pET 20b vector, instead of a Tac promoter in a pUC19 vector. However, compared to wild-type cholesterol oxidase, the protein yield was severely impaired by the mutation of 4 cysteines to alanines. Typically, 1-5 mg pure protein was obtained per liter of culture.

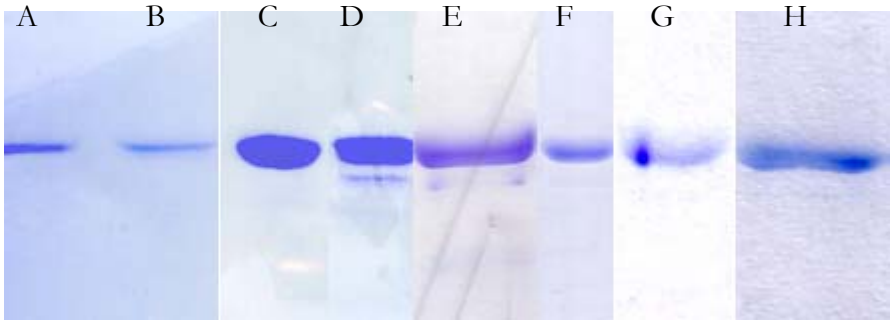

Figure 2.5. SDS-PAGE gel for A), Wild-type CO; B), L274C/4CA-Ad; C), L80C/4CA-Ad; D), I427C/4CA-Ad; E), M154C/4CA-Ad; F), N88C/4CA-Ad; G), A393C/4CA-Ad; H), W333C/4CA-Ad.

Fluorescence Labeling of Cholesterol Oxidase Mutants. Separating the labeled protein from free label is essential for the later fluorescence measurements. The purity of the acrylodan-labeled mutants was confirmed by SDS-PAGE analysis. Stoichiometry of labeling for each cysteine mutant was estimated from a comparison of acrylodan concentration (by absorption at 391 nm, extinction coeffient 19,200 $cm^{-1}M^{-1}$ (*101*)) and

protein concentration (by absorption at 280 nm, extinction coefficient 81924 $cm^{-1}M^{-1}$, calculated from the molar absorptivities of tryptophan and tyrosine (*102*)). Absorption at 391 nm from acrylodan is obtained by subtracting absorption at 391 nm of the FAD cofactor from total absorption at 391 nm, absorption at 391 nm from FAD was calculated using the ratio of A_{280}/A_{391} of *Streptomyces* cholesterol oxidase, which is 11.1 (*89*). The labeling efficiencies of the cysteine mutants were obtained ranged from 30 to 43% indicating the newly introduced cysteine residues were labeled as expected. However, problems were encountered with W333C/4CA (5% labeling efficiency) and M154C/4CA (8% labeling efficiency). The low labeling efficiency could be ascribed to the fact that the hydrophobic residues are not exposed to the solution completely.

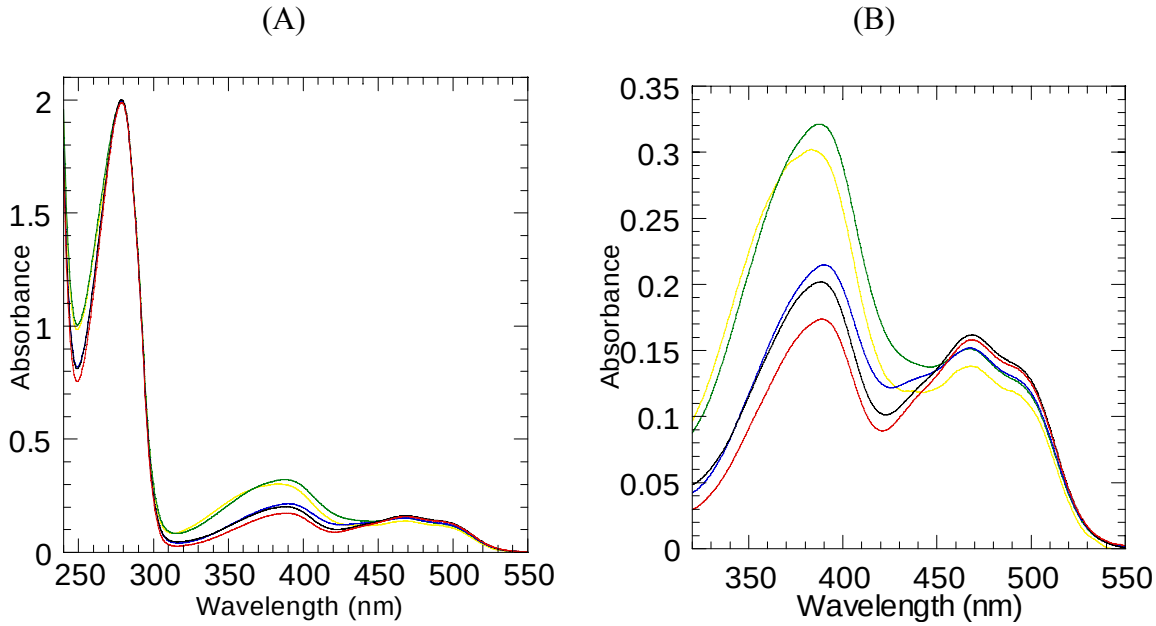

Figure 2.6. UV spectra of 24 μM wild type (—), L274C/4CA-Ad (—), W333 C/4CA-Ad (—), L80 C/4CA-Ad (—), and M154 C/4CA-Ad (—) in sodium phosphate buffer, pH 7.0. Spectra were normalized at 280 nm. (A), Spectra from 240 nm to 550 nm; (B), Closeup of FAD region, from 320 nm to 550 nm.

Structural and functional analysis. The UV spectra of the bound FAD cofactors of the labeled mutant cholesterol oxidases have λ_{max}s identical to wild type at 391 and 468 nm (Figure 2.6). To confirm the folding and functional properties of all mutants, the intrinsic Trp fluorescence and steady state enzyme kinetics were determined (Table 2.2). A Trp λ_{em}(max) value near 329 nm for wild-type cholesterol oxidase indicates properly folded protein. Trp λ_{em}(max) value of acrylodan-labeled mutant cholesterol oxidases range from 325 nm to 329 nm, suggesting that the newly incorporated cysteine residues did not affect the structural integrity of the enzyme. Activity assays of all mutants showed that the purified fluorophore-labeled mutants retained wild-type activity. Structural and functional

analysis of the acrylodan-labeled cholesterol oxidase mutants demonstrated that these mutants fold properly and have catalytic activities similar to wild-type cholesterol oxidase, which allowed the next step to study the orientation of the enzyme on the membrane.

Table 2.2 Michaelis-Menten constants for wild-type and mutant cholesterol oxidases [a]

	k_{cat} (S^{-1})	K_m (μM)	k_{cat}/K_m ($M^{-1}S^{-1}$)	λ_{max} Trp (nm)[b]
Wild-type	44 ± 2	4.8 ± 0.8	9.2×10^6	329
L274C/4CA-Ad	16 ± 0.6	4.6 ± 0.8	3.5×10^6	329
L80C/4CA-Ad	64 ± 3	11 ± 1	5.8×10^6	325
W333C/4CA-Ad	41 ± 3	5.5 ± 1	7.4×10^6	325
M154C/4CA-Ad	18 ± 1	4.5 ± 2	4.0×10^6	329
A393C/4CA-Ad	36 ± 4	4.6 ± 2	7.8×10^6	328
N88C/4CA-Ad	30 ± 4	18 ± 6	1.7×10^6	327
I427C/4CA-Ad	41 ± 4	7.0 ± 3	5.9×10^6	327

[a] Assays conducted in 50 mM sodium phosphate, pH7.0, 0.025% Triton-X-100, 2% propan-2-ol at 37 °C. [b] Excitation wavelength was 280 nm, protein was in PBS buffer (138 mM NaCl, 2.67 mM potassium chloride, 10.0 mM sodium phosphate, pH 7.4).

CHAPTER 3 The Orientation of Cholesterol Oxidase on Model Membranes Using Fluorescence Spectrometry-based Approach

I. Introduction

Membranes are essential because they separate the cell from the outside world. Compartments inside the cell are also separated by membranes to protect important processes and events. Many fundamental cellular processes occur on a cell membrane. Cell membranes are semi-permeable, composed of a variety of biological molecules, primarily proteins and lipids (Figure 3.1). Protein to lipid ratios in membranes vary depending on membrane function. The lipid bilayer is the structural foundation of the plasma membrane. The lipid fraction of the complex mixture varies according to the membrane source. The lipid is amphipathic with a hydrophilic head and a hydrophobic tail(s). The two layers of lipids are positioned such that their polar groups face toward the aqueous environment and their hydrophobic carbon tails face toward the interior of the membrane (*103*).

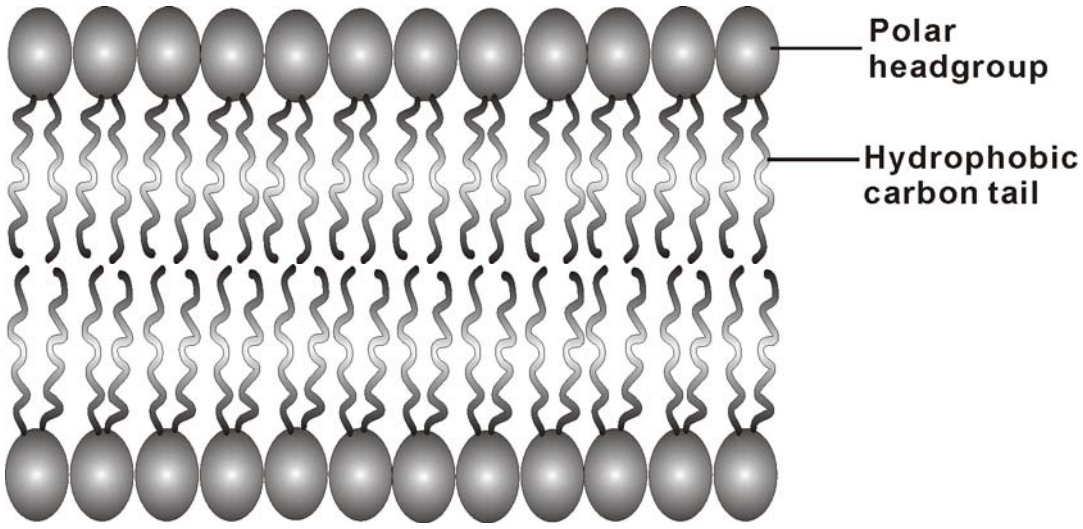

Figure 3.1. Schematic of lipid bilayer architecture. This figure was made with CorelDRAW.

The most abundant lipids in all cell membranes are phospholipids with a phosphodiester head group and two fatty acid hydrocarbon tails. Membrane structure is maintained mainly by phosphatidylcholine (PC), phosphatidylserine (PS), phosphatidylethanolamine (PE), sphingomyelin (SM) and cholesterol, the four types of phospholipids are different in their head group structure and charge (Figure 3.2) (*103*).

In mammalian cells, cholesterol is normally found dispersed in varying degrees throughout cell membranes. Its polar 3-OH group points toward the head groups of the phospholipids and orients the steroid ring and hydrocarbon tail to associate with the fatty acid carbon chains (Figure 3.3). Cholesterol molecules affect membrane fluidity in two ways (*104, 105*). At low concentrations of cholesterol, the rigidity of the planar steroid ring of cholesterol prevents the highly flexible movement of the lipid carbon tail, reducing membrane fluidity; while at high concentrations of cholesterol, it prevents tight packing between lipid chains, making the membrane plastic (*105*). Cholesterol alters other membrane biological properties, including membrane permeability (*106*), and regulating function of membrane proteins (*107*).

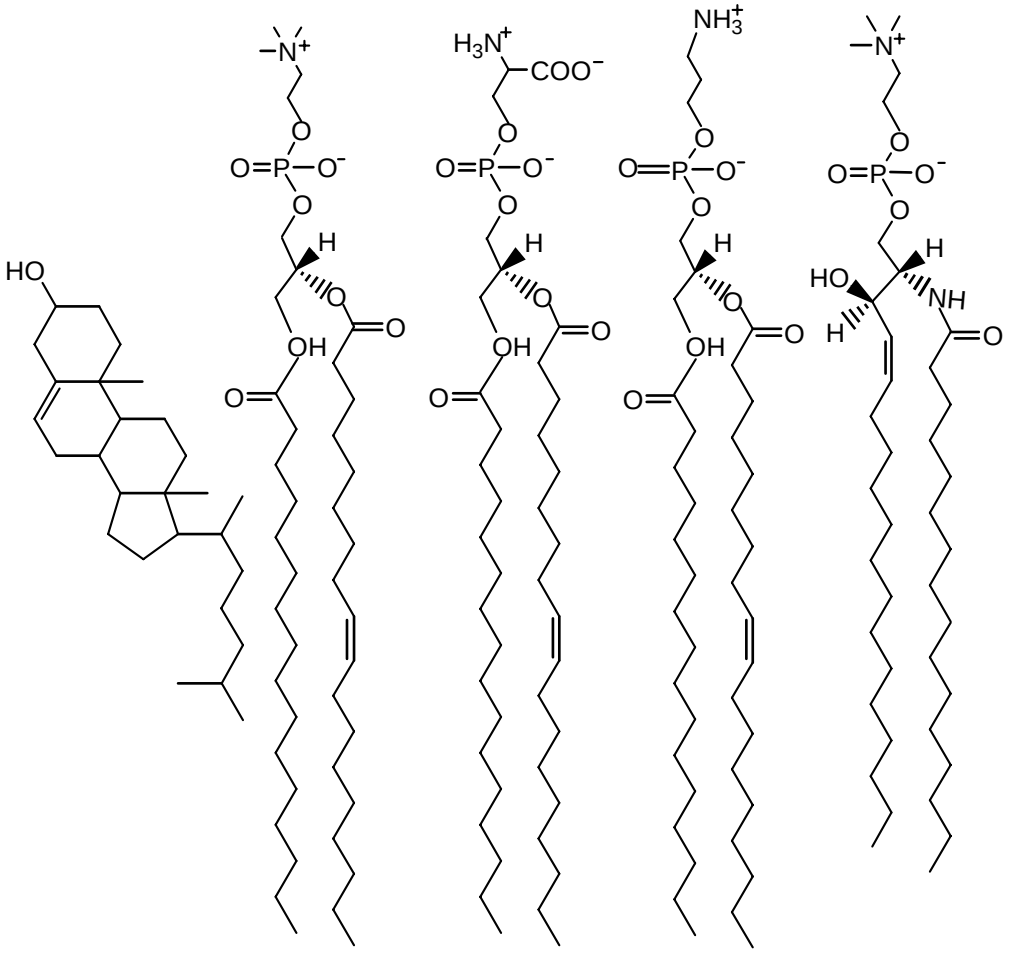

Figure 3.2. Structures of four phospholipids abundant in mammalian cells and cholesterol. The same fatty acid chains are shown for simplicity. In lipid bilayers the cholesterol molecule is in the same orientation as phospholipids, the polar group is positioned toward the head groups of the phospholipids and the hydrophobic part, including the steroid ring and hydrocarbon tail, is associated with the fatty acid chains.

Besides cholesterol molecules in the lipid bilayer, membrane fluidity can be influenced by the length and the level of unsaturation in the fatty acid carbon tail. Shorter hydrocarbon tails increase the fluidity of the membrane. Fatty acid double bonds, generally with the *cis* configuration, put a rigid 30 degree bend in the hydrocarbon chain of unsaturated lipids that interferes with their efficient packing to fill the space, resulting in a decrease in lipid melting point. This effect has important consequences for membrane properties, as well as membrane protein functions (*103*).

The cell membrane plays host to many proteins, which can be identified as integral membrane proteins, and peripheral membrane proteins. Integral membrane proteins, such as Na^+-K^+ ATPase and hormone receptors, are permanently attached to the lipid bilayer. They are both structurally and functionally an integral component of a membrane. Because the transmembrane domains of integral membrane proteins penetrate the hydrophobic regions of the lipids, these proteins can only be removed from the membrane using detergent to disrupt the hydrophobic interactions of the membrane. Peripheral membrane proteins only adhere temporarily to the cell membrane, and usually attach to integral membrane proteins, or penetrate the peripheral regions of the lipid bilayer. Examples include the regulatory protein subunits of many ion channels and transmembrane receptors. Membrane proteins play diverse roles, such as receptors in signal transduction pathways, transporters in membrane trafficking, enzymes catalyzing many membrane-associated reactions, and structural linkers mediating specific interactions among integral membrane proteins, cytoskeletal proteins and contractile proteins (*103*).

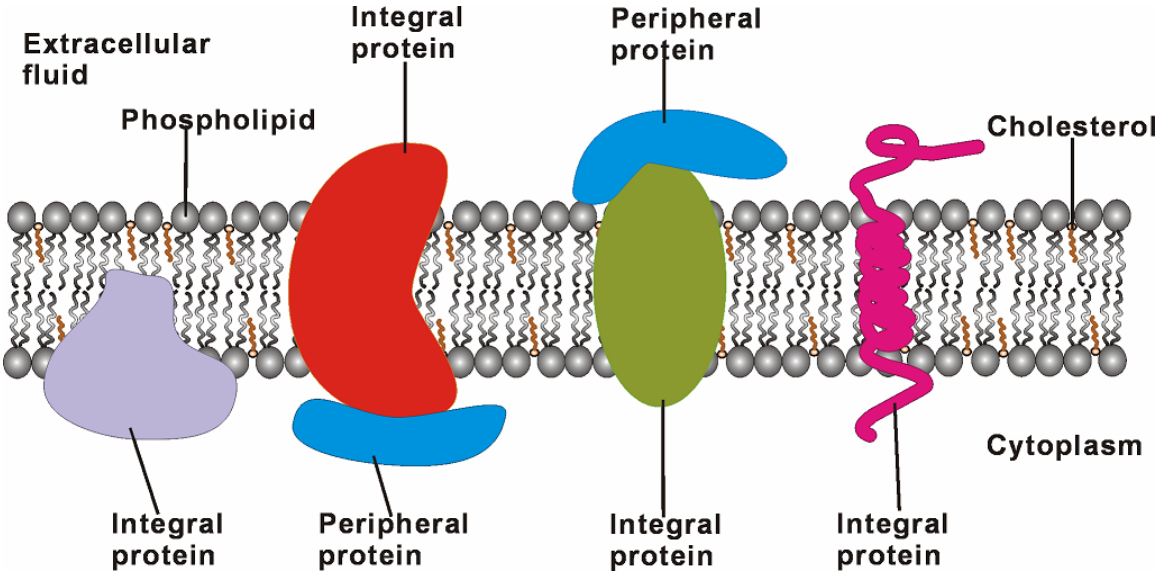

Figure 3.3 Schematic diagram of a cell membrane. Integral proteins are embedded in phospholipid bilayers containing cholesterol, with transmembrane domain(s) or attached via lipid modification. Peripheral proteins are attached noncovalently to the integral protein, generally loosely associated with the membrane. This figure was made with CorelDRAW.

Peripheral membrane proteins are only loosely associated with a membrane and the association of the protein with a lipid bilayer may involve significant conformational changes (*108*). The specific lipid composition of the membrane with which many peripheral proteins are associated affects the membrane binding affinities of these proteins (*109*). Proteins bind to membranes through hydrophobic interactions (*110*), covalent bonds(*111*), and electrostatic or ionic interactions (Figure 3.4) (*28, 112*). Peripheral membrane proteins are involved in the metabolism of different membrane components, such as lipids (phospholipases and cholesterol oxidases), cell wall oligosaccharides, or proteins.

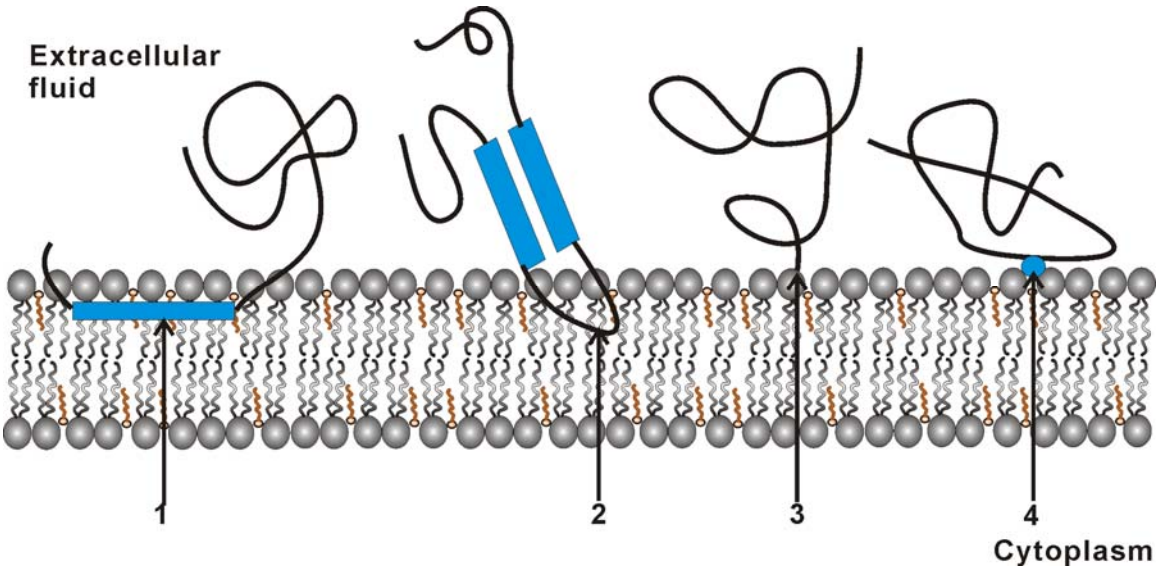

Figure 3.4. Schematic representation of the different types of interactions between peripheral membrane proteins and lipid bilayers: 1. Interaction with an α-helix parallel to the membrane plane; 2. Interaction with a hydrophobic protein loop; 3. Interaction with a covalent bond between the protein and the membrane lipid; 4. Electrostatic or ionic interactions with the lipid bilayer, e.g. via a calcium ion. This figure was adapted from http://en.wikipedia.org/wiki/Peripheral_protein, and was made with CorelDRAW.

For membrane-associated enzymes that access substrate from either a monolayer or a bilayer, understanding the biophysical steps involved in interfacial recognition and association is essential. However, knowledge regarding these steps remain relatively poorly understood (*5*). The enzyme phospholipase A2 (PLA_2) is considered a well studied interfacial enzyme (Figure 3.5). Knowledge gained from studies of this enzyme can be applied toward investigation of other interfacial enzyme mechanisms.

PLA2s are water soluble proteins with phospholipid substrates. They are found both in intracellular and secreted forms. The members of the secreted PLA_2 ($sPLA_2$) family are small (~14 kDa) disulfide-rich proteins, catalyzing the Ca^{2+}-dependent hydrolysis of fatty acid esters at the *sn*-2 position of 1,2-diacyl or 1-alkyl-2-acyl-glycero-sn-3-phospholipids (Scheme 3.1). Considerable attention has been focused on the structural and functional characterization of the surface of $sPLA_2$s that contact the phospholipid interface (*113-118*).

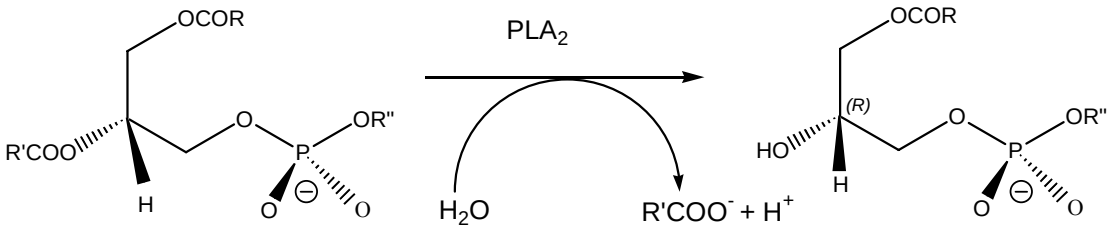

Scheme 3.1. The reaction catalyzed by phospholipase A_2.

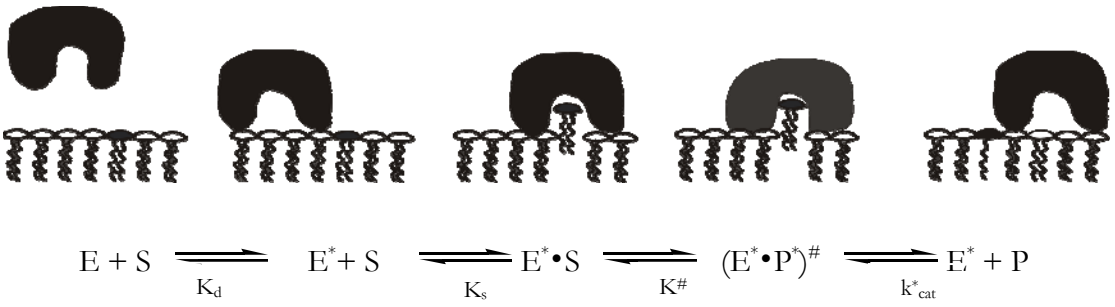

Figure 3.5. Interfacial catalysis by phospholipase A_2. This figure was adapted from Winget, Pan and Bahnson (*5*), and made with CorelDRAW. Key features of catalysis of PLA2. E represents free enzyme in the aqueous state and E* denotes the enzyme bound to the interface. E*·S is the enzyme-substrate complex of the interface bound form. (E*·P*)# stands for an additional anion activation step. PLA2 catalyzes the formation of the enzyme-product complex once activated on the interface. After releasing the product, the enzyme can diffuse to bind the substrate and continue the processive turnover for multiple cycles.

Examination of the X-ray crystal structures of different $sPLA_2$s revealed highly conserved catalytic sites, located on an external flat face, which is believed to be the interfacial binding surface, *i*-face (*119, 120*). This planar face of the enzyme consists of ~20 amino acids, the surface area of which is about 1500 $Å^2$ (*121*). The *i*-faces of $sPLA_2$s contain a ring of hydrophobic residues surrounding the opening to the catalytic site, and two or more cationic arginine or lysine residues (*122*). Quantification of interfacial binding indicates that $sPLA_2$s typically bind much tighter to vesicles of anionic phospholipids than to zwitterionic phosphatidylcholine vesicles (*122*). A positive electrostatic potential on the *i*-face resulting from the basic residues might explain the high affinity of these enzymes for anionic lipids (*122*). Besides the contribution of electrostatic effects to interfacial binding,

aromatic residues, particularly tryptophan, have been recently postulated to contribute to interfacial binding for some PLA_2 family members, which bind well to zwitterionic surfaces, e.g. cobra venom sGIA PLA_2s (*122-125*). On the *i*-faces of these enzymes, one or more tryptophans are present. Because the hydrophobic catalytic site of the enzyme is functionally and physically distinct from the *i*-face, it was proposed that PLA_2s protect the hydrophobic regions of the substrate from the bulk solvent, allowing the phospholipids to transfer from their aggregates into the active site (*126, 127*).

Cholesterol oxidase is a water soluble interfacial enzyme with a membrane-bound substrate and it is thought to follow an interfacial catalysis mechanism like the phospholipases. However, the substrate of this enzyme, cholesterol, is a neutral, hydrophobic molecule. It resides in the hydrophobic part of the lipid bilayer or micelle. Crystal structures of cholesterol oxidases reveal a deeply buried hydrophobic active site. Conformational changes are required to shield the hydrophobic region from the aqueous environment in the free enzyme state, and to facilitate the transfer of cholesterol from the membrane to the active site (*81, 82*).

Previous membrane binding studies using a site-specifically fluorophore labeled type I *R. equi.* cholesterol oxidase showed direct evidence of membrane insertion via a protein loop, suggesting that the protein sits on the surface of the lipid bilayer (*27*). The studies also suggested that protein-membrane interactions are not affected by ionic strength, and are primarily driven by hydrophobic effects. Therefore, the surface of the enzyme containing this loop, composed of hydrophobic residues, could be the potential *i*-face. The goal of my work described in this chapter is to map out the *i*-face, obtaining more structural information about the interactions between the protein and the membrane. The knowledge

gained will be very important for cholesterol oxidase as a molecular probe for characterizing cell membrane structure, especially determining the existence of lipid rafts.

Fluorescence spectroscopic approaches were employed and performed on the fluorophore-labeled cysteine cholesterol oxidase mutants described in chapter 2. To measure only the $E\text{-}E^*$ step, conditions that prevent oxidation and isomerization of cholesterol were used, including the use of synthetic phospholipids with the absence of cholesterol, and the use of temperatures below physiological temperature for the enzyme.

II. Materials and Methods

Materials. Cholesterol was purchased from Sigma Chemical Co. (St. Louis, MO). Lipids were purchased from Avanti Polar Lipids (Alabaster, AL). Unless otherwise specified, all chemicals, solvents and other materials, were supplied by Fisher Scientific (Pittsburgh, PA). Water for assays and chromatography was distilled, followed by passage through a Barnstead NANOpure filtration system (Barnstead International, Dubuque, IA) to give a resistivity better than 18 M .

General Methods. Unless otherwise noted, fluorescence measurements were taken on a PTI Spectrofluorimeter (Photon Technology International, Lawrenceceville, NJ). The buffers used were A: 50 mM sodium phosphate, pH 7.0; B: 138 mM NaCl, 2.67 mM potassium chloride, 10.0 mM sodium phosphate, pH 7.4.

Synthesis of Lipid Vesicles. 100-nm unilamellar vesicles were made from mixtures of lipids by extrusion (*128*). Lipids (18 μmol) were mixed as $CHCl_3$ solutions in a round-bottomed flask, dried as a thin film under reduced pressure in a rotary evaporator, and evacuated under high vacuum for 2 h. The lipids were resuspended in 6 mL buffer A with vortexing. Five freeze-thaw cycles, at -80 °C and 37 °C, followed by 10 extrusion cycles through two stacked 100-nm filters (Whatman, Newton, MA) using a nitrogen gas pressure of 350-400 psi, provided a homogeneous batch of vesicles.

Activity assay of cholesterol oxidase with vesicles. The activity of wild-type and mutant ChoA was measured by following the appearance of conjugated enone at 240 nm (ε_{240} = 12 100 M^{-1} cm^{-1} (*100*)). Cholesterol was added as a lipid mixture of DOPC:Chol (X_{Chol}=0.5). 2-3 nM of the enzyme was added and the absorbance at 240 nm corresponding to the first 10% of total cholesterol conversion was measured as a function of time. The

assays were conducted in buffer B at 31 °C. Independent sets of data were fit simultaneously to a binding isotherm using Kaleidagraph:

$$V_i=(V_i^{sat}*[L])/(K_{app}+[L]) \quad \text{(Eq.1)}$$

V_i, initial rate; V_i^{sat}, V_i when cholesterol oxidase binding to the vesicle is saturated; K_{app}, apparent K_d for coupled equilibrium of binding of the enzyme to vesicles and of binding substrate to the enzyme; [L], monomeric lipid concentration that is proportional to the number of vesicles added.

Steady-State Spectra of Intrinsic Trp and Conjugated Acrylodan Fluorescence. Unless otherwise stated, a 0.5-1.0 μM protein sample in buffer B was used for all measurements. Measurements were made in a semi-micro cuvette. Tryptophan was excited at 280 nm, and the spectrum was acquired from 320 to 450 nm; acrylodan was excited at 360 nm, and the spectrum was acquired from 420 to 600 nm. The excitation and emission slit widths used were 8.0 nm and 8.0 nm, respectively. Corrections were made for the appropriate blank, sample signals were corrected for light fluctuations by simultaneously monitoring the exciting light on a reference photomultiplier. The fluorescence emission maximum ($\lambda_{em,max}$) values were determined from the first derivative of the smoothed spectra.

Steady State Fluorescence Binding Measurements. Binding of cholesterol oxidase to vesicles was assayed through the change in tryptophan fluorescence. All binding assays were conducted in buffer B at 31 °C. The cuvettes were washed with nitric acid before each assay. For intrinsic tryptophan fluorescence studies, 320-nm and 410-nm cut-on filters were placed before the emission monochromator to eliminate any contribution from scattered light. The binding assay was performed on both ePC and a mixture of SM[1] and cholesterol

with a mole ratio of 7:3, respectively. Protein (0.5– 1.0μM) was titrated with increasing amounts of lipid vesicles (0-200 μL of a 3 mM stock solution) to a final concentration of 500 μM. Emission was corrected for dilution and any background signal by performing a titration in the absence of protein. Each of the assays was repeated for at least 2 times. The integrated fluorescence was fitted to Eq. 2 using KaleidaGraph software:

$$\Delta F = (\Delta F_{max}[L])/([L] + K_D) \quad \text{(Eq.2)}$$

[L], monomeric lipid concentration; K_D, dissociation constant; ΔF, change in fluorescence intensity; ΔF_{max}, maximum change in fluorescence intensity.

Fluorescence Quenching Measurements. Fluorescence quenching data for acrylodan-labeled cholesterol oxidase in the membrane-bound state was analyzed by using nitroxide spin-labeled quenchers. The fluorescence emission intensity for acrylodan at its λ_{em}(max), 534 nm for L274C/4CA-Ad, 521 nm for L80C/4CA-Ad, 520 nm for W333C/4CA-AD and 525 nm for M154C/4CA-Ad, upon excitation at 360 nm in the presence of the quencher (tempo-PC, 5-doxyl-PC, or 10-doxyl-PC) in the lipid membrane was compared with the fluorescence emission intensity in the absence of the quencher in lipid bilayers. The quenching ratio ($Q=F/F_0$) is corrected for unbound enzyme.

$$F/F_0=[F_{(E+L)}-F_E(100\%-\%bound)]/[F_{(E+Q)}-F_E(100\%-\%bound)] \quad \text{(Eq. 3)}$$

F, corrected fluorescence in the presence of quencher in the membrane; F_0, corrected fluorescence in the absence of quencher in the membrane; $F_{(E+L)}$, fluorescence in the absence of quencher in the membrane; F_E, fluorescence of the unbound enzyme; $F_{(E+Q)}$, fluorescence in the presence of quencher in the membrane.

Parallax Method of Depth-Dependent Fluorescence Quenching. Fluorescence quench data for acrylodan-labeled cholesterol oxidase in the membrane-bound state was

analyzed according to Chattopadhyay and London(*25*). The quenching ratio for conjugated acrylodan obtained from fluorescence quenching measurement in the presence of the shallow quencher (tempo-PC or 5-doxyl-PC) was compared with the fluorescence intensity in the presence of the more deeply located quencher (5-doxyl-PC or 12-doxyl-PC). At a fixed lipid concentration, the calculated quenching ratio for each quencher was used for F_1 and F_2. The data were analyzed according to the following equations:

$$Z_{IF}=[(1/(-\pi C))\ln(F_1/F_2)-L^2_{21}]/2L_{21} \quad \text{(Eq. 4)}$$

$$Z_{IF} = Z_{IF} + L_{C1} \quad \text{(Eq. 5)}$$

where Z_{1F} is the distance from the fluorophore to the shallow quencher, C is the concentration of quencher within the bilayer, F_1 is the calculated quenching ratio in the presence of the shallow quencher, F_2 is quenching ratio in the presence of the deep quencher, L_{21} is the distance from shallow to deep quencher, L_{C1} is the distance from the center of the bilayer to the shallow quencher, L_{C2} is the distance from the center of the bilayer to the deep quencher, and Z_{CF} is the distance from the center of the bilayer to the fluorophore. F_1 and F_2 values are the average values of at least two independent experiments.

III. Results and Discussion

Part I. Investigation of the orientation of cholesterol oxidase on model membranes in the absence of cholesterol.

Catalytic Activity Measurements. Catalytic activity measurements of wild-type and fluorophore-labeled mutant ChoA were carried out by following the appearance of cholest-4-en-3-one as described in chapter 2, and results indicated that fluorophore-labeled mutants retained wild type activity. In this case, cholesterol was in the form of micelles of nonionic detergent Triton X-100. In this chapter, the kinetic activity was measured at 31 °C using wild-type and fluorophore-labeled mutant ChoA, and cholesterol was added as medium-sized, unilamellar phospholipid vesicles (MUV) with a cholesterol mole fraction of 0.5. Activity assays of all mutants showed that they retained wild-type activity, confirming that the covalently attached fluorophore and mutated amino acids did not interfere with the catalytic activity of the enzyme upon binding to 100 nm vesicles (Table 3.1).

Table 3.1. Kinetic constants for wild-type and mutant cholesterol oxidases with 100 nm vesicles[a]

	V_i^{sat}/[E] (s^{-1})	K_{app} (μM)
WT ChoA	21 ± 1	24 ± 5
L274C/4CA-Ad	35 ± 2	31 ± 1
L80C/4CA-Ad	26 ± 1	8.9 ± 1
W333C/4CA-Ad	16 ± 1	29 ± 5
M154C/4CA-Ad	26 ± 1	38 ± 6

[a] Assays were conducted in 138 mM NaCl, 2.67 mM potassium chloride, 10.0 mM sodium phosphate, pH 7.4, 31 °C. DOPC:Chol (X_{Chol}=0.5) was used.

Membrane Binding Affinity Measurements. Except W333C/4CA-Ad, the change in wild-type and mutant cholesterol oxidase intrinsic tryptophan fluorescence emission intensity upon binding to medium-sized, unilamellar lipid vesicles was measured and fit to a binding isotherm (Table 3.2, Table 3.3). For W333C/4CA-Ad, the covalently attached acrylodan was used as a reporter to measure the dissociation constant. There are 10 intrinsic Trp in wild-type ChoA that could potentially contribute to the change of fluorescence intensity upon binding to the membrane, due to a change in their surroundings. Both conformational change of the protein when it binds to the lipid and possible membrane contact of some of Trp could cause the change in their surroundings. Two types of lipids were employed, ePC and DOPC, and emission spectra were acquired at 31 °C. ePC and DOPC are in a liquid-disordered phase (*129-131*) at 31 °C.

The quantum yield of tryptophan and acrylodan fluorescence generally decreased

upon binding to the lipid. There was only a 10-20% decrease in Trp fluorescence intensity when the enzyme is fully in a membrane-bound form compared to the fluorescence intensity of free enzyme was detected, suggesting that the enzyme does not embed into the membrane deeply, and may only loosely associate with the lipid bilayer. Membrane binding affinity of W333C/4CA-Ad using intrinsic Trp fluorescence as the reporter could not be determined because tryptophan fluorescence emission intensity upon binding to lipid vesicles could not be fit to a binding isotherm. Such difficulties with the determination of the dissociation constant of W333C/4CA-Ad using intrinsic Trp fluorescence suggest that Trp 333 might be one of the main reporters upon binding to the lipid. However, the quenching measurements and λ_{em}(max) measurement as described later indicate that this residue is not in membrane contact. Therefore, Trp 333 may detect a conformational change of the protein upon binding to the lipid, and reflect this effect on its fluorescence, thus contributing as a main reporter.

Table 3.2. Dissociation constants for binding of mutant ChoA to 100 nm vesicles.[a]

	K_d (μM)	
ChoA mutants	ePC	DOPC
WT ChoA	9.8 ± 1	19 ± 4
L274C/4CA-Ad	11 ± 2	17 ± 5
L80C/4CA-Ad	4.2 ± 1	14 ± 3
W333C/4CA-Ad	7.0 ± 1	18 ± 3
M154C/4CA-Ad	8.9 ± 2	22 ± 8

[a]Binding assays were performed in 138 mM NaCl, 2.67 mM potassium chloride, 10.0 mM sodium phosphate, pH 7.4, 31 °C.

Acrylodan Fluorescence Emission Spectra. The fluorescence of the 6-acyl-2-dimethylaminonaphthalene moiety is extremely sensitive to the polarity of its surrounding environment (*132*). The quantum yield of acrylodan is markedly enhanced after it reacts with thiols, and as expected, this thiol adduct is very sensitive to dipolar perturbation from its surroundings (*133*). Compared to the λ_{em}(max) of an acrylodan-mercaptoethanol adduct in water, which is 540 nm (*133*), all of the mutant acrylodan λ_{em}(max) values were less than 540 nm, confirming that conjugation of the fluorophore with targeted residues had occurred (Figure 3.6, Table 3.1).

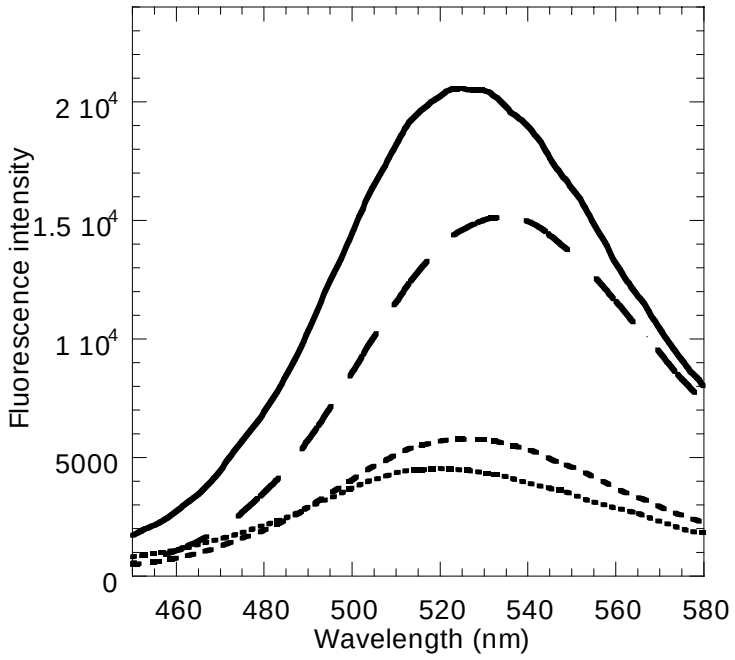

Figure 3.6. Acrylodan fluorescence emission spectra of 100 nM acrylodan-labeled cholesterol oxidase mutants, (⋯⋯) 0.20 μM W333C/4CA-Ad, (──) 0.41μM L80C/4CA-Ad, (─ ─) 0.19 μM L274C/4CA-Ad, and (─ ─ ─) 0.25 μM M154C/4CA-Ad. Spectra were acquired in 138 mM NaCl, 2.67 mM potassium chloride, 10.0 mM sodium phosphate, pH 7.4. The excitation wavelength was 360 nm.

Acrylodan λ_{em}(max) values were measured upon binding to the lipid to determine if the selected residue could detect a change in polarity of its surrounding environment. No obvious change in λ_{em}(max) values was observed upon binding to lipids, indicating that upon binding to the membrane, the environment around the acrylodan-labeled residues does not change (Table 3.3). However, these results can not exclude the possibility of a shallow membrane contact, e.g., the polar headgroup of the lipid bilayer. Further studies needed to be pursued to know if there is any shallow membrane contact. Measurement of fluorescence quenching between a conjugated fluorophore and a quencher within the lipid

is an effective way to address this question, especially using a tempo PC, whose quencher group is attached on the headgroup of the lipid.

Table 3.3. The fluorescence emission maximum (λem(max)) of acrylodan labeled Cys mutants.[a]

	λ_{max} Ad (nm)		
Ad-labeled mutant ChoA	Vesicle free[b]	ePC	DOPC
L274C/4CA-Ad	534	534	535
L80C/4CA-Ad	524	524	525
W333C/4CA-Ad	520	521	521
M154C/4CA-Ad	525	523	525

[a]Fluorescence emission spectra were acquired in 138 mM NaCl, 2.67 mM potassium chloride, 10.0 mM sodium phosphate, pH 7.4, 31 °C. Phospholipid concentration was 272 μM. The excitation wavelength was 360 nm. Protein concentration was 0.2-0.8μM.

Fluorescence Quenching Measurements. The degree of exposure of conjugated acrylodan to the membrane as well as its depth are reflected by the overall level of quenching since nitroxide quenching is a short-range process, <30 Å (*134, 135*). At a fixed lipid concentration of 272 μM, the quenching ratios in the presence of Tempo-PC, 5-doxyl PC and 12-doxyl PC were compared. Quenching measurements were performed on these fluorophore-labeled ChoA mutants using lipids in the absence of cholesterol at 31 °C to measure only the E-E* step.

The initial fluorescence quenching measurements were performed with the lipid containing 10 mole percent of quencher. The surface area per lipid molecule is 60-70 Å^2*(136)*.

The foot print of the enzyme on the membrane is predicted to be about 1200 $Å^2$. That is, one protein molecule could cover approximately 20 lipid molecules, two of which are quenchers. To increase the probability of a fluorophore covalently attached to the enzyme being located within a short range of the quencher dispersed in the lipid, 30 mole percent of quencher was used in the measurements using ePC to see if quenching observed with a ChoA mutant would increase as the mole percent of quencher increases. Basically, no difference in fluorescence quenching was observed between lipids containing 10 and 30 mole percent quencher. Because the incorporation of quenchers in the lipid may alter membrane structure, the mole percent of quencher should be low. For DOPC, only 10% mole quencher was used. With ePC and DOPC, the amounts of fluorescence quenching by spin-labeled quenchers in the absence of the substrate, so that the membrane were in an l_d phase, were determined. The results are summarized in Table 3.4.

Table 3.4. Fluorescence Quenching Ratio[a] of Acrylodan in Cholesterol Oxidase Mutants.

ChoA mutants	Quenchers	ePC	DOPC
L80C/4CA-Ad	Tempo PC	0.96 ± 0.01	0.96 ± 0.01
	5-doxyl PC	0.97 ± 0.01	0.97 ± 0.01
	12-doxyl PC	0.98 ± 0.02	0.98 ± 0.01
L274C/4CA-Ad	Tempo PC	0.99 ± 0.01	0.91 ± 0.01
	5-doxyl PC	1.00 ± 0.01	0.98 ± 0.01
	12-doxyl PC	1.05 ± 0.01	0.99 ± 0.01
W333C/4CA-Ad	Tempo PC	0.99 ± 0.02	0.97 ± 0.01
	5-doxyl PC	0.97 ± 0.04	0.98 ± 0.01
	12-doxyl PC	0.98 ± 0.01	0.99 ± 0.01
M154C/4CA-Ad	Tempo PC	1.01 ± 0.02	0.99 ± 0.01
	5-doxyl PC	0.98 ± 0.02	0.97 ± 0.03
	12-doxyl PC	0.97 ± 0.01	0.97 ± 0.02

[a]The quenching ratio F/F_0 is corrected for unbound enzyme, lipid concentration was 272 μM. $F/F_0 = [F_{(E+L)} - F_E(100\text{-}\%bound)]/[F_{(E+Q)} - F_E(100\text{-}\%bound)]$. F, corrected fluorescence with the presence of quencher in the membrane; F_0, corrected fluorescence with the absence of quencher in the membrane; $F_{(E+L)}$, fluorescence with the absence of quencher in the membrane; F_E, fluorescence of the enzyme without lipids; $F_{(E+Q)}$, fluorescence in the presence of quencher in the membrane. Quenching measurements were performed at 31 °C in 138 mM NaCl, 2.67 mM potassium chloride, 10.0 mM

sodium phosphate, pH 7.4, excitation wavelength was 360 nm. Protein concentration was 0.2-0.8μM

Binding of all the acrylodan-labeled mutants to ePC or DOPC vesicles with quencher resulted in no appreciable quenching. Acrylodan λ_{em}(max) measurements showed that no obvious change in λ_{em}(max) values was observed upon binding to lipids. As shown earlier in the emission spectra of acrylodan-labeled ChoA mutants, fluorescence of covalently conjugated acrylodan is very sensitive to the polarity of its surrounding environment. If the selected residue is in the membrane contact, a change in λ_{em}(max) value should be observed. All of these results indicate that the selected sites across the surface of the enzyme, including residues 80, 154, 274 and 333, are not in membrane contact when the enzyme binds to lipids without cholesterol.

Membrane binding affinity measurements using the intrinsic Trp as a reporter showed a dissociation constant with a value of 10-20 μM upon binding to ePC or DOPC, suggesting that the enzyme binds to the membrane without the substrate. Although we have selectively incorporated fluorophore into the sites across the surface of the enzyme, the interface of this enzyme may be small, and the selected sites are not included in the interface.

As already mentioned, residue 80 from *Rhodococcus equi* cholesterol oxidase was known to be in membrane contact, cholesterol oxidase from *Rhodococcus equi* and *Streptomyces* are nearly identical in sequence and structure. Therefore, residue 80 of *Streptomyces* cholesterol oxidase was predicted to be in membrane contact as is the corresponding residue of *Rhodococcus equi* cholesterol oxidase. Moreover, ChoA has a

much higher protein expression level than *Rhodococcus equi* cholesterol oxidase. However, a slight difference in the protein loop containing residue 80 in these two oxidases does exist, and this difference now seems critical. Since results described earlier suggested that residue 80 of ChoA in not in membrane contact, to map out the interface of cholesterol oxidase upon binding to the membrane in the absence of cholesterol using current available structural information of *Rhodococcus equi* cholesterol oxidase, same strategy performed on ChoA mutants should be carried out using *Rhodococcus equi* cholesterol oxidase. A library of single cysteine mutants, whose cysteine resides near residue 80, needs to be constructed. Binding measurements should be employed with these mutants one by one to determine which residue(s) is in membrane contact, thus to define *i*-face of the enzyme.

Part II. Investigation of the orientation of cholesterol oxidase on model membranes in the presence of cholesterol, under conditions that prevent the oxidation and isomerization of cholesterol.

WT ChoA and fluorophore-labeled ChoA mutant are catalytically active when cholesterol was added to vesicles, and the enzyme must first interact with the membrane to recruit a cholesterol molecule into its active site. Comparison of X-ray crystal structures of free cholesterol oxidase and the complex formed with the substrate analog revealed that a conformational change of two surface loop regions (residue 79-83, 432-438) must occur during the steroid binding event, and this conformational change was believed to provide a hydrophobic pathway for the substrate molecule to move between the membrane and the active site. Deletion mutagenesis studies suggested that loop 79-83 residues are essential for packing with the "tail" of cholesterol. Again, Chen and Sampson showed the tip of this loop of *Rhodococcus equi* cholesterol oxidase inserts into the lipid bilayer upon binding to the membrane without cholesterol. All of the facts point to the same direction that loop 79-83 is an important region during catalysis.

However, our fluorescence quenching measurements using fluorophore-labeled ChoA mutants indicate that in the absence of cholesterol, the selected sites, including residue 80 that is on the tip of this loop, are not in membrane contact upon binding to the lipid. It is possible that the enzyme binds to the lipid in the presence of the substrate through different region(s), which may include this loop; or, for ChoA, this loop inserts into the membrane only when the substrate presents in the lipid during catalysis process. It is known that cholesterol-4-en-3-one alters membrane structure. However, the effect of cholesterol-4-en-3-one on membrane structure is poorly understood. Therefore, orientation

of the enzyme on the membrane currently can not be determined under the conditions in which the enzyme is catalytically active. We made tentative efforts to investigate if the selected sites are in membrane contact using a temperature lower than the physiological temperature to prevent the formation of the product. Conditions include 20 °C and two types of lipids, ePC:Chol (X_{Chol}=0.3) and DOPC:Chol (X_{Chol}=0.3). With these lipid mixtures, the enzyme had nearly no catalytic activity at 20 °C.

Membrane binding affinity measurements were performed at 20 °C with wild-type ChoA using two types of lipids, ePC:Chol (X_{Chol}=0.3) and DOPC:Chol (X_{Chol}=0.3), respectively. Dissociation constants were measured using intrinsic tryptophan fluorescence emission intensity upon binding to the lipid. Previously Ahn and Sampson had shown that binding affinity was not temperature dependent (*65*). Similar dissociation constants were obtained for both of these two types of lipids, as well as ePC and DOPC without cholesterol as mentioned earlier (Table 3.2, Table 3.5).

Table 3.5. Dissociation constants for binding of WT ChoA to 100 nm vesicles.

	K_d (μM)	
	ePC:Chol (X_{Chol}=0.3)	DOPC:Chol (X_{Chol}=0.3)
WT ChoA	17 ± 2	11 ± 3

Binding assays were performed in 138 mM NaCl, 2.67 mM potassium chloride, 10.0 mM sodium phosphate, pH 7.4, at 20 °C. Dissociation constants were measured using intrinsic tryptophan fluorescence emission intensity upon binding to the lipid. Excitation wavelength was 280 nm.

Acrylodan λ_{em}(max) values were measured upon binding to ePC:Chol (X_{Chol}=0.3) and DOPC:Chol (X_{Chol}=0.3) at 20 °C, respectively (Table 3.6). No obvious change in λ_{em}(max) values was observed upon binding to lipids, indicating that upon binding to the membrane with the substrate at 20 °C, the environment around the acrylodan-labeled residues does not change.

Table 3.6. The fluorescence emission maximum ($\lambda_{em(max)}$) of acrylodan labeled Cys mutants.[a]

	λ_{max} Ad (nm)		
Ad-labeled mutant ChoA	Vesicle free[b]	ePC:Chol (X_{Chol}=0.3)[c]	DOPC:Chol (X_{Chol}=0.3)[c]
L274C/4CA-Ad	534	535	536
L80C/4CA-Ad	524	523	523
W333C/4CA-Ad	520	522	523
M154C/4CA-Ad	525	526	525

[a]Fluorescence emission spectra were acquired in 138 mM NaCl, 2.67 mM potassium chloride, 10.0 mM sodium phosphate, pH 7.4. Phospholipid concentration was 272 μM. The excitation wavelength was 360 nm. Spectra were recorded at 20 °C. Protein concentration was 0.2-0.8μM

At 20 °C, a mixture of POPC:Chol with X_{Chol} of 0.3 has been reported to be in a two-phase, l_o-l_d, coexistence region (*137*), and DOPC:Chol (X_{Chol}=0.3) is in the l_d phase(*129*). ePC is a mixture of several PC species, the most predominant component is 16:0–18:1 (*138*), which is the same as POPC. Due to the extra unsaturation in the carbon tails of a small fraction of phospholipids in the mixture, ePC has a higher fluidity and a lower melting temperature than POPC (*139*). The nitroxide group on the acyl chain of lipids, e.g., 5-doxyl PC and 12-doxyl PC, behaves like a double bond to prevent tight packing, and the tempo group of tempo-PC also inhibits tight packing by enlarging the

head group size of the lipid (personal communication, E. London and N. Sampson). Therefore, addition of these quenchers into ePC or DOPC will not change the lipid phase and these quenchers should disperse in the membrane evenly in these lipids, allowing the measurement of fluorescence quenching between covalently conjugated acrylodan and nitroxide spin-labeled quencher in the lipid.

With ePC:Chol (X_{Chol}=0.3) and DOPC:Chol (X_{Chol}=0.3), the amounts of fluorescence quenching by spin-labeled quenchers in the presence of the substrate at 20 °C were determined. The results are summarized in Table 3.7. For L80C/4CA using DOPC:Chol (X_{Chol}=0.3), instead of an acrylodan-labeled protein, a monobromobimane (mBBr) labeled enzyme was employed for the quenching measurements. The reason will be discussed in Part III.

Table 3.7. Fluorescence Quenching Ratio[a] of Acrylodan in Cholesterol Oxidase Mutants.

ChoA mutants	Quenchers	ePC:Chol (X_{Chol}=0.3)	DOPC:Chol (X_{Chol} =0.3)
L80C/4CA-Ad	Tempo PC	0.93 ± 0.02	1.01 ± 0.06[b]
	5-doxyl PC	0.96 ± 0.01	1.00 ± 0.01[b]
	12-doxyl PC	0.98 ± 0.01	1.00 ± 0.03[b]
L274C/4CA-Ad	Tempo PC	1.00 ± 0.01	0.94 ± 0.01
	5-doxyl PC	1.00 ± 0.01	1.00 ± 0.01
	12-doxyl PC	1.00 ± 0.02	0.98 ± 0.01
W333C/4CA-Ad	Tempo PC	0.98 ± 0.01	0.99 ± 0.01
	5-doxyl PC	0.98 ± 0.01	0.97 ± 0.01
	12-doxyl PC	0.98 ± 0.01	0.99 ± 0.03
M154C/4CA-Ad	Tempo PC	1.01 ± 0.01	0.98 ± 0.01
	5-doxyl PC	0.97 ± 0.01	0.97 ± 0.01
	12-doxyl PC	1.01 ± 0.01	0.96 ± 0.01

[a]The quenching ratio F/F_0 is corrected for unbound enzyme, lipid concentration was 272 μM. $F/F_0 = [F_{(E+L)} - F_E(100\text{-}\%bound)]/[F_{(E+Q)} - F_E(100\text{-}\%bound)]$. F, corrected fluorescence with the presence of quencher in the membrane; F_0, corrected fluorescence in the absence of quencher in the membrane; $F_{(E+L)}$, fluorescence in the absence of quencher in the membrane; F_E, fluorescence of the enzyme without lipids; $F_{(E+Q)}$, fluorescence in the presence of quencher in the membrane. Quenching measurements were performed at 20 °C, excitation wavelength was 360 nm. Protein

concentration was 0.2-0.8μM

[b]Quenching ratios were obtained using mBBr-labeled mutant cholesterol oxidase.

Binding of all the fluorophore-labeled mutants to ePC:Chol (X_{Chol}=0.3) and DOPC:Chol (X_{Chol}=0.3) with quencher resulted in no appreciable quenching (Table 3.7). Acrylodan λ_{em}(max) measurements showed that no obvious change in λ_{em}(max) values was observed upon binding to lipids (Table 3.6). Under the conditions that cholesterol oxidase has nearly no catalytic activity, residue 80, 154, 274 and 333 are not in membrane contact in the presence of cholesterol (X_{Chol}=0.3).

Part III. Is Acrylodan a Problematic Fluorophore?

When an acrylodan labeled cysteine mutant, L80C/4CA-Ad, was employed for the quenching measurements, no obvious change in acrylodan λ_{em}(max) value and fluorescence intensity was observed upon binding to DOPC:Chol (X_{Chol}=0.3). However, compared to the case of binding to this lipid in the absence of quencher, a decrease in fluorescence intensity and a blue-shift at acrylodan λ_{em}(max) upon binding to the lipid containing quenchers, including tempo PC, 5-doxyl PC and 12-doxyl PC, were observed. In the meantime, a new fluorescence peak at 440 nm appeared, which did not appear when using the lipid without quencher. When mBBr labeled L80C/4CA was employed for the same quenching measurements, no appreciable change in acrylodan λ_{em}(max) value and fluorescence quenching was observed upon binding to DOPC:Chol (X_{Chol}=0.3), indicating that the decrease in acrylodan fluorescence intensity observed using L80C/4CA-Ad was not caused by fluorescence quenching between the nitroxide group of the quencher lipid and acrylodan incorporated to residue 80.

In addition of vesicles containing cholesterol under conditions that the enzyme is catalytically active, a fluorescence peak was observed at 440 nm using L80C/4CA-Ad in the presence or in the absence of catalase, a common enzyme decomposing hydrogen peroxide. After 30 min incubation at 31 °C, fluorescence intensity at 440 nm increased less with the sample containing catalase than the one without catalase. Therefore, catalase inhibited the increase in fluorescence intensity at 440 nm, suggesting that the peak was a result of the formation of hydrogen peroxide, and acrylodan fluorescence was affected by it. However, the mechanism is not clear. When vesicles (without quencher) containing cholesterol were added, although the turnover of cholesterol catalyzed by the enzyme at 20

°C is so slow that acrylodan fluorescence was not affected by the formation of the product, the presence of quencher in the lipid may alter the membrane structure sufficiently that acrylodan was more exposed to hydrogen peroxide.

Acrylodan is extremely sensitive to the polarity of its environment, and this property makes it an excellent fluorescence probe to study protein-membrane interactions. However, the environmental sensitivity also allows it to detect nonspecific change, which makes interpretation complicated. Moreover, when acrylodan is covalently conjugated to a cysteine, the acrylodan-cysteine linker provides degrees of conformational freedom that allow the fluorophore to move up and down within the bilayer. The position of acrylodan e.g., whether the linker is an extended or kinked chain, is difficult to estimate. When the parallax method is applied to measure membrane depth using acrylodan as a fluorescence probe, this linker would limit the accuracy of the depth. Therefore, a different fluorophore needs to be considered. mBBr, a fluorophore with high water solubility, was used to label L274C/4CA, L80C/4CA and W333C/4CA. For mBBr, there will be a smaller linker problem, and because this molecule is water soluble, unreacted mBBr is easy to remove. However, compared to acrylodan, it has a lower labeling efficiency (~2 fold lower) and fluorescence intensity. The low labeling efficiency may be due to its hydrophilicity, which makes it hard to access residues on the hydrophobic surface of the protein. An ideal fluorophore is needed with the following properties: small molecule with short length, mild hydrophibicity, high fluorescence intensity when reacts with a thiol group.

IV. Conclusion and Future Work

Binding measurements were carried out under conditions that included using lipid without substrate at 31 °C and with substrate at 20 °C, in both cases there is no turnover of cholesterol. Binding of all the acrylodan-labeled mutants to ePC or DOPC vesicles with quencher at 31 °C, ePC:Chol (X_{Chol}=0.3) and DOPC:Chol (X_{Chol}=0.3) at 20 °C, resulted in no appreciable fluorescence quenching between the covalently conjugated fluorophore and the quencher within the lipid bilayer. Acrylodan λ_{em}(max) measurements showed that no obvious change in λ_{em}(max) values was observed upon binding to lipids under the above conditions. We conclude that residue 80, 154, 274 and 333 are not in membrane contact upon binding to the lipid in the absence of the substrate; under conditions in which the enzyme has nearly no activity, they are not in membrane contact upon binding to the membrane in the presence of cholesterol.

A derivative of an inactive ChoA mutant, H447E/E361Q, with incorporated cysteine across the surface of the enzyme is another way to define the interface of the enzyme under a physiological temperature with lipids containing cholesterol. Ye and Sampson showed that membrane binding affinity was not affected by these mutations (*140*). However, since H447E/E361Q is catalytically inactive, it must bind to the membrane in a different way from a catalytically active enzyme, and the possible conformational change of cholesterol oxidase upon binding to the membrane during catalysis would not occur. Moreover, to map out sites in membrane contact, the protein can only have one cysteine residue. A single cysteine mutant derived from H447E/E361Q cholesterol oxidase contains totally 7 mutated amino acids, e.g., L80C/C56A/C282A/C445A/C452A/H447E/E363Q. Protein expression levels and purification would be issues of concern, as well as structural integrity of the

protein.

A library composed of single cysteine mutants, which are derivatives of *Rhodococcus equi*. cholesterol oxidase, should be considered. Since residue 80 is known to be in membrane contact, cysteine would be considered to incorporate to positions near residue 80. Binding measurements would be employed with these mutants one by one to determine which residue(s) is in membrane contact, and thus to define *i*-face of the enzyme.

A new method using a different approach, mass spectrometry, for modeling the orientation of cholesterol oxidase on the membrane is under development as described in Chapter 4. With this method, there is no need to remove the 4 intrinsic cysteines, making plasmid construction and protein purification much easier.

CHAPTER 4 Development of a Mass Spectrometry-Based Approach for Modeling the Orientation of Cholesterol Oxidase on the Lipid Bilayer

I. Introduction

Mass spectrometry (MS) is an important and well established analytical technique, and has been used in a wide range of applications. An intrinsic property of a molecule, its mass/charge ratio, is measured by MS with high sensitivity. However, traditional ionization techniques in mass spectrometry were limited in their application to macromolecules, which are large and not easily transferred into the gas phase and ionized.

The invention of "soft-ionization" techniques, i.e., electrospray ionization (ESI) (*141*) and matrix-assisted laser desorption ionization (MALDI) (*142*), opened up applications in the biological sciences, because gentle ionization enables the analysis of biomolecules of higher molecular weight without major fragmentation. ESI ionizes the analytes out of a solution and is used for a wide range of compounds, including proteins, oligonucleotides, sugars, and polar lipids, which are sufficiently polar to carry a charge; while MALDI ionizes the analytes out of a solid, a dry, crystalline matrix and can only be applied to the analysis of peptides since the power required to ionize large proteins causes fragmentation (*143*). This chapter will be exclusively dedicated to MALDI-TOF MS analysis.

MALDI utilizes an ultraviolet-absorbing matrix that is mixed with the sample of interest. Upon laser irradiation of the UV absorbing matrix, the analyte is desorpted into the gas phase (*144*); matrix ions are formed as a result of direct laser activation (*145*), and matrix-derived ions interact with the analyte to yield analyte ions (*146*). The precise nature of the ionization process is unknown. The ions are accelerated in an electric field to a fixed velocity before entering a flight tube where they travel down in a linear or a reflecting mode. Ions of smaller mass have a higher velocity and reach the detector earlier. For the reflecting mode, an ion reflector is used to compensate for the difference in flight times of

the same m/z ions carrying slightly different kinetic energies, and the effective flight path is lengthened. Therefore a higher mass resolution can be obtained.

Currently, mass spectrometry is the key technique in proteomics (*43*). In quantitative proteome analysis, the combination of isotope coded affinity tag (ICAT) reagents and tandem mass spectrometry allows accurate quantification and identification of individual proteins in complex mixtures, and its application has expanded greatly. A new method, which is inspired by ICAT strategy, is proposed in this chapter, and preliminary results are also included.

ICAT was originally developed in the laboratory of Ruedi Aebersold (*147*). The ICAT reagents consist of three functional components (Figure 4.1). The first element is biotin, which provides an affinity tag for ICAT-labeled peptides to isolate them from complex peptide mixtures. The second is an ethylene glycol linker that can incorporate stable isotopes to allow 8 daltons difference between "heavy" and "light" tags. The third component is a reactive group with specificity toward thiol groups (cysteines).

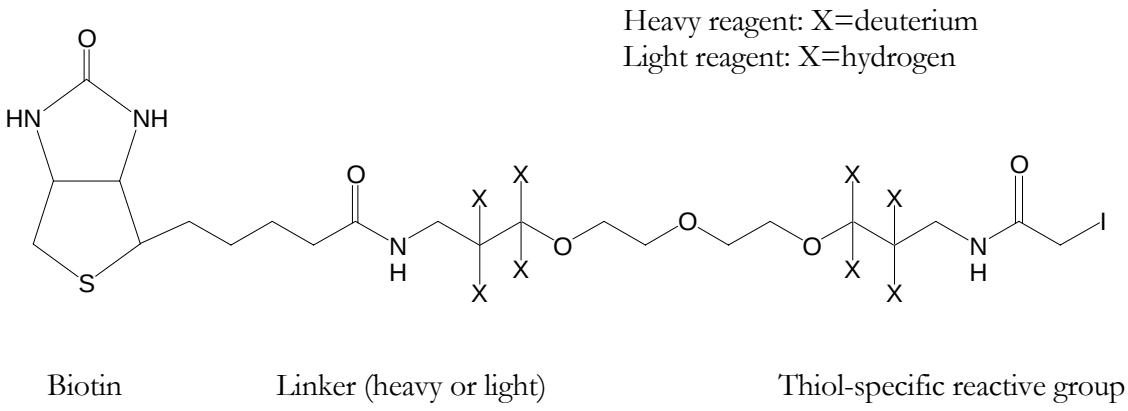

Figure 4.1. Structure of the ICAT reagent.

In the ICAT strategy, two separate protein mixtures are treated with the isotopically light and heavy ICAT reagents, and each cysteine residue in every protein covalently reacts with an ICAT reagent. The protein mixtures are combined and enzymatically digested to peptides, and the biotin tag is utilized to isolated ICAT-labeled peptides by avidin affinity chromatography. The isolated peptides are separated and analyzed by microcapillary high-performance liquid chromatograghy and tandem mass spectrometry. The ratio of the pair of ICAT-labeled peptides is used to determine the relative quantity of each peptide, and identification of the protein is achieved by computer searching the recorded sequence information against a protein database (Figure 4.2).

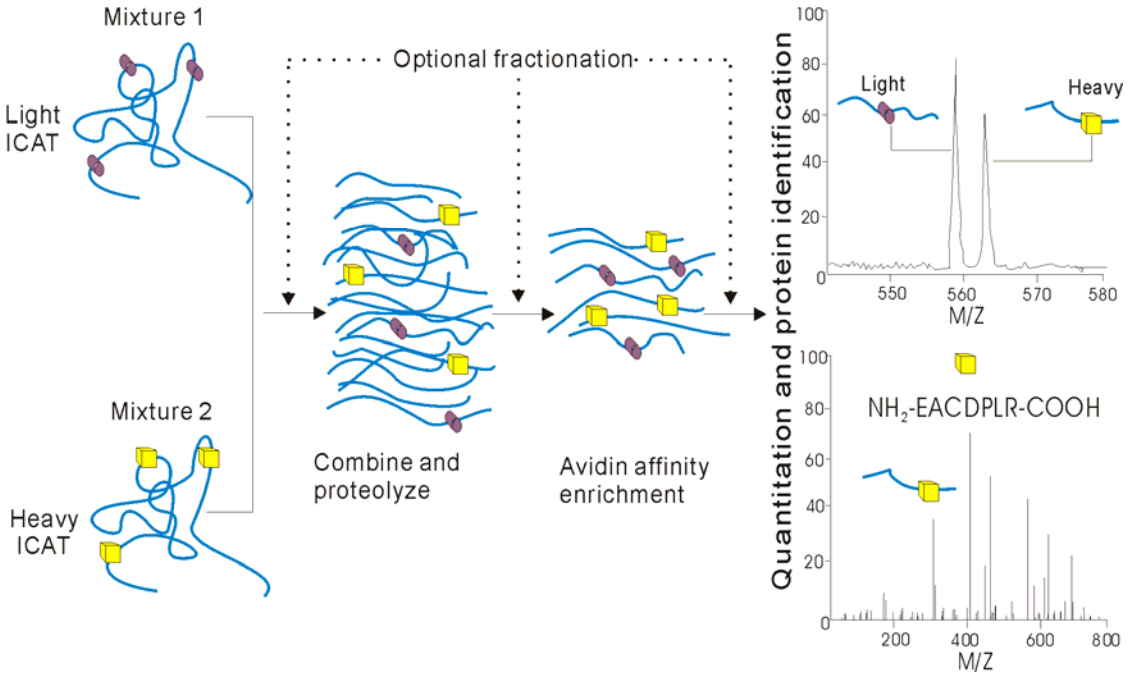

Figure 4.2. The ICAT strategy for quantitative proteome analysis. This figure was adapted from Shiio, Y. and Aebersold, R. (*148*), the drawings were generated using CorelDRAW. Light or heavy ICAT reagent is attached to each of two protein samples. The two labeled protein samples are combined and enzymatically cleaved to peptides. The ICAT-labeled peptides are isolated using the biotin tag, and are analyzed by microcapillary liquid chromatography–tandem mass spectrometry for protein quantification and identification.

A mass spectrometry-based method for modeling the orientation of cholesterol oxidase on the membrane, which involves an isotope-coded mass tag (ICMT), is under development. This method will be first performed on the cysteine mutants described in Chapter 2. It will be used to confirm the membrane bound model for cholesterol oxidase, and should be a general method for studying other interfacial proteins.

In this strategy, instead of ICAT reagents, new reagents are required, which consist of two functional elements: a specific chemical reactivity, and an isotopically coded linker. Since this method will be used to map out the membrane binding sites of an interfacial enzyme, the reagents have to be water soluble and membrane impermeable. The strategy includes the following sequential steps (Figure 4.3). 1) Protein mutant, in the presence of lipids, is treated with heavy ICMT reagents for a limited incubation time. 2) DTT is added to quench the excess heavy ICMT reagent, and reduce disulfide bonds formed during denaturation that may form between unreacting cysteine residues. 3) Before enzymatic cleavage, a light ICMT reagent with excess amount is allowed to react with the remaining cysteines, as well as DTT. 4) The ICMT-labeled peptides are purified using immobilized chromatography, such as C18 Zip Tips, and are analyzed by MALDI-TOF MS. The ratio of heavy ICMT labeled peptides containing the target cysteine to that of light ICMT labeled peptides are compared between the cysteine mutants. A mutant in which the cysteine is in contact with the membrane will have a lower heavy/light mass ratio than a mutant with a cysteine not in membrane contact. By comparing this ratio from several mutants, the residues that are in membrane contact will be identified.

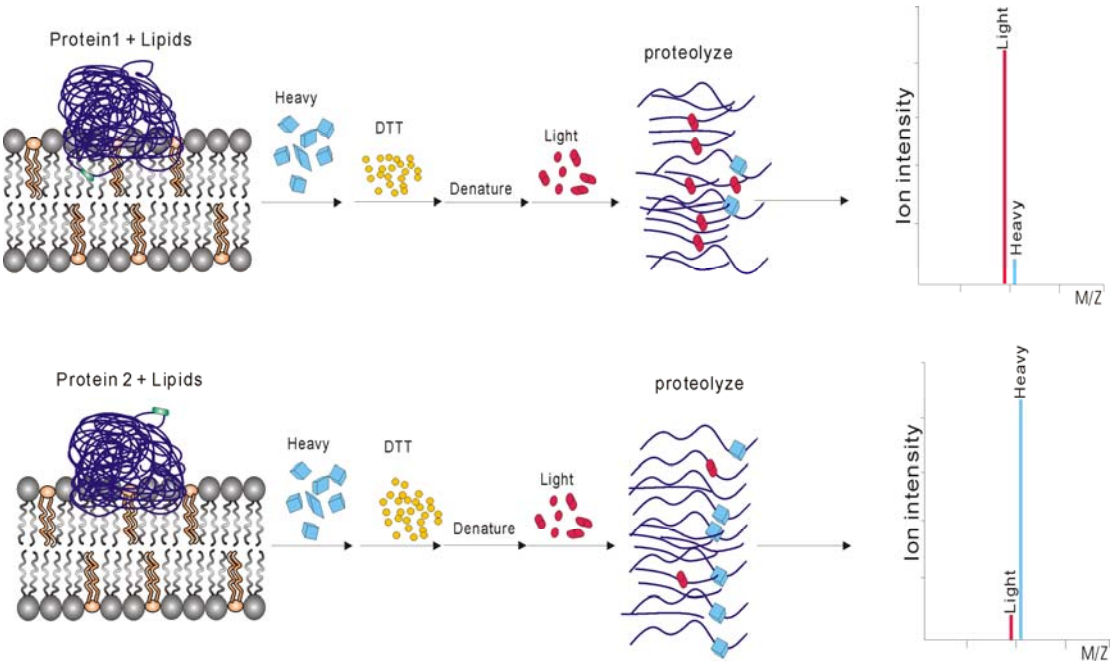

Figure 4.3. The ICMT strategy for mapping out the binding site of an interfacial enzyme on the membrane. This figure was made using CorelDRAW. Two cysteine mutants, in the presence of lipids, are treated separately with heavy ICMT reagent. DTT is used to quench the excess ICMT reagent and reduce the disulfide during denaturation. Excess light ICMT reagent is added before enzymatic cleavage. The relative quantity of the peptides is determined by the ratio of the peptide pairs.

II. Materials and Methods

Materials. Trifluoroacetic acid (TFA), dithiothreitol (DTT), iodoacetamide (IAM), N-ethylmaleimide (NEM), and Promega sequencing grade modified trypsin, were purchased from Sigma Chemical Co. (St. Louis, MO). α-Cyano-4-hydroxycinnamic acid (α-matrix) and peptide calibration standards were purchased from Bruker Daltonics (Billerica, MA). All other chemicals and solvents were supplied by Fisher Scientific (Pittsburg, PA), unless otherwise specified. All aqueous solutions were made in high purity water filtered through a Barnstead NANOpure filtration system (Barnstead International, Dubuque, IA) to give a resistivity better than 18 MΩ.

Labeling Targeted Protein. The labeling reagents used were IAM and NEM. The reactions were carried out as follows: 20-200 μg of the targeted protein was diluted into 500 μL of 50 mM Tris•HCl buffer, pH 8.2. Iodoacetamide (5 molar equivalent) was added into the protein (1 molar equivalent) solution. The reaction mixture was incubated for 2 h at rt in an eppendorf tube protected from light. The reaction was stopped by adding DTT to a final concentration of 200 μM. For quenching with NEM after denaturation, the same procedure was used except that NEM was added to a final concentration of 1 mM.

Protein Denaturation and Protease Digestion. Proteins generally need to be denatured and their disulfide bonds cleaved before protease digestion can go to completion (*149*). The protein (20-200 μg) was diluted into denaturation buffer containing 6 M urea, 2 mM DTT, 50 mM Tris-HCl, pH 8.2, in a reaction volume of 1 mL. The sample mixture was incubated at 37 ºC for at least 2 h. After denaturation, 50 mM ammonium bicarbonate and 1 mM calcium chloride were added until the urea concentration was below 1M. The sample solution was concentrated down to 500 μL using a Microcon (Millipore, Bedford, MA)

with a molecular weight cut off of 10 kDa. Protease was added to a final protease:protein ratio of 1:50, and incubated at 37 ºC in the dark 1-24 h. The protease activity was terminated by freezing at -20 ºC. Prior to mass spectrometry analysis, the sample was frozen in liquid nitrogen, and lyophilized overnight to obtain a powder form of the peptides.

Peptide Desalting. C18 Zip Tips (Millipore, Bedford, MA) were used to desalt the peptide sample. The pipette tip was wetted with wetting solution (50% acetonitrile in water), and the tip was equilibrated for binding by washing with 0.1% TFA solution. The lyophilized peptide was dissolved in 100 µL of 0.1% TFA solution, peptides were bound to the tip by aspirating and dispensing the sample for 10 times. The tip was washed with 0.1% TFA solution, and peptides were eluted with 10 µL of elution solution containing 0.1% TFA and 50% acetonitrile.

Sample Preparation for MALDI Analysis. The MALDI matrix was prepared by dissolving α-cyano-4-hydroxycinnamic acid in a mixture of 0.01% TFA and 30% acetonitrile with a matrix concentration of 10 mg/mL. An MTP 384 target plate (Bruker Daltonic, Billerica, MA) was used for MALDI-TOF analysis as described below. Prior to application to the sample plate, the purified peptide samples were mixed at a peptide:matrix ratio of 1:1 and 1:10, respectively. 1.0 µL of sample-matrix mixture was applied onto the target plate, the sample was allowed to air dry naturally before placing it into the mass spectrometer.

Mass Spectrometry. Spectra were acquired using a Bruker Autoflex II MALDI-TOF/TOF mass spectrometer (Bruker Daltonic, Billerica, MA), operated in the reflectron mode. A nitrogen UV laser (337 nm, 1-5 ns pulse of max energy 140 µJ, 10 Hz)

was used to accomplish desorption/ionization. The positive ions were subjected to an accelerating potential of 19.0 kV and 16.9 kV for ion source 1 and ion source 2, respectively, and 8.35 kV for the optical lens, reflected by reflectron electrodes (20.0 and 9.52 kV), and detected by a microchannel plate (MCP) detector using 4× voltage gain. The pulsed ion extraction time was 100 ns. Matrix ions were suppressed using low mass (m/z 500) cutoffs. The spectra were obtained by accumulating data from 5 sites on each spot using 40 laser shots per site. A PC workstation running Flexcontrol (Bruker Daltonic) was used to record the data. The laser attenuation used was 60%-90% (10-40% of the total laser intensity**)**, 90-100 μJ per laser pulse was used for ionization. FlexAnalysis software served for data analysis (Bruker Daltonic). Peptide calibration standards II (Bruker Daltonic) with mass range between 700 and 4000 Da were used to provide an external calibration of the instrument, using a quadratic order fit.

Peptide mass analysis. Amino acid sequences of the target protein were entered into PeptideMass (*150*) using the Swiss-Prot database to obtain the theoretical peptide masses of the protein. The search parameters were monoisotopic masses, $[M+H]^+$, 2 possible missed cleavages, carbamidomethylation of cysteine, and selected enzymatic cutting.

III. Results and Discussion

Tryptic digest. The influence of digestion time on the cleavage efficiency was evaluated, using two analytical parameters, amino acid coverage of the protein sequence, and number of peptides identified in a protein digest (Figure 4.4 and Table 4.1). This measurement was performed on wild-type cholesterol oxidase, with a digestion time of 1 h, 2 h, 3 h, 4 h, 5 h and 20 h. Examination of the analytical parameters with different digestion times revealed that the highest cleavage efficiency under the conditions that had been attempted, with 45.1% coverage and a total of 20 peptides, was obtained at 5 h. Cleavage efficiency was reduced a little using L80C ChoA in the presence of an alkylation reagent, IAM, during the enzymatic degradation; while in the absence of IAM, the enzymatic activity was supressed substantially (Figure 4.5).

Table 4.1. Tryptic peptides from WT ChoA identified by MALDI-TOF mass spectrometry.[a]

Residues	Sequence
1-50	AKSAADNGGYVPAVVIGTGYGAAVSALRLGEAGVQTLMLEMGQLWNQPGP
51-100	DGNIFCGMLNPDKRSSWFK**NRTEAPLGSFLWLDVVNRNIDPYAGVLDRVN**
101-150	**YDQMSVYVGR**GVGGGSLVNGGMAVEPK**RSYFEEILPRVDSSEMYDRYFPR**
151-200	ANSMLRVNHIDTK**WFEDTEWYK**FARVSREQAGK**AGLGTVFVPNVYDFGYM**
201-250	**QR**EAAGEVPK**SALATEVIYGNNHGK**QSLDKTYLAAALGTG KVTIQTLHQV
251-300	KTIRQTKDGGYALTVEQK**DTDGKLLATKEISCRYLFLGAGSLGSTELLVR**
301-350	AR**DTGTLPNLNSEVGAGWGPNGNIMTAR**ANHMWNPTGAHQSSIPALGIDA
351-400	WDNSDSSVFAEIAPMPAGLETWVSLYLAITKNPQR**GTFVYDAATDR**AKLN
401-450	WTRDQNAPAVNAAKALFDRINK**ANGTIYRY DLFGTQLKAFADDFCYHPLG**
451-500	**GCVLGK**ATDDYGRVAGYK**NLYVTDGSLIPGSVGVNPFVTITALAER**NVER
501-559	IIK**QDVTAS**

[a] Conditions: 9.4 nM protein and 0.2 nM trypsin in 42 mM ammonium bicarbonate buffer (pH 8.2), 5 h incubation at 37 °C. Identified sequences are shown in bold-face, underlined, amino acids are given in single-letter code.

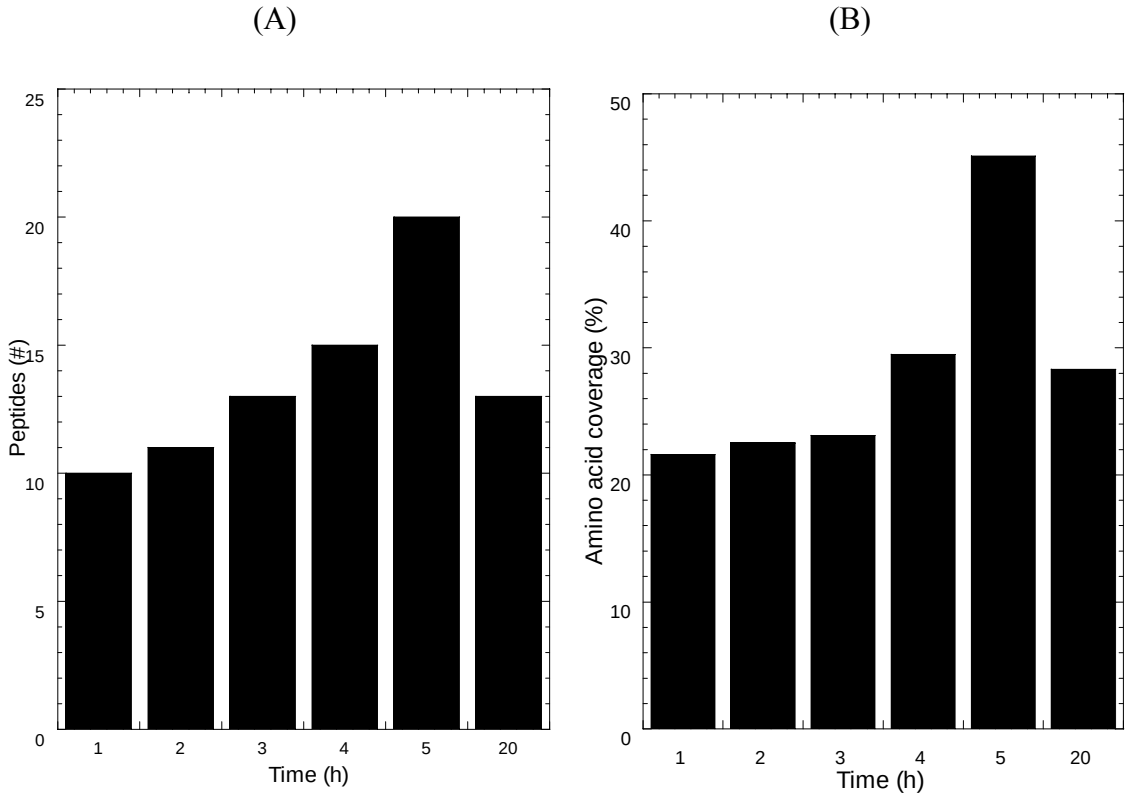

Figure 4.4. Tryptic cleavage efficiency. (A) Number of peptides; (B) Amino acid coverage, percentage of the number of identified amino acids over total number of amino acids. Conditions: 9.4 nM protein and 0.2 nM trypsin in 42 mM ammonium bicarbonate buffer (pH 8.2), incubated at 37 °C.

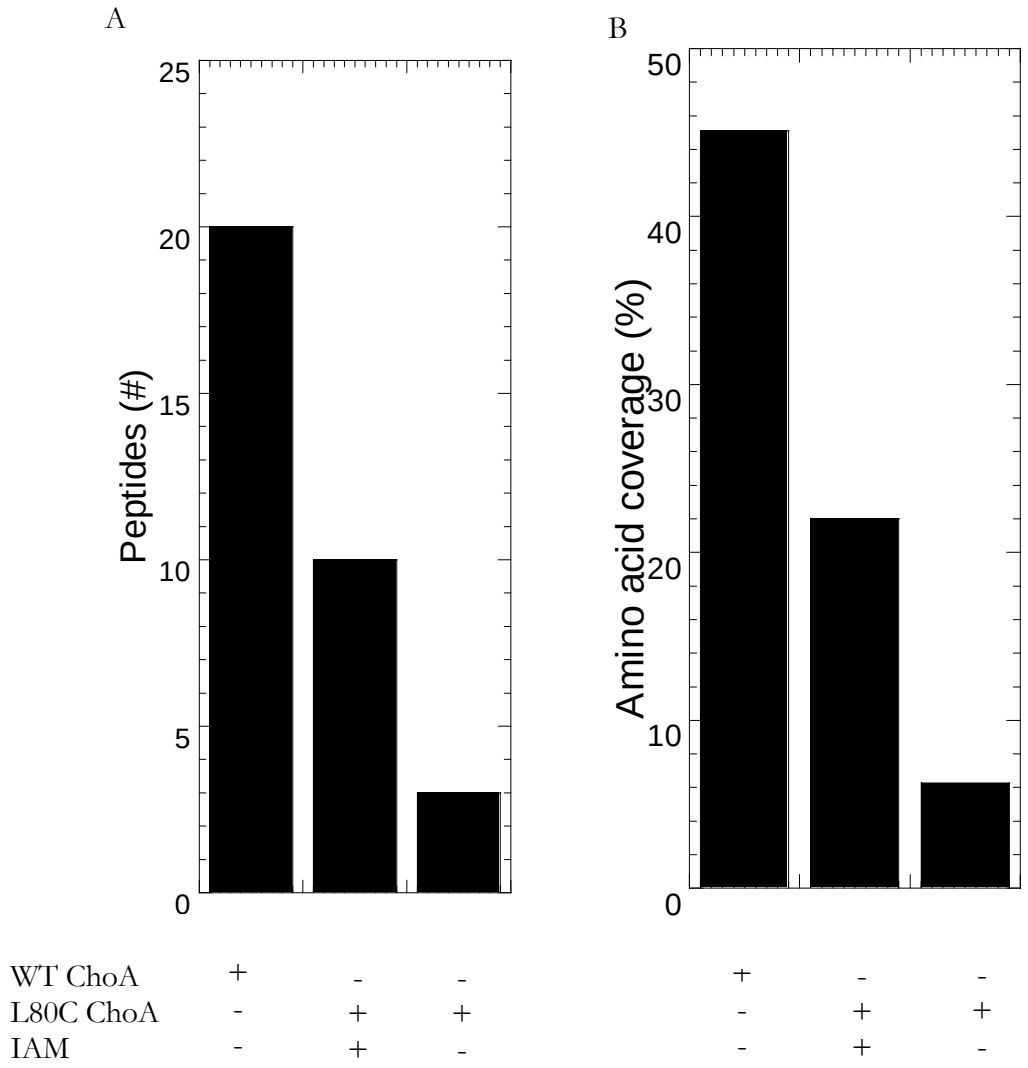

Figure 4.5. Tryptic cleavage efficiency. A) Number of peptides; B) Amino acid coverage percentage. Conditions: 9.4 nM protein and 0.2 nM trypsin in 42 mM ammonium bicarbonate buffer (pH 8.2), 5 h incubation at 37 °C.

Mass Spectrometry. C18 zip-tip was employed to wash away the buffers and salts used during protein denaturation and trypsin digestion; desalting is necessary because salts may lower the signal during the original measurements (*151*). The disadvantage for washing the sample through zip-tip was the loss of a considerable amount of peptides. Generally, no less than 1 nM of peptide provided a reasonable ion signal.

IAM and NEM were used as two thiol-reactive reagents, respectively. Because both the reagents are membrane permeable (*152*), they can not be used to determine which residue is in membrane contact. Prior to the decision of ICMT reagent, they were used to investigate how well the target residues would be labeled, and if the target residues would be included in the mass peaks shown in a MALDI-TOF MS spectrum. Since residue 80 was known to contact the membrane, the L80C ChoA mutant was used to test the accuracy of the ICMT strategy.

Labeling reactions were first performed on wild-type ChoA using IAM, which was added during protein denaturation; a control experiment was carried out with wild-type ChoA in the absence of IAM. The purpose of the studies was to find out if trypsin peptide fragments observed in mass spectra would include residue 80, and whether cysteine residues would react with IAM. Comparison of the enzymatically digested peptides from the two protein samples revealed that fragments containing residue Leu80 were present in the mass spectra with m/z 1817.278 (Figure 4.6A); fragments (m/z 1911.198) containing residue 439-456, including a disulfide bond between cys445 and cys452, were obtained in the absence of IAM (Figure 4.6B); in the presence of IAM, the related fragment appeared at m/z 2027.289, indicating that both cys445 and cys452 reacted with IAM (Figure 4.6C). The

results indicate that trypsin is the proper protease that could be used in future experiments, and IAM can label the side chains of cysteine residues under denaturing conditions.

The L80C mutant ChoA was then allowed to react with these two labeling reagents, and this study was carried out in three parallel experiments. The first one was performed with the addition of IAM during protein denaturation, the analysis of the resulting peptide fragments (Figure 4.7) enabled the identification of IAM labeled cysteine 80 (m/z 1864.230). In the second experiment, NEM was employed as the only alkylation reagent during protein denaturation, peptides containing NEM labeled cysteine 80 (m/z 1931.916) were observed (Figure 4.8). The third one was carried out by adding IAM prior to denaturation, after 30 min incubation at rm temperature, DTT was added to quench excess IAM, NEM was added during denaturation. Enzymatically cleaved peptides containing both IAM labeled cys80 (m/z 1863.778) and NEM labeled cys80 (m/z 1931.788) were present in the mass spectra (Figure 4.9).

The simultaneous presence of IAM and NEM labeled cys80 suggested that only part of the cysteines react with IAM within a 30 min incubation time, this incomplete IAM labeling may be due to the partial exposure of Leu80 to solution, or the time used for the labeling reaction. A control would be needed using a sample without lipids in the ICMT strategy, it would tell us the maximum labeling efficiency with the time used for the incubation with heavy ICMT reagents prior to denaturation. Therefore, for the cysteine mutant with the mutating site that is not in membrane contact, the difference in the ratio of heavy to light labeled fragments between protein samples with or without lipids may tell if a conformational change of the site where the mutation resides takes place upon binding to the membrane.

Examination of the mass spectra revealed that peptide fragments containing free residue 80 using a L80C ChoA mutant did not appear in the mass spectra in the presence or absence of IAM. The efficiency of tryptic digestion was suppressed using a L80C mutant in the absence of IAM, these results indicate that a possible conformational change induced by the introduction of cysteine may occur, resulting in a reduction of tryptic cleavage. However, the exact mechanism is unclear. The absence of this fragment will not be an issue in our strategy because only the ratio of heavy to light labeled fragments is required to determine the membrane binding residue(s).

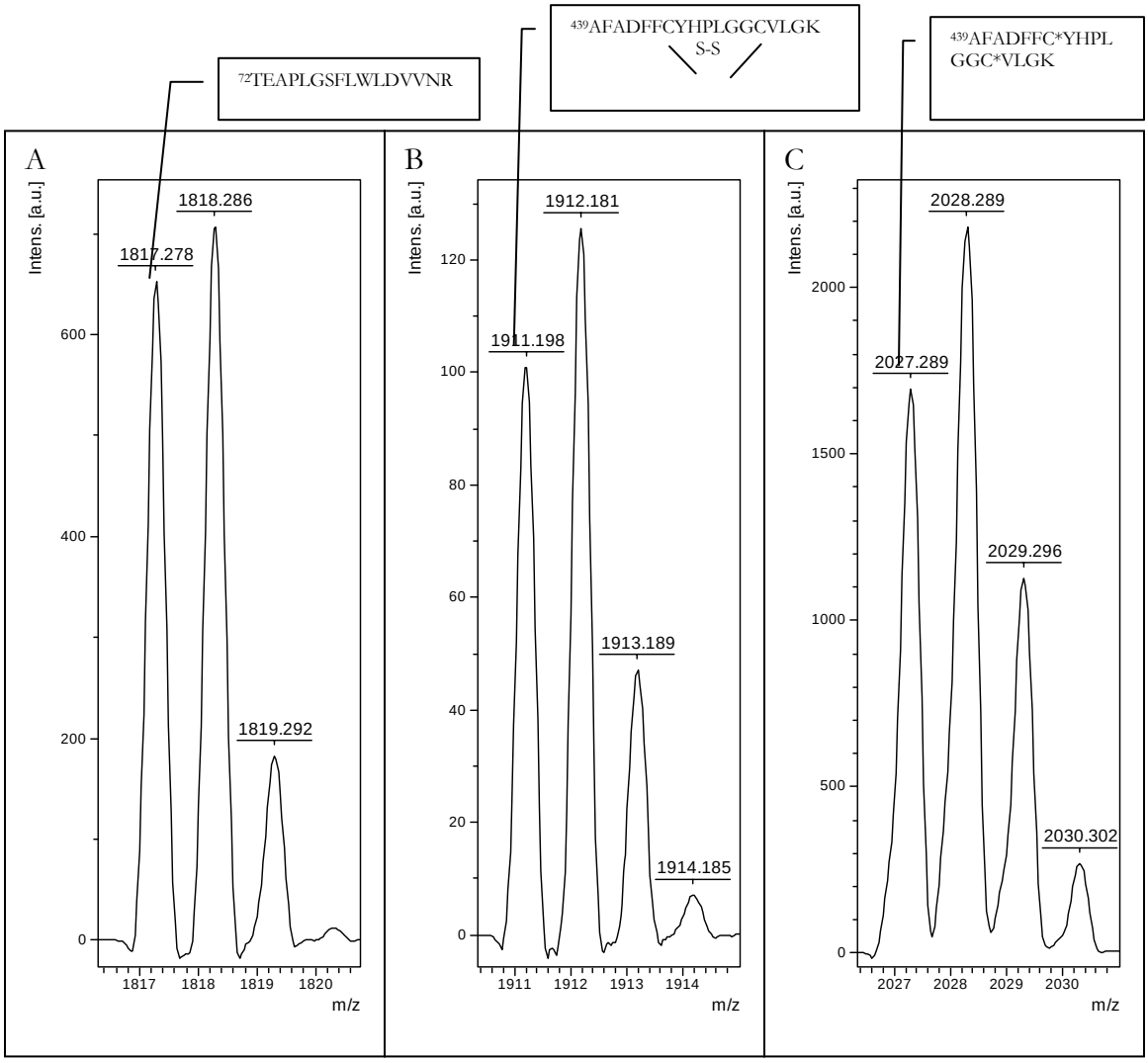

Figure 4.6. MALDI-TOF MS spectrum of peptides after digesting WT cholesterol oxidase in the presence or absence of IAM. A) m/z 1817.278 corressponding to the 72-86 fragment, containing Leu80; B) m/z 1911.198 corresponding to the 439-456 fragment, containing a disulfide bond between Cys 445 and Cys 452; C) m/z 2027.289 corresponding to the 439-456 fragment, with both Cys 445 and Cys 452 labeled with IAM. Conditions: 31 nM of protein in 42 mM ammonium bicarbonate buffer (pH 8.0), 20 h incubation at 37 °C. *IAM labeled residue.

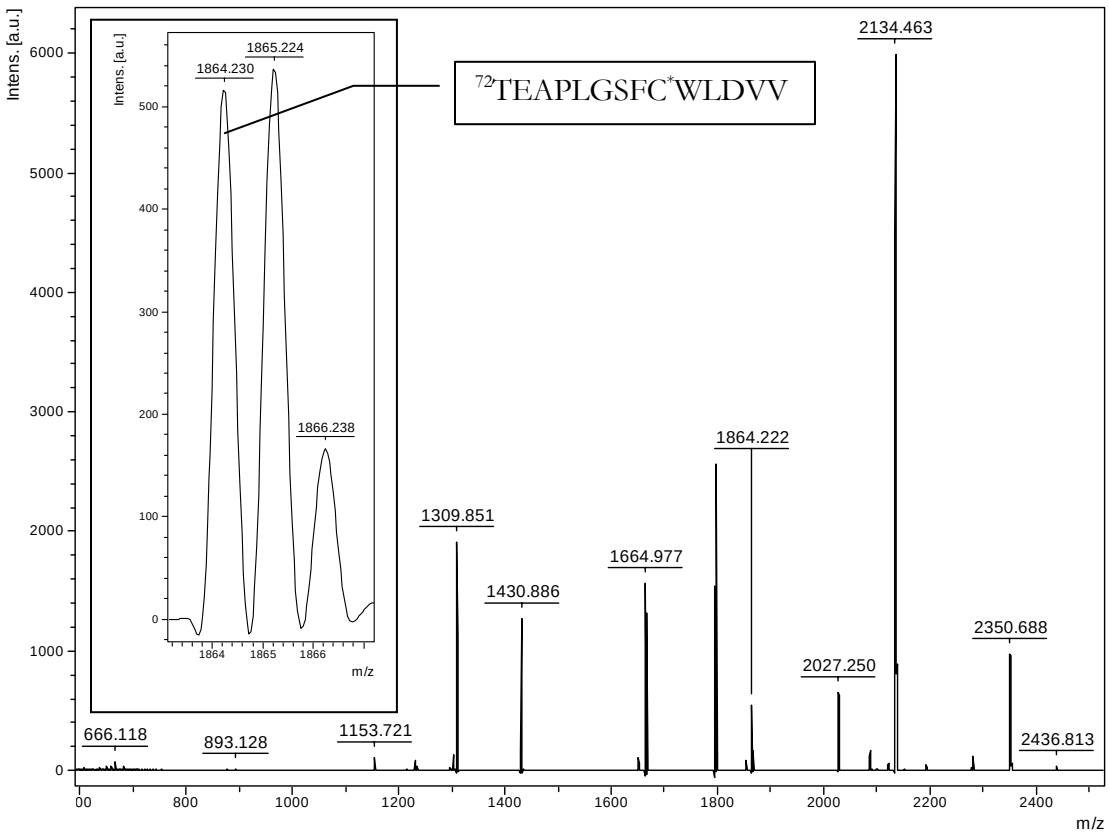

Figure 4.7. MALDI-TOF MS spectrum obtained from the digestion of IAM treated L80C cholesterol oxidase. The inset shows the m/z 1864.230 fragment. * labeled with IAM. The first residue in the peptide sequence is Thr72. Conditions: 76 nM of protein in 42 mM ammonium bicarbonate buffer (pH), 24 h incubation at 37 °C.

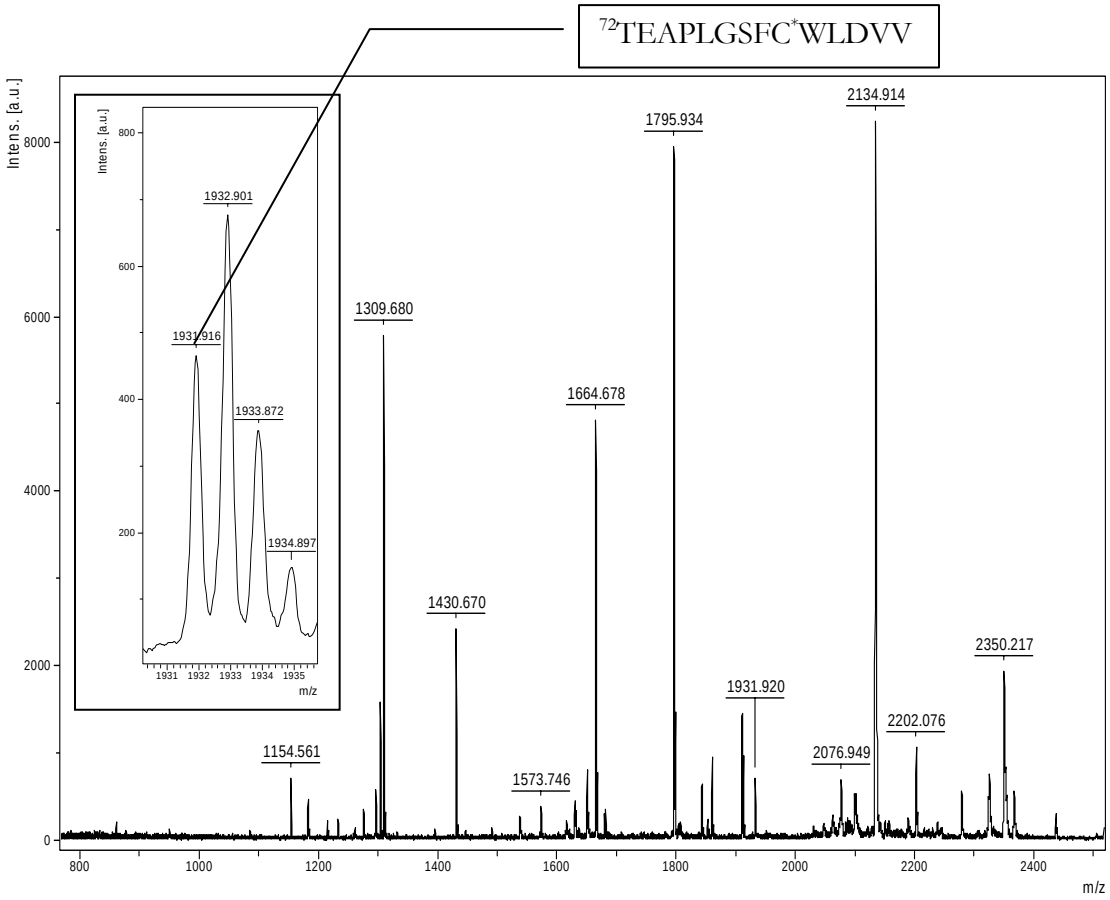

Figure 4.8. MALDI-TOF MS spectrum of peptides after digesting NEM treated L80C cholesterol oxidase. The inset shows the m/z 1931.916 fragment. Conditions: 76 nM of protein in 37.5 ammonium bicarbonate buffer (pH 8.0), 24 h incubation at 37 °C. * labeled with NEM. The first residue in the peptide sequence is Thr72.

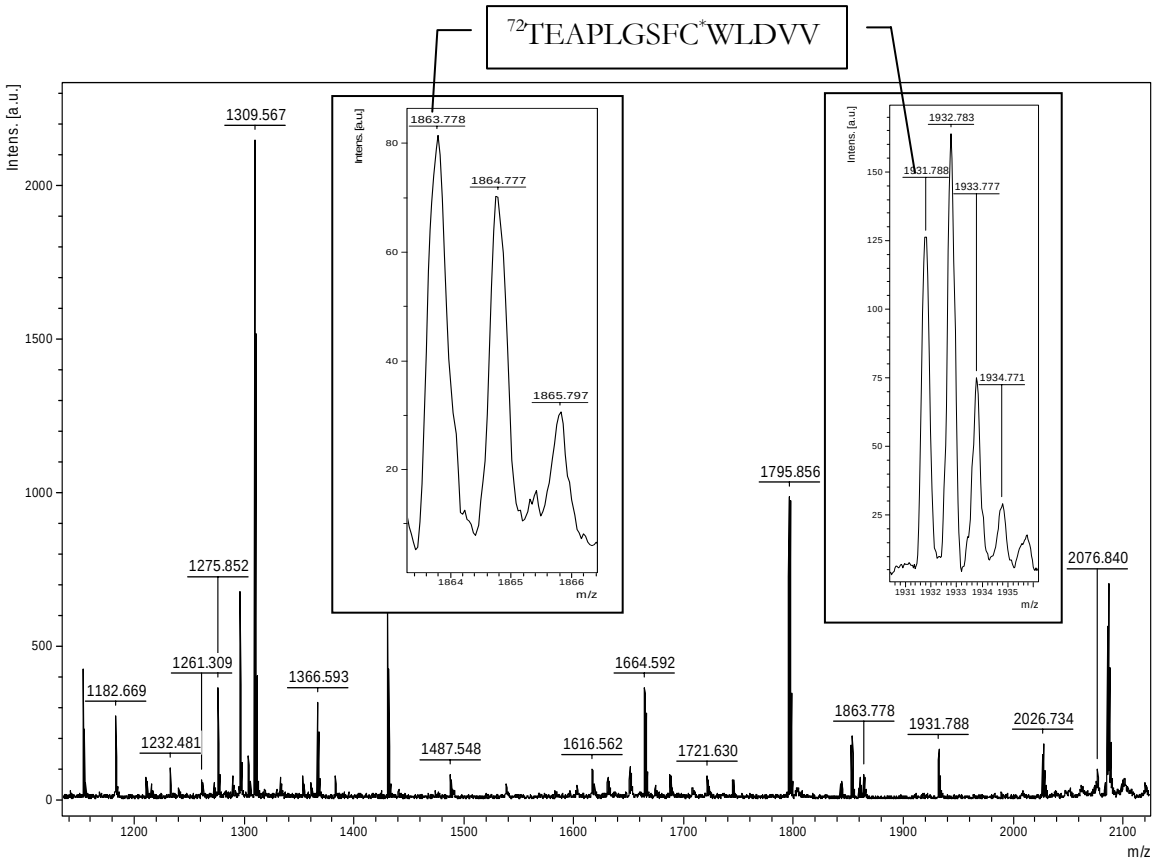

Figure 4.9. MALDI-TOF MS spectrum of peptides after digesting IAM-NEM treated L80C cholesterol oxidase. The inset shows the m/z 1863.778 and 1931.788 fragments. * Labeled with IAM (m/z 1863.778) or NEM (1931.788). The first residue in the peptide sequence is Thr72. Conditions: 76 nM of protein in 37.5 mM ammonium bicarbonate buffer (pH 8.0), 24 h incubation at 37 °C.

Isotope-Coded Mass Tags (ICMT). The design of a new reagent requires the following features: (1) a thiol reactive group that will covalently bind to the sulfhydryl group of reduced cysteine via an irreversible reaction; (2) a linker group that occurs in a deuterated (isotopically heavy) or non-deuterated (isotopically normal) form to allow ~8 Da difference between "heavy" and "light" tags; (3) a reagent that is water soluble and membrane impermeable.

The alkylation reaction can be carried out through a reaction between an iodoacetyl moiety or a maleimide moiety and thiol group (Scheme 4.1). Moreover, the products are stable in water under reducing conditions due to a newly formed covalent bond. Therefore, molecules containing an iodoacetyl or a maleimide group should be considered. A spacer arm can be employed to allow the incorporation of a deuterated or non-deuterated moiety. It also can be formed from different chemical groups to provide water solubility and membrane-impermeability.

The spacer arm can be formed from polyethylene glycol (PEG) subunits with abundant oxygen atoms to provide water solubility. (PEO)n will make the molecule both water-soluble and unable to penetrate lipid membranes. Maleimide-$(PEO)_n$ is a membrane-impermeant Cys-specific reagent and has been widely used to study the topology of membrane proteins(*153, 154*). However, commercially available pegylation reagents typically are a heterogeneous mixture composed of a distribution of chain lengths. Synthesis of a short arm PEO chain with a monodisperse number of PEG subunits will be required to obtain an ICMT reagent, the length of the PEO chain should be short and should not affect its water solubility and membrane impermeability. Maleimide-$(PEO)_n$-biotins are water soluble because the hydrophilic PEO spacer arm

imparts water solubility that is transferred to the biotinylated molecule. Maleimide-PEO_2-biotin has been reported as a membrane impermeable reagent (*155*). Therefore, compound **1** is proposed as a proper ICMT reagent (Figure 4.10).

The ICAM strategy is currently under development, further studies should be carried out to make the ICMT reagent. This mass spectrometry-based approach will provide an efficient way to study protein-membrane interactions.

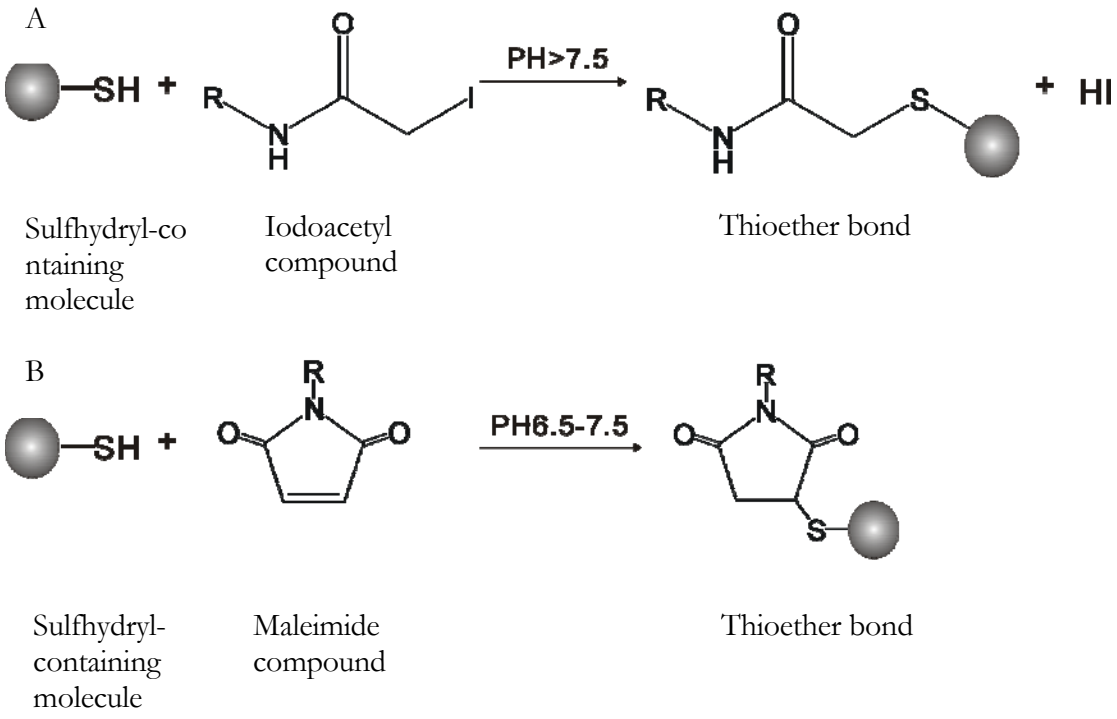

Scheme 4.1. Reaction scheme of A) Active halogen, B) Maleimide.

Heavy reagent: X=deuterium
Light reagent: X=hydrogen

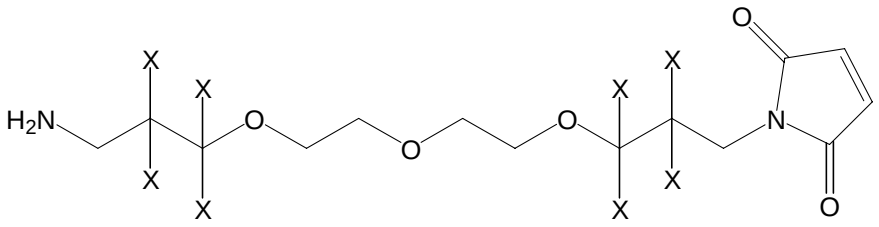

Figure 4.10. Structure of proposed ICMT reagent, compound **1**

CHAPTER 5 Characterization of Cholesterol Oxidase Activity with Glycerol: Investigation of the Interplay among Glycerol, FAD and Active residues, Found in the Steroid-binding Cavity and the Active Site.

- The crystallography experiments in this chapter were performed by Artem Y. Lyubimov in the laboratory of Professor Alice Vrielink at University of California, Santa Cruz.

I. Introduction

Cholesterol oxidase is a flavoenzyme, it is utilized by bacteria, actinomycetes in particular, to produce energy through metabolizing 3β-hydroxy sterols to 3-ketosteroids (*50, 156, 157*). Interests are arising on investigation of the role of this enzyme in pathogenic bacteria, such as *Rhodococcus equi*, and it has been proposed that cholesterol oxidase is required for bacterial maintenance of the infection in the host macrophage (*71*). Since cholesterol oxidase is unique to bacteria, a specific inhibitor of the enzyme would be an attractive candidate for novel antibiotics. Detailed understanding of substrate binding and catalysis at a molecular level is required to guide the design of inhibitors of cholesterol oxidase.

The exact structure of either type I or type II oxidase with a bound substrate is not known. A structure of cholesterol oxidase in complex with dehydroepiandrosterone (DHEA) was obtained under anaerobic conditions (*82*). In this complex, the enzyme underwent a single turnover event, and the reoxidation of the cofactor could not be accomplished because of lacking of oxygen. Therefore, the reduced form of the cofactor was observed in the active site, which resulted in the structural difference from the Michaelis (E·S) complex of many other flavoenzyme oxidases (*158*). Generally, in flavoenzymes that catalyze dehydrogenation reactions, the positioning of the reactive part of the substrate with respect to the FAD cofactor is conserved (*158*). The hydride donor binds in front of the flavin at a distance of ~3.5 Å from N5-FAD, and the N10-N5-CH angle (where CH is the hydride donor) is in the narrow range of 96-117°. In the DHEA-ChoD complex, the steroid binds in the active site, the distance between the steroid C3 atom and N5-FAD is longer than 3.5 Å.

A Michaelis complex model for type I enzyme was proposed based on the atomic

resolution structural work (*90*) and the structure of enzyme-DHEA complex (*82*). In this model (*90*), the steroid C3 atom is placed within a hydrogen bond distance (~3.0 Å) of N5-FAD, and the positioning of hydride donor with respect to the cofactor is similar to those in many other flavoproteins (*158*). To confirm the accuracy of this model, a structure of the complex of oxidized cholesterol oxidase with a substrate or a substrate analog is required. In the enzyme-substrate analog complex, the cofactor is in it native form, the rate of the reaction in the active site, catalyzed by cholesterol oxidase is so slow that crystals of the complex of enzyme-substrate can be obtained, where the substrate has not been oxidized yet. The structure of the enzyme in the presence or absence of a bound ligand would reveal if a conformational rearrangement of the active site is caused by substrate binding. In addition, a better understanding of the effect of the protein microenvironment on subatrate binding and the conformational change of flavin cofactor would also be obtained from the same type of structural studies.

Trapping the Michaelis complex by crystallography requires cocrystallizing cholesterol oxidase with its substrate or a substrate analog under aerobic conditions. A double mutant of the enzyme, H447Q/E361Q, was selected for this study by our collaborator, Alice Vrielink and her coworker, Artem Y. Lyubimov. This mutant has a ~ 600-fold lower catalytic activity (k_{cat}) than wild type with a minimally affected apparent K_m, the apparent equilibrium constant of the enzyme-substrate complex (*140*). The hydrogen-bonding interactions with the substrate were expected to be conserved with the substitution of His447 by glutamine, and the catalysis was slowed down by this substitution without a serious disruption of substrate binding (*87, 159*). The substitution of Glu361 by Gln affects oxidation in concert with the H447Q mutation (*88*). Therefore, under aerobic

conditions, soaking this inactive cholesterol oxidase mutant with its substrate or a substrate analog will provide crystals of the enzyme in its native form, bound with a substrate or a substrate analog, that is, the Michaelis complex. In Lyubimov's experiments, he soaked crystals of the enzyme in a solution containing 20% glycerol, and obtained crystals of an enzyme-glycerol complex (*160*).

In Lyubimov's structural studies, two atomic resolution structures of H447Q/E361Q in the presence and absence of glycerol, respectively, were solved. Four distinct populations of glycerol in the active site were observed in the crystal structures of the enzyme-bound glycerol complex, including a structure with a covalent adduct between oxidized and dehydrated glycerol and N5 of the flavin (Figure 3.1). The glycerol bound structures showed two geometries of the isoalloxazine moiety of the FAD cofactor, "planar" ($\Phi = 166.54° \pm 0.65$) and "bent" ($\Phi = 149.55° \pm 0.59$), Φ is the angle between the pyrimidine and dimethylbenzene rings (Figure 3.2), while only the "planar" conformation with a Φ value of $167.64° \pm 0.58$ was observed in the absence of glycerol. The Φ angle of a reduced isoalloxazine has been predicted to be approximately 150° through molecular geometry calculations (*161, 162*), and crystallographic studies have confirmed the association of the Φ angle with a reduced isoalloxazine (*163, 164*), although it is not always found in crystal structures of reduced flavins bound to flavoproteins (*165*). The distortion of FAD geometry seemed to be caused by the movement of the "aromatic triad" of Tyr107, Phe444 and Tyr446, upon the binding of glycerol in the active site.

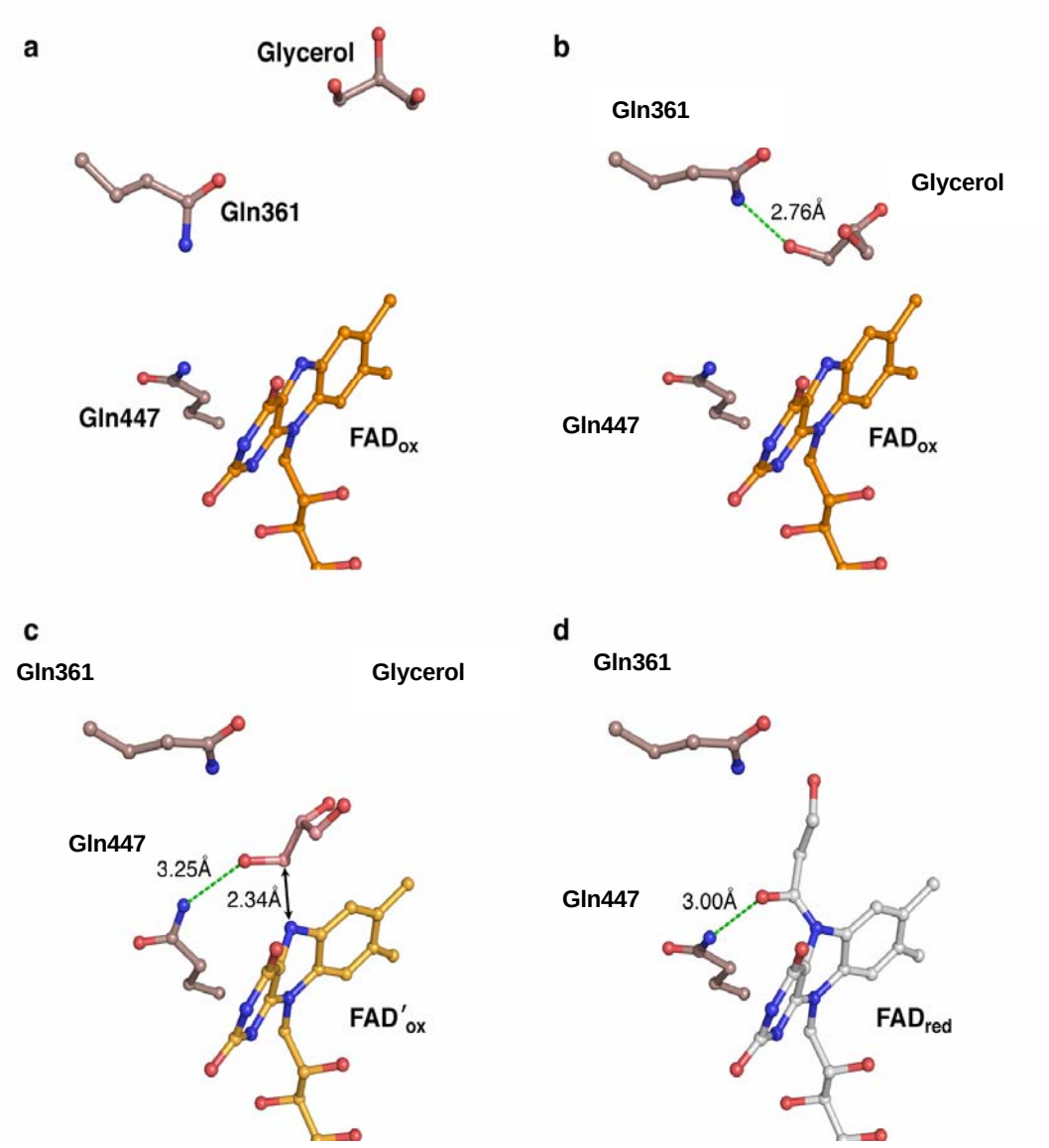

Figure 5.1. Glycerol binding and reaction with FAD (*160*) (This figure was made by A. Y. Lyubimov). FADox and FAD'ox are the oxidized forms of the FAD cofactor with a "planar" and "bent" conformation, respectively; FADred is the reduced form of the FAD cofactor with a "bent" conformation. a-d) A time-resolved interpretation of multiple glycerol conformations found in the steroid-binding cavity and the active site. a) Glycerol binds in the distal part of the steroid-binding cavity; b) glycerol moves to the proximal part

of the steroid-binding cavity and forms a hydrogen bond (green dashed line) with Gln361; c) glycerol binds in the active site in a Michaelis complex-like orientation; d) the covalent FAD-ketopropanol adduct.

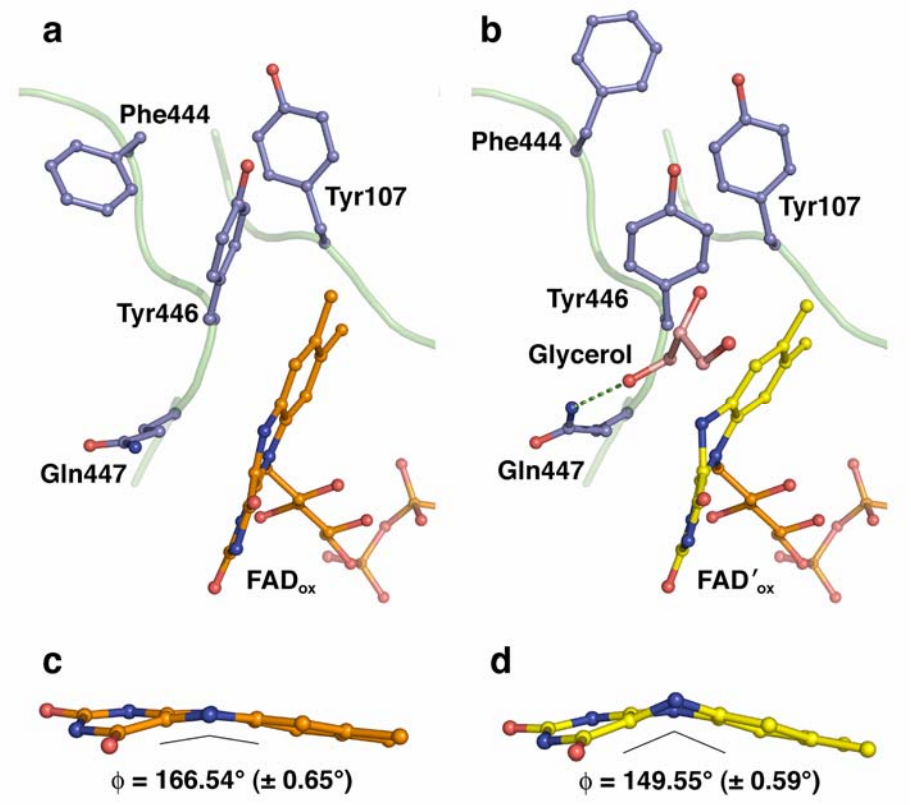

Figure 5.2. Effect of glycerol binding on the "aromatic triad" and FAD Φ-angle (*160*) (This figure was made by A. Y. Lyubimov). FADox and FAD'ox are the oxidized forms of the FAD cofactor with a "planar" and "bent" conformation, respectively a,b) A comparison of Tyr107, Phe444, Tyr446 and Gln447 conformations before (a) and after (b) glycerol binding. c,d) A comparison of the isoalloxazine "butterfly bend" before (c) and after (d) glycerol binding; the angle (Φ) between the dimethylbenzene and pyrimidine rings was calculated using SHELX.

Atomic resolution crystallography provides more structural information about how the state of enzymes changes than lower resolution crystallograhy, which generally yields static, average structures that carry little information about the dynamic nature of enzymes. Lyubimov's structural studies showed multiple glycerol conformations in the steroid-binding cavity and the active site, including a glycerol binding in the active site in a

Michaelis complex-like orientation, and a formation of a covalent adduct between glycerol and the cofactor, which suggested that a redox reaction take place in the active site. Therefore, glycerol appears to be a substrate analog for cholesterol oxidase. To determine if glycerol is a substrate of cholesterol oxidase, that is, does cholesterol oxidase catalyze the oxidation of glycerol to glyceraldehyde in solution, activity assays were required to detect the product of the reaction catalyzed by cholesterol oxidase. Direct binding between an electrochemically reduced cofactor and glyceraldehyde in solution was monitored to look for the direct evidence of the existence of the covalent FAD adduct. Enzyme kinetics was performed on wild-type cholesterol oxidase and the HQ/EQ double mutant to determine if glycerol inhibits the catalytic activity of the enzyme with its substrate. This chapter describes these efforts to characterize cholesterol oxidase activity with glycerol.

II. Materials and Methods

Materials. Cholesterol, DHEA, HRP, p-HPAA, ABTS, BSA, safranin O and methylviologen were purchased from Sigma Chemical Co. (St. Louis, MO), all other chemicals and solvents were supplied by Fisher Scientific (Pittsburg, PA), unless otherwise specified. The following buffers were used: buffer A, 50 mM sodium phosphate buffer, pH 7.0; buffer B, buffer A + 0.025% Triton X-100 (w/v) + 0.020% BSA; buffer C, 10 mM sodium phosphate buffer, 137 mM NaCl, and 2.67 mM KCl, pH 7.0.

Oxygen Consumption Measurements. Measurements were carried out at 37 °C in buffer A + 1 M glycerol. The reaction was initialized by adding cholesterol oxidase to a final concentration of 5 μM. The dissolved oxygen level was monitored with a YSI model 53 oxygen meter as a function of time.

Hydrogen Peroxide Production Measurements. Glycerol (1M), HRP (2000 units/mL), p-HPAA (200 mM) and ABTS (100 mM) stock solutions were prepared in buffer A. The concentration of enzyme used in the assays was as follows: wild type cholesterol oxidase, 50 nM to 500 nM; H447Q/E361Q cholesterol oxidase, 5 μM. The concentration of each reagent used in the assays was as follows: glycerol, 0.5 – 1 M; HRP, 40 units/mL; p-HPAA, 4 mM; or ABTS, 2 mM. To detect the formation of H_2O_2 with p-HPAA, the reaction was followed by excitation at 325 nm and monitoring the fluorescence emission at 415 nm; with ABTS, the absorbance was monitored at 600 nm as a function of time. Initial velocities measured in this assay, as well as the assays described below, were determined by following less than 10% reaction by monitoring the product absorbance.

Assay for Irreversible Inhibition. Glycerol (up to 1 M) was incubated with 200 nM WT cholesterol oxidase or 10 μM H447Q/E361Q in buffer A at 37 °C. At various time

intervals, the amount of active cholesterol oxidase remaining was measured by removing an aliquot (100 μL), diluting to 1 mL with buffer B containing 50 μM cholesterol and 2% propan-2-ol, and following the appearance of cholest-4-en-3-one at 240 nm to determine remaining enzyme activity. The inhibition assay for glyceraldehyde was carried out in an identical manner using a maximum concentration of 0.1 M glyceraldehyde due to its limited solubility in the buffer.

Assay for Competitive Inhibition. A stock solution of DHEA (3.7 mM) was prepared by dissolving DHEA in ethanol. This solution was filtered through a 0.45-μm nylon filter. Measurements of the activity of WT cholesterol were carried out at 37 °C in buffer C + 2 mM ABTS, 40 units/mL HRP, 4% ethanol. The enzyme was added at a final concentration of 40 nM to initiate the reaction. DHEA concentrations ranged from 6 μM to 150 μM, and glycerol concentrations were varied from 0 to 4 M.

Binding Titration. H447Q/E361Q (30 μM) was electrochemically reduced as described by Pellett and Stankovich (*166*) at pH 7.0, 25 °C in buffer A, with 4 μM safranin O and 100 μM methylviologen under anaerobic conditions. One equivalent of glycerol or glyceraldehyde was added from a sidearm, and absorbance spectra were recorded from 330 to 825 nm.

III. Results and Discussion

Activity Assays. Formation of the covalent FAD-ketopropanol adduct in the crystal structure suggested that a redox reaction was occurring in the active site. If this reaction was catalyzed by cholesterol oxidase using an FAD cofactor, the glycerol would be oxidized, and FAD would be reduced. The cofactor would be regenerated by the reduction of O_2 to hydrogen peroxide (Scheme 1.1). Therefore, cholesterol oxidase activity with glycerol can be detected by measuring hydrogen peroxide production.

Generation of hydrogen peroxide was probed using a horseradish peroxide coupled assay. In this assay, an indicator dye is used as the substrate to reduce hydrogen peroxide. The assay is very sensitive, and can detect the formation of a very subtle amount of hydrogen peroxide, which is essential when a cholesterol oxidase mutant with a greatly reduced catalytic activity is used. ABTS (Scheme 5.1A) and *para*-hydroxyphenyl acetic acid (HPAA) (Scheme 5.1B) were chosen as the indicator molecules.

The activity assays were performed with wild-type cholesterol oxidase and the H447Q/E361Q mutant, using HPAA or ABTS, respectively. Neither an increase in fluorescence at 415 nm using HPAA, nor an increase in absorbance at 600 nm using ABTS, was observed at pH 7.0 and pH 5.0 in aqueous solution containing glycerol (0.5-1 M), indicating that no hydrogen peroxide was produced with glycerol as substrate.

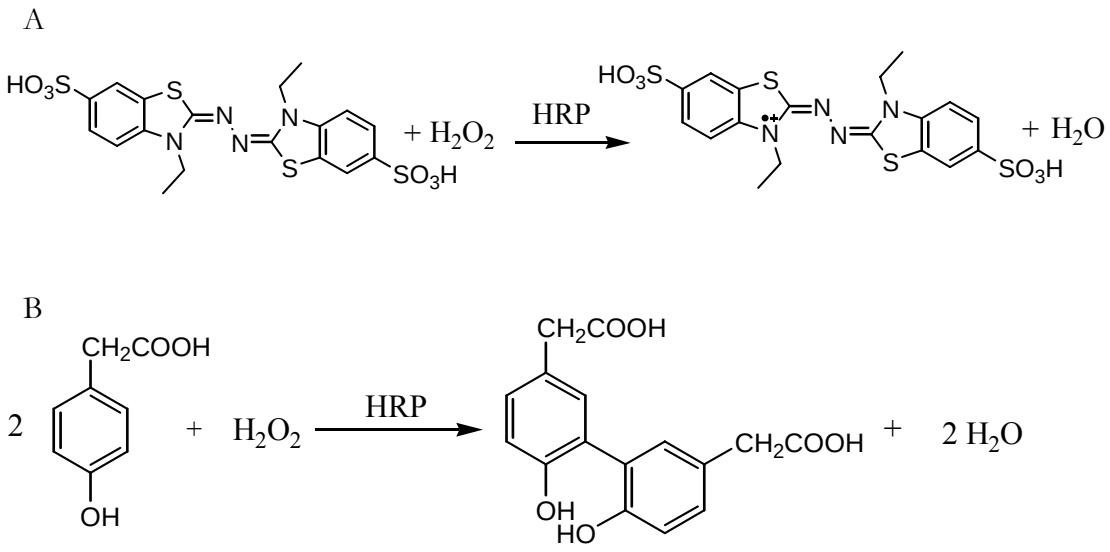

Scheme 5.1 HRP-catalyzed oxidation of A) ABTS and B) HPAA in the presence of hydrogen peroxide (*167, 168*).

To confirm that there is no redox reaction taking place in the active site, the consumption of oxygen was monitored. Adding wild-type cholesterol oxidase into 50 mM sodium phosphate buffer containing cholesterol initiated a reduction in oxygen concentration in the solution, confirming that oxygen is consumed in a redox reaction catalyzed by cholesterol oxidase with cholesterol as a substrate; consumption of oxygen was not observed when cholesterol was replaced with glycerol as a substrate. The results confirmed that oxygen was not utilized for regenerating the cofactor when glycerol was employed as a substrate. Thus, in solution, cholesterol oxidase can't catalyze the oxidation of glycerol to glyceraldehyde, and glycerol is not a substrate of cholesterol oxidase. Formation of the covalent FAD-ketopropanol adduct in the crystal structure maybe caused by another reaction, perhaps initiated by high energy X-rays.

Enzyme kinetics In solution, assays of irreversible inhibition of WT cholesterol oxidase by glycerol were performed with 10 μM and 100 μM under glycerol. The remaining cholesterol oxidase specific activity was plotted as a function of time (Figure 3.3). The remaining active cholesterol oxidase (uninhibited) was measured with cholesterol as a substrate and compared to a control incubation without glycerol. No irreversible inhibition of WT cholesterol oxidase was observed by glycerol. Identical assays were carried out with HQ/EQ cholesterol oxidase, using glycerol or glyceraldehyde as the inhibitor. Neither glycerol nor glyceraldehyde reduced the catalytic activity of HQ/EQ (Figure 3.3).

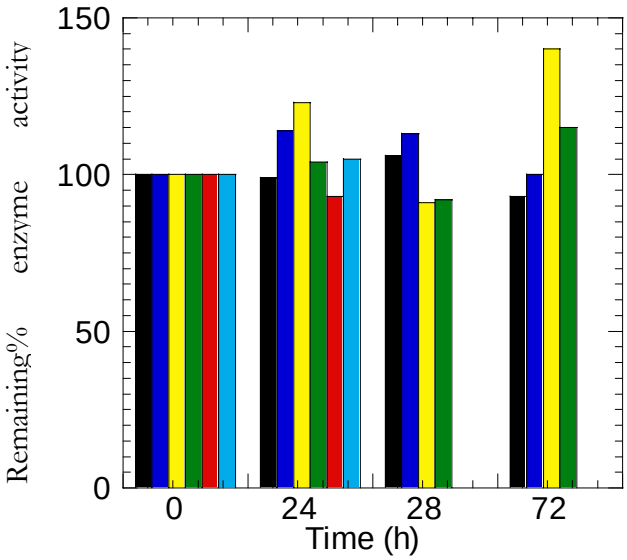

Figure 5.3. Assay for irreversible inhibition of WT by glycerol and H447Q/E361Q cholesterol oxidase by glycerol or glyceraldehyde. E*, remaining enzyme activity with glycerol or glyceraldehyde; E0, remaining enzyme activity without glycerol or glyceraldehyde. WT cholesterol oxidase (0.2 μM) and glycerol (10 μM 100 μM), HQ/EQ cholesterol oxidase (9.2 μM) and glycerol (13.3 μM and 133μM), HQ/EQ cholesterol

oxidase (10 μM) and glyceraldehyde (25 μM and 250 μM), were incubated at pH 7.0, 37 °C. The remaining enzyme activity was measured by removing an aliquot of the incubation mixture at various time intervals, diluting into 50 mM sodium phosphate buffer containing 0.025% Triton X-100, 0.020% BSA, 50 μM cholesterol, and 2% propan-2-ol, and following the formation of cholest-4-en-3-one. Remaining enzyme activity (%) was obtained by dividing enzyme activity measured in the aliquot from the incubation mixture with glycerol or glyceraldehyde by enzyme activity measured in the aliquot from the incubation mixture without glycerol or glyceraldehyde at the same time interval. Remaining activity (%) of WT cholesterol oxidase in the presence of glycerol with a molar ratio of: ■ , 1:50 (enzyme:glycerol); ■ , 1:500 (enzyme:glycerol); remaining activity (%) of HQ/EQ cholesterol oxidase in the presence of glycerol with a molar ratio of: ■ , 7:10 (enzyme:glycerol); ■ , 7:100 (enzyme:glycerol); remaining activity (%) of HQ/EQ cholesterol oxidase in the presence of glyceraldehyde with a molar ratio of: ■ , 2:5 (enzyme:glycerol); ■ , 2:50 (enzyme:glycerol).

Glycerol was tested as a competitive inhibitor of steroid using DHEA as a substrate. The enzyme activity with DHEA was measured by detecting the formation of H_2O_2 with ABTS at 600 nm as a function of time, at four glycerol concentrations: 0 M, 1M, 2M and 4M. DHEA was used as the substrate in this study because its aqueous solubility made the assay conditions less complicated. Detergent micelles, e.g., triton X-100, which are required for assays with cholesterol, interfere with K_i determinations. Initial velocity data with WT cholesterol oxidasewere identical in the absence and presence of glycerol. That is, no inhibition was observed up to 4M glycerol (Figure 3.4). The crystal structure reveals that glycerol is a useful substrate analog (*160*), enzyme activity assay and kinetics data show a lack of observed glycerol turnover in solution, and no inhibition of WT cholesterol oxidase by glycerol, suggesting that glycerol has a very weak affinity for the enzyme and will only bind in the absence of competitive ligands.

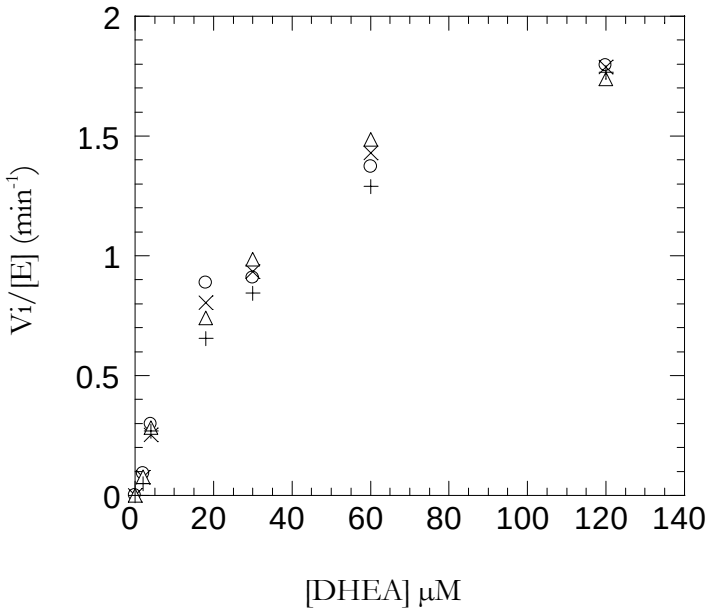

Figure 5.4. Glycerol inhibition kinetics of WT cholesterol oxidase. Initial velocities were measured over a range of DHEA concentrations at varied glycerol concentrations, in phosphate buffered saline (10 mM sodium phosphate, 137 mM sodium chloride and 2.67 mM potassium chloride, pH 7.3) containing 2 mM ABTS, 40 units/mL HRP, and 4% ethanol, 37 °C. The glycerol concentrations used were: ○, 0 M; ×, 1 M; △, 2 M; ＋, 4 M.

Formation of a covalent adduct between oxidized and dehydrated glycerol and N5 of FAD was revealed in the crystal structure (*160*). The electron density is clearly a result of the reaction with glycerol. However, activity data suggested that glycerol was not oxidized in solution. Perhaps high-energy X-rays initiate a covalent reaction through free electrons generated in the X-ray beam. It is well known that radiolysis of water takes place during data collection due to the exposure of crystals to X-rays at typical experimental wavelengths (1.0Å – 1.5Å, which corresponds to ~12 keV). Regions of electron deficiency in the form of hydroxyradicals are produced by the radiolysis of water at temperatures as low as 100 K, the temperature at which the diffraction experiments are performed (*169*). Because glycerol is an electron hole-trapping agent (*170*), hydroxyradicals formed from the water molecules present in the crystal could be used to form a covalent adduct with the flavin cofactor. However, the exact mechanism of this process is unclear.

Binding Titration. In order to monitor binding directly by visible spectroscopy, an aerobic titration of 30 μM H447Q/E361Q cholesterol oxidase with glycerol was carried out. Addition of glycerol resulted in precipitation of the concentrated protein. In a second experiment, an anaerobic spectroelectrochemical cell and the method of Stankovich (*166*) were employed to conduct a binding titration of reduced H447Q/E361Q cholesterol oxidase under anaerobic conditions. The enzyme was monitored by UV/visible spectroscopy. Again, the concentrated protein precipitated upon addition of glyceraldehyde. These results indicate that direct binding could not be monitored in solution.

The binding measurements were originally designed to detect the change in FAD redox potential upon the binding of substrate analogs. Thus a relationship between the geometric distortion of FAD and reduction potential could be elucidated. The difficulty of

the binding titration makes it hard to explain the distortion of the isoalloxazine geometry from a thermodynamic viewpoint.

However, the structural studies suggest the cause behind the "butterfly bend" in FAD. Theoretical calculations predicted that the oxidized flavin prefers a planar Φ-angle. Two geometries of the isoalloxazine moiety of the FAD cofactor, "planar" (Φ = 166.54° ± 0.65) and "bent" (Φ = 149.55° ± 0.59), were observed in the glycerol bound structure. The extra 15° bending observed in the oxidized FAD cofactor is proposed to result from substrate binding that forces rearrangement of the "aromatic triad", not from X-ray exposure. An atomic resolution structure of a photoreduced *Streptomyces* sp. cholesterol oxidase demonstrates that only reduction of cholesterol oxidase bound FAD is insufficient to cause a significant change of isoalloxazine geometry. During data collection, the region of a crystal of wild type cholesterol oxidase lost its yellow coloring, indicating that the high energy X-ray beam reduced the FAD cofactor (Lario and Vrielink, personal communication). The reduction took place in the absence of any substrate in the active site. In these structures, the geometry of the reduced FAD is unchanged with respect to that observed in the oxidized FAD (PDB ID: 1N1P). Furthermore, both in the presence and absence of glycerol, crystals of HQ/EQ double mutant retained their yellow color, indicating that in both cases FAD was in its oxidized form. These observations strengthen the hypothesis that glycerol binding causes the bending of the isoalloxazine moiety of the FAD cofactor.

Bibliography

1. Malmberg, N. J., and Falke, J. J. (2005) Use of EPR power saturation to analyze the membrane-docking geometries of peripheral proteins: Applications, *Annu. Rev. Biophys. Biomol. Struct. 34*, 71-90.

2. Hurley, J. H., and Misra, S. (2000) Signaling and subcellular targeting by membrane-binding domains, *Annu. Rev. Biophys. Biomol. Struct. 29*, 49-79.

3. Ron, D., and Kazanietz, M. G. (1999) New insights into the regulation of protein kinase C and novel phorbol ester receptors, *FASEB J. 13*, 1658-1676.

4. Jain, M. K., and Berg, O. G. (2006) Coupling of the i-face and the active site of phospholipase A2 for interfacial activation, *Curr. Opin. Chem. Biol. 10*, 473-479.

5. Winget, J. M., Pan, Y. H., and Bahnson, B. J. (2006) The interfacial binding surface of phospholipase A2s, *Biochim. Biophys. Acta. 1761*, 1260-1269.

6. Gelb, M. H., Min, J. H., and Jain, M. K. (2000) Do membrane-bound enzymes access their substrates from the membrane or aqueous phase: interfacial versus non-interfacial enzymes, *Biochim. Biophys. Acta. 1488*, 20-27.

7. Grobler, J. A., Essen, L. O., Williams, R. L., and Hurley, J. H. (1996) C2 domain conformational changes in phospholipase C-delta 1, *Nat. Struct. Biol. 3*, 788-795.

8. Ball. A, N., R., Gelb, M. H., Robinson, B. H. . (1999) Interfacial membrane docking of cytosolic phospholipase A2 C2 domain using electrostatic potential-modulated spin relaxation magnetic resonance, *Proc. Natl. Acad. Sci. USA 96*, 6637-6642.

9. Xu, G. Y., McDonagh, T., Yu, H. A., Nalefski, E. A., Clark, J. D., and Cumming, D. A. (1998) Solution structure and membrane interactions of the C2 domain of cytosolic phospholipase A2, *J. Mol. Biol. 280*, 485-500.

10. Medkova, M., and Cho, W. (1999) Interplay of C1 and C2 domains of protein kinase C-alpha in its membrane binding and activation *J. Biol. Chem. 274*, 19852-19861.

11. Bittova, L., Sumandea, M., and Cho, W. (1999) A structure-function study of the C2 domain of cytosolic phospholipase A2. Identification of essential calcium ligands and hydrophobic membrane binding residues, *J. Biol. Chem. 274*, 9665-9672.

12. Rizo, J., and Sudhof, T. C. (1998) C2-domains, structure and function of a universal Ca2+-binding domain, *J. Biol. Chem. 273*, 15879-15882.

13. Nalefski, E. A., and Falke, J. J. (1996) The C2 domain calcium-binding motif: structural and functional diversity, *Protein Sci. 5*, 2375-2390.

14. Simonsen, A., Lippe, R., Christoforidis, S., Gaullier, J. M., Brech, A., Callaghan, J., Toh, B. H., Murphy, C., Zerial, M., and Stenmark, H. (1998) EEA1 links PI(3)K function to Rab5 regulation of endosome fusion, *Nature 394*, 494-498.

15. Stenmark, H., Aasland, R., Toh, B. H., and D'Arrigo, A. (1996) Endosomal localization of the autoantigen EEA1 is mediated by a zinc-binding FYVE finger, *J. Biol. Chem. 271*, 24048-24054.

16. Wurmser, A. E., Gary, J. D., and Emr, S. D. (1999) Phosphoinositide 3-kinases and their FYVE domain-containing effectors as regulators of vacuolar/lysosomal membrane trafficking pathways, *J. Biol. Chem. 274*, 9129-9132.

17. Luecke, H., Schobert, B., Richter, H. T., Cartailler, J. P., and Lanyi, J. K. (1999) Structure of bacteriorhodopsin at 1.55 Å resolution, *J. Mol. Biol. 291*, 899-911.

18. Gonen, T., Cheng, Y., Sliz, P., Hiroaki, Y., Fujiyoshi, Y., Harrison, S. C., and Walz, T. (2005) Lipid-protein interactions in double-layered two-dimensional AQP0 crystals, *Nature 438*, 633-638.

19. Galdiero, S., and Gouaux, E. (2004) High resolution crystallographic studies of alpha-hemolysin-phospholipid complexes define heptamer-lipid head group interactions: implication for understanding protein-lipid interactions *Protein Sci. 13*, 1503-1511.

20. Mulgrew-Nesbitt, A., Diraviyam, K., Wang, J., Singh, S., Murray, P., Li, Z., Rogers, L., Mirkovic, N., and Murray, D. (2006) The role of electrostatics in protein-membrane interactions, *Biochim. Biophys. Acta. 1761*, 812-826.

21. Diraviyam, K., and Murray, D. (2006) Computational analysis of the membrane association of group IIA secreted phospholipases A2: a differential role for electrostatics, *Biochemistry 45*, 2584-2598.

22. Diraviyam, K., Stahelin, R. V., Cho, W., and Murray, D. (2003) Computer modeling of the membrane interaction of FYVE domains., *J. Biol. Chem. 328*, 721-736.

23. Hurley, J. H., Tsujishita, Y., and Pearson, M. A. (2000) Floundering about at cell membranes: a structural view of phospholipid signaling, *Curr. Opin. Struct. Biol. 10*, 737-743.

24. Ren, J., Lew, S., Wang, Z., and London, E. (1997) Transmembrane orientation of hydrophobic alpha-helices is regulated both by the relationship of helix length to bilayer thickness and by the cholesterol concentration, *Biochemistry 36*, 10213-10220.

25. Chattopadhyay, A., and London, E. (1987) Parallax method for direct mesurement of membrane penetrating depth utilizing fluorescence quenching by spin-labeled phospholipids, *Biochemistry 26*, 39-45.

26. Abrams, F. S., and London, E. (1993) Extension of the parallax analysis of membrane penetration depth to the polar region of model membranes: use of fluorescence quenching by a spin-label attached to the phospholipid polar headgroup, *Biochemistry 32*, 10826-10831.

27. Chen, X., Wolfgang, D. E., and Sampson, N. S. (2000) Use of the parallax-quench method to determine the position of the active-site loop of cholesterol oxidase in lipid bilayers, *Biochemistry 39*, 13383-13389.

28. Cho, W., and Stahelin, R. V. (2005) Membrane-protein interactions in cell signaling and membrane trafficking, *Annu. Rev. Biophys. Biomol. Struct. 34*, 119-151.

29. Caputo, G. A., and London, E. (2003) Using a novel dual fluorescence quenching assay for measurement of tryptophan depth within lipid bilayers to determine hydrophobic alpha-helix locations within membranes, *Biochemistry 42*, 3265-3274.

30. Smith, S. O., and Peersen, O. B. (1992) Solid-State NMR Approaches for Studying Membrane Protein Structure, *Annu. Rev. Biophys. Biomol. Struct. 21*, 25-47.

31. Saito, H., Yamamoto, K., Tuzi, S., and Yamaguchi, S. (2003) Backbone dynamics of membrane proteins in lipid bilayers: the effect of two-dimensional array formation as revealed by site-directed solid-state 13C NMR studies on [3-13C]Ala- and [1-13C]Val-labeled bacteriorhodopsin, *Biochim. Biophys. Acta. 1616*, 127-136.

32. Saito, H., Yamaguchi, S., Okuda, H., Shiraishi, A., and Tuzi, S. (2004) Dynamic aspect of bacteriorhodopsin as a typical membrane protein as revealed by site-directed solid-state 13C NMR, *Solid State Nucl. Magn. Reson. 25*, 5-14.

33. Tuzi, S., Uekama, N., Okada, M., Yamaguchi, S., Saito, H., and Yagisawa, H. (2003) Structure and dynamics of the phospholipase C-delta1 pleckstrin homology domain located at the lipid bilayer surface, *J. Mol. Biol. 278*, 28019-28025.

34. Frazier, A. A., Roller, C. R., Havelka, J. J. Hinderliter, A., and Cafiso, D. S. (2003) Membrane-bound orientation and position of the synaptotagmin I C2A domain by site-directed spin labeling, *Biochemistry 42*, 96-105.

35. Frazier, A. A., Wisner, M. A., Malmberg, N. J., Victor, K. G. and Fanucci, G. E. (2002) Membrane orientation and position of the C2 domain from cPLA2 by site-directed spin labeling, *Biochemistry 41*, 6282-6292.

36. Kohout, S. C., Corbalan-Garcia, S., Gomez-Fernandez, J. C., and Falke, J. J. (2003) C2 domain of protein kinase C alpha: elucidation of the membrane docking surface by site-directed fluorescence and spin labeling, *Biochemistry 42*, 1254-1265.

37. Malmberg, N. J., Van Buskirk, D. R., and Falke, J. J. (2003) Membrane-docking loops of the cPLA2 C2 domain: detailed structural analysis of the protein-membrane interface via site-directed spin-labeling, *Biochemistry 42*, 13227-13240.

38. Tieleman, D. P., Marrink, S. J., and Berendsen, H. J. C. (1997) A computer perspective of membranes: molecular dynamics studies of lipid bilayer systems, *Biochim. Biophys. Acta. 1331*, 235-270.

39. Tobias, D. J., Tu, K., and Klein, M. L. (1997) Atomic-scale molecular dynamics simulations of lipid membranes, *Curr. Opin. Colloid Interface Sci. 2*, 15-26.

40. Hyvonen, M. T., Oorni, K., Kovanen, P. T., and Ala-Korpela, M. (2001) Changes in a phospholipid bilayer induced by the hydrolysis of a phospholipase A2 enzyme: a molecular dynamics simulation study, *Biophys. J. 80*, 565-578.

41. Zhou, F., and Schulten, K. (1996) Molecular dynamics study of phospholipase A2 on a membrane surface, *Proteins 25*, 12-27.

42. Schiller, J., Suss, R., Arnhold, J., Fuchs, B., Lessig, J., Muller, M., Petkovic, M., Spalteholz, H., Zschornig, O., and Arnold, K. (2004) Matrix-assisted laser desorption and ionization time-of-flight (MALDI-TOF) mass spectrometry in lipid and phospholipid research, *Prog. Lipid Res. 43*, 449-488.

43. Aebersold, R., and Mann, M. (2003) Mass spectrometry-based proteomics, *Nature 422*, 198-207.

44. Wyttenbach, T., and Bowers, M. T. (2006) Intermolecular interactions in biomolecular systems examined by mass spectrometry, *Annu. Rev. Phys. Chem. 58*, 511-533.

45. Baumketner, A., Bernstein, S. L., Wyttenbach, T., Bitan, G., Teplow, D. B., Bowers, M. T., and Shea, J. E. (2006) Amyloid β-protein monomer structure: a computational and experimental study, *Protein Sci. 15*, 420-428.

46. Bernstein, S. L., Wyttenbach, T., Baumketner, A., Shea, J. E., Bitan, G., Teplow, D. B., and Bowers, M. T. (2005) Amyloid β-protein: monomer structure and early aggregation states of Aβ42 and its pro19 alloform, *J. Am. Chem. Soc. 127*, 2075-2084.

47. Yang, M., and Thompson, R. (2004) Comparative stability determination of oligonucleotide duplexes in gas and solution phase, *J. Am. Soc. Mass Spectrom 15*, 1354-1135.

48. Loo, J. A., Berhane, B., Kaddis, C. S., Wooding, K. M., Xie, Y., Kaufman, S. L., and Chernushevich, I. V. (2005) Electrospray ionization mass spectrometry and ion mobility analysis of the 20S proteasome complex, *J. Am. Soc. Mass Spectrom 16*, 998-1008.

49. Turfit, G. E. (1948) The microbiological degradation of steroids. Part IV: Oxidation of cholesterol by *Proactinomyces* spp, *Biochem. J. 42*, 376-393.

50. Turfit, G. E. (1944) The microbiological degradation of steroids. Part II: Oxidation of cholesterol by *Proactinomyces* spp, *Biochem. J. 38*, 49-62.

51. Turfit, G. E. (1946) The microbiological degradation of steroids. Part III: Oxidation of cholesterol by *Proactinomyces* spp, *Biochem. J. 40*, 79-81.

52. Schatz, A., Savard, K., and Pintner, I. J. (1949) The ability of soil microorganisms to decompose steroids, *J. Bacteriol. 1949*, 117-125.

53. Stadtman, T. C., Cherkes, A., and Anfinsen, C. B. (1954) Studies on the microbiological degradation of cholesterol, *J. Biol. Chem. 206*, 511-523.

54. Flegg, H. M. (1973) An investigation of the determination of serum cholesterol by an enzymic method, *Ann. Clin. Biochem. 10*, 79-84.

55. Richmond, W. (1972) The development of an enzymatic technique for the assay of cholesterol in biological fluids, *Scan. J. Clin. Lab. Invest. 29*, 25.

56. Richmond, W. (1973) Preparation and properties of a bacterial cholesterol oxidase from *Nocardia* sp. and its application to enzyme assay of total cholesterol in serum, *Clin. Chem. 19*, 1350-1356.

57. Nakaminami, T., Kuwabata, S., and Yoneyama, H. (1997) Electrochemical oxidation of cholesterol catalyzed by cholesterol oxidase with use of an artificial electron mediator, *Anal. Chem. 69*, 2367-2372.

58. Devadoss, A., Palencsar, M. S., Jiang, D., Honkonen, M. L., and Burgess, J. D. (2005) Enzyme modification of platinum microelectrodes for detection of cholesterol in vesicle lipid bilayer membranes, *Anal. Chem. 77*, 7393-7398.

59. Lange, Y. (1992) Tracking cell cholesterol with cholesterol oxidase, *J. Lipid. Res. 33*, 315-321.

60. Lange, Y., and Steck, T. L. (1996) The role of intracellular cholesterol transport in cholesterol homeostasis, *Trends in Cell Biol. 6*, 205-208.

61. Lange, Y., Ye, J., and Steck T. L. (2005) Activation of membrane cholesterol by displacement from phospholipids, *J. Biol. Chem. 280*, 36126-36131.

62. El-Yandouzi, E. H., and Le-Grimellac, C. (1992) Cholesterol heterogeneity in the plasma membrane of epithelial cells, *Biochemistry 31*, 547-551.

63. Stevens, V. L., Xu, T. S., and Lambeth, J. D. (1992) Cholesterol pools in rat adrenal mitochondria Ð use of cholesterol oxidase to infer a complex pool structure, *Endocrinology 130*, 1557-1563.

64. Lange, Y., Matthies, H., and Steck, T. L. (1984) Cholesterol oxidase susceptibility of the red cell membrane, *Biochim. Biophys. Acta. 769*, 551-562.

65. Ahn, K. W., and Sampson, N. S. (2004) Cholesterol oxidase senses subtle changes in lipid bilayer structure, *Biochemistry 43*, 827-836.

66. Purcell, J. P., Greenplate, J. T., Jennings, M. G., Ryerse, J. S., Pershing, J. C., Sims, S. R., Prinson, M. J., Corbin, D. R., Tran, M., Sammons, D., and Stonard, R. J. (1993) Cholesterol oxidase: a potent insecticidal protein active against boll weevil larvae, *Biochem. Biophys. Res. Commun. 196*, 1406-1413.

67. Cho, H. J., Choi, K. P., Yamashita, M., Morikawa, H., and Murooka, Y. (1995) Introduction and expression of the *Streptomyces* cholesterol oxidase gene (ChoA), a potent insecticidal protein active against boll weevil larvae, into tobacco cells, *Chem. Mater. Sci. 44*, 133-138.

68. Corbin, D. R., Greenplate, J. T., Wong, E. Y., and Purcell, J. P. (1994) Cloning of an insecticidal cholesterol oxidase gene and its expression in bacteria and in plant protoplasts, *Appl. Environ. Microbiol. 60*, 4239-4244.

69. Corbin, D. R., Grebenok, R. J., Ohnmeiss, T. E., Greenplate, J. T., and Purcell, J. P. (2001) Expression and chloroplast targeting of cholesterol oxidase in transgenic tobacco plants, *Plant Physiol. 126*, 1116-1128.

70. Schaller, H., Bouvier-Navei, P., and Benveniste, P. (1998) Overexpression of an *Arabidopsis* cDNA encoding a sterol-C24-methyltransferase in tobacco modifies the ratio of 24-methylcholesterol to sitosterol and is associated with growth reduction, *Plant Physiol. 118*, 461-469.

71. Linder, R., and Bernheimer, A. W. (1997) Oxidation of macrophage membrane cholesterol by intracellular Rhodococcus equi., *Vet. Microbiol. 56*, 269-276.

72. Aviram, M. (1992) Low density lipoprotein modification by cholesterol oxidase induces enhanced cholesterol accumulation in cells, *J. Biol. Chem. 267*, 218-225.

73. Ladron, N., Fernandez, M., Aguero, J., Gonzalez Zorn, B., Vazquez-Boland, J. A., and Navas, J. (2003) Rapid identification of *Rhodococcus equi.* by a PCR assay targeting the choE gene, *J. Clin. Microbiol. 41*, 3241-3245.

74. Gatfield, J., and Pieters, J. (2000) Essential role for cholesterol in entry of mycobacteria into macrophages, *Science 288*, 1647-1650.

75. Reading, P. C., Moore J. B., and Smith G. L. (2003) Steroid hormone synthesis by vaccinia virus suppresses the inflammatory response to infection, *J. Exp. Med. 197*, 1269-1278.

76. Geize, R. V. D., Yam, K., Heuser, T., Wilbrink, M. H., Hara, H., Anderton, M. C., Sim, E., Dijkhuizen, L., Davies, J. E., Mohn, W. W., and Eltis, L. D. (2007) A gene cluster encoding cholesterol catabolism in a soil actinomycete provides insight into Mycobacterium tuberculosis survival in macrophages, *Proc. Natl. Acad. Sci. 104*, 1947-1952.

77. Navas, J., Gonzalez-zorn, B., Ladron, N., Garrido, P., and Vazquez-boland, J. A. (2001) Indentification and mutagenesis by allelic exchange of *choE,* encoding a cholesterol oxidase from the intracellular pathogen *Rhodococcus equi*, *J. Bacteriol. 183*, 4796-4805.

78. Pei, Y., Dupont, C., Sydor, T., Haas, A., and Prescott, J. F. (2006) Cholesterol oxidase (ChoE) is not important in the virulence of *Rhodococcus equi*, *Vet. Microbiol. 118*, 240-246.

79. Coulombe, R., Yue, K. Q., Ghisla, S., and Virelink, A. (2001) Oxygen access to the active site of cholesterol oxidase through a narrow channel is gated by an Arg-Glu pair, *J. Biol. Chem. 276*, 30435-30441.

80. Vrielink, A., and Sampson, N. S. (2003) Sub-Ångstrom resolution enzyme X-ray structures: is seeing believing?, *Curr. Opin. Struct. Biol. 13*, 709-715.

81. Vrielink, A., Lloyd, L. F., and Blow, D. M. (1991) Crystal structure of cholesterol oxidase from *Brevibacterium sterolicum* refined at 1.8 Å resolution, *J. Mol. Biol. 219*, 533-554.

82. Li, J., Vrielink, A., Brick, P., and Blow, D. M. (1993) Crystal structure of cholesterol oxidase complexed with a steroid substrate: implications for flavin adenine dinucleotide dependent alcohol oxidases, *Biochemistry 32*, 11507-11515.

83. Yin, Y., Lario, P., Vrielink, A., and Sampson, N. S. (2001) The presence of a hydrogen bond between asparagine 485 and the π system of FAD modulates the redox potential in the reaction catalyzed by cholesterol oxidase, *Biochemistry 40*, 13779-13787.

84. Motteran, L., Pilone, M. S., Molla, G., Ghisla, S., and Pollegioni, L. (2001) Cholesterol oxidase from *Brevibacterium sterolicum*, *J. Biol. Chem. 276*, 18024-18030.

85. DeLano, W. L. (2002) The PyMOL molecular graphics system, http://www.pymol.org.

86. Cavener, D. R. (1992) GMC oxidoreductases. A newly defined family of homologous proteins with diverse catalytic activities, *J. Mol. Biol. 223*, 811-814.

87. Yue, K., Kass, I. J., Sampson, N. S., and Vrielink, A. (1999) Crystal structure determination of cholesterol oxidase from *Streptomyces* and strucutral characterization of key active site mutants, *Biochemistry 38*, 4277-4286.

88. Kass, I. J., and Sampson, N. S. (1998) The importance of Glu361 position in the reaction catalyzed by cholesterol oxidase, *Bioorg. Med. Chem. Lett. 8*, 2663-2668.

89. Sampson, N. S., and Kass, I. J. (1997) Isomerization, but not oxidation, is suppressed by a single point mutation, E361Q, in the reaction catalyzed by cholesterol oxidase, *J. Am. Chem. Soc. 119*, 855-862.

90. Lario, P., Sampson, N. S., and Vrielink, A. (2003) Sub-atomic resolution crystal structure of cholesterol oxidase: What atomic resolution crystallography reveals about enzyme mechanism and the role of the FAD cofactor in redox activity, *J. Mol. Biol. 326*, 1635-1650.

91. Gadda, G., Wels, G., Pollegioni, L., Zucchelli, S., Ambrosius, D., Pilone, M. S. and Ghisla, S. (1997) Characterization of cholesterol oxidase from *Streptomyces hygroscopicus* and *Brevibacterium sterolicum*, *Eur. J. Biochem. 250*, 369-376.

92. Sampson, N. S., Kass, I. J., and Ghoshroy, K. B. (1998) Assessment of the role of an omega loop of cholesterol oxidase: a truncated loop mutant has altered substrate specificity, *Biochemistry 37*, 5770-5778.

93. Heller, H., Schaefer, M., and Schulten, K. (1993) Molecular Dynamics Simulation of a Bilayer of 200 Lipids in the Gel and in the Liquid-crystal Phases, *J. Phys. Chem 97*, 8343-8360.

94. Rodrigueza, W. V., Wheeler, J. J., Klimuk, S. K., Kitson, C. N., and Hope, M. J. (1995) Transbilayer movement and net flux of cholesterol and cholesterol sulfate between liposomal membranes, *Biochemistry 34*, 6208-6217.

95. Sampson, N. S., and Vrielink, A. (2003) Cholesterol oxidase: A study of nature's approach to protein design, *Acc. Chem. Res. 36*, 713-722.

96. Nomura, N., Choi, K. P., and Murooka, Y. (1995) Genetic modification of the *Streptomyces* cholesterol oxidase gene for expression in *Escherichia Coli* and developement of promoter-probe vectors for use in enteric bacteria, *J. Ferm. Bioeng. 79*, 410-416.

97. Sambrook, J., and Russell, D. W. (2001) Molecular cloning: A laboratory manual. Cold spring harbor, *Cold Spring Harbor Laboratory Press*.

98. Xiang, J., and Sampson, N. S. (2004) Library screening studies to investigate substrate specificity in the reaction catalyzed by cholesterol oxidase, *Protein Eng. Des. Sel. 17*, 341-348.

99. Fasman, G. D. (1992) Practical handbook of biochemistry and molecular biology, *C. R. C. Press, Boca Raton, FL*.

100. Smith, A. G., and Brooks, C. J. W. (1977) The substrate specificity and stereochemistry, reversiblility and inhibition of the 3-oxo steroid 4-5 isomerase component of cholesterol oxidase, *Biochem. J. 167*, 121-129.

101. Certificate of analysis, *Molecular Probes, Inc.*

102. Fasman, G. D. (1992) *Practical Handbook of Biochemistry and Molecular Biology*, CRC Press, Boca Raton, FL.

103. Voet, D., and Voet, E. (1995) Biochemistry, *John Wiley & Sons, Inc.*

104. Kusumi, A., Tsuda, M., Akino, T., Ohnishi, S., and Terayama, Y. (1983) Protein-phospholipid-cholesterol interaction in the photolysis of invertebrate rhodopsin, *Biochemistry 22*, 1165-1170.

105. Papahadjopoulos, D., Cowden, M., and Kimelberg, H. (1973) Role of cholesterol in membranes. Effects on phospholipid-protein interactions, membrane permeability and enzymatic activity, *Biochim. Biophys. Acta. 330*, 8-26.

106. Haines, T. H. (2001) Do sterols reduce proton and sodium leaks through lipid bilayers?, *Prog. Lipid Res. 40*, 299-324.

107. Simons, K., and Toomre, D. (2000) Lipid rafts and signal transduction, *Nat. Rev. Mol. Cell Biol. 1*, 31-39.

108. Goñi, F. (2002) Non-permanent proteins in membranes: when proteins come as visitors *Mol. Membr. Biol. 19*, 237-245.

109. McIntosh, T., and Simon, S. (2006) Roles of bilayer material properties in function and distribution of membrane proteins, *Annu. Rev. Biophys. Biomol. Struct. 35*, 177-198.

110. Hanakam, F., Gerisch, G., Lotz, S., Alt, T., and Seelig, A. (1996) Binding of hisactophilin I and II to lipid membranes is controlled by a pH-dependent myristoyl-histidine switch, *Biochemistry 35*, 11036-11044.

111. Silvius, J. R., pp. 371–395. (2003) Lipidated peptides as tools for understanding the membrane interactions of lipid-modified proteins, *In Current Topics in Membranes (52) Academic Press*, 371-395.

112. Ben-Tal, N., Honig, B., Miller, C., and McLaughlin, S. (1997) Electrostatic binding of proteins to membranes. Theoretical predictions and experimental results with charybdotoxin and phospholipid vesicles, *Biophys. J. 73*, 1717-1727.

113. Dijkstra, B. W., Kalk, K. H., Hol, W. G., and Drenth, J. . (1981) Structure of bovine pancreatic phospholipase A2 at 1.7A resolution, *J. Mol. Biol. 147*, 97-123.

114. Dijkstra, B. W., Drenth, J., and Kalk, K. H. (1981) Active site and catalytic mechanism of phospholipase A2, *Nature 289*, 604-606.

115. Renetseder, R., Brunie, S., Dijkstra, B. W., Drenth, J., and Sigler, P. B. (1985) A comparison of the crystal structures of phospholipase A2 from bovine pancreas and Crotalus atrox venom, *J Biol Chem. 260*, 11627-11634.

116. Dufton, M. J., Eaker, D., and Hider, R. C. (1983) Conformational properties of phospholipases A2. Secondary-structure prediction, circular dichroism and relative interface hydrophobicity, *Eur. J. Biochem. 137*, 537-544.

117. Dijkstra, B. W., Kalk, K. H., Drenth, J., de Haas, G. H., Egmond, M. R., and Slotboom, A. J. (1984) Role of the N-terminus in the interaction of pancreatic phospholipase A2 with aggregated substrates. Properties and crystal structure of transaminated phospholipase A2, *Biochemistry 23*, 2759-2766.

118. Scott, D. L., White, S. P., Otwinowski, Z., Yuan, W., Gelb, M. H., and Sigler, P. B. (1990) Interfacial catalysis: the mechanism of phospholipase A2, *Science 250*, 1541-1546.

119. Lin, Y., Nielsen, R., Murray, D., Hubbell, W. L., Mailer, C., Robinson, B. H., and Gelb, M. H. (1998) Docking phospholipase A2 on membranes using electrostatic potential-modulated spin relaxation magnetic resonance, *Science 279*, 1925-1929.

120. Snitko, Y., Koduri, R. S., Han, S. K., Othman, R., Baker, S. F., Molini, B. J., Wilton, D. C., Gelb, M. H., and Cho, W. (1997) Mapping the interfacial binding surface of human secretory group IIa phospholipase A2, *Biochemistry 36*, 14325-14333.

121. Pan, Y. H., Epstein, T. M., Jain, M.K. and Bahnson, B.J. (2001) Five coplanar anion binding sites on one face of phospholipase A2: relationship to interface binding, *Biochemistry 40*, 609-617.

122. Gelb, M. H., Cho, W., and Wilton, D. C. (1999) Interfacial binding of secreted phospholipases A(2): more than electrostatics and a major role for tryptophan, *Curr. Opin. Struct. Biol. 9*, 428-432.

123. Han, S. K., Kim, K. P., Koduri, R., Bittova, L., Munoz, N. M., Leff, A. R., Wilton, D. C., Gelb, M. H. and Cho, W. (1999) Roles of Trp31 in high membrane binding and proinflammatory activity of human group V phospholipase A2, *J. Biol. Chem. 274*, 11881-11888.

124. Bezzine, S., Bollinger, J. G., Singer, A. G., Veatch, S. L., Keller, S. L., and Gelb, M. H. (2002) On the binding preference of human groups IIA and X phospholipases A2 for membranes with anionic phospholipids, *J. Biol. Chem. 277*, 48523-48534.

125. Beers, S. A., Buckland, A. G., Giles, N., Gelb, M. H., and Wilton, D. C. (2003) Effect of tryptophan insertions on the properties of the human group IIA phospholipase A2: Mutagenesis produces an enzyme with characteristics similar to those of the human group V phospholipase A2, *Biochemistry 42*, 7326-7338.

126. Jain, M. K., and Vaz, W. L. . (1987) Dehydration of the lipid–protein microinterface on binding of phospholipase A2 to lipid bilayers, *Biochim. Biophys. Acta. 905*, 1-8.

127. Berg, O. G., Gelb, M. H., Tsai, M., andJain, M. K. (2001) Interfacial enzymology: the secreted phospholipase A2-Paradigm, *Chem. Rev. 101*, 2613-2654.

128. Hope, M. J., Bally, M. B., Webb, G., and Cullis, P. R. (1985) Production of large unilamellar vesicles by rapid extrusion procedure. Characterization of size distribution, trapped volume and ability to maintain a membrane potential, *Biochim. Biophys. Acta. 812*, 55-65.

129. Feigenson, G. W. (2006) Phase behavior of lipid mixtures, *Nat. Chem. Biol. 2006 Nov;2(11):560-3 2*, 560-563.

130. Frazier, M. L., Wright, J. R., Pokorny, A., and Almeida, P. F. F. (2007) Investigation of domain formation in sphingomyelin/cholesterol/POPC mixtures by fluorescence resonance energy transfer and Monte Carlo simulations, *Biophys. J. 92*, 2422-2433.

131. Róg, T., and Pasenkiewicz-Gierula, M. (2006) Cholesterol-sphingomyelin interactions: a molecular dynamics simulation study, *Biophys. J. 91*, 3756-3767.

132. Weber, G., and Farris, F. J. . (1979) Synthesis and spectral properties of a hydrophobic fluorescent probe: 6-propionyl-2-(dimethylamino)naphthalene, *Biochemistry 18*, 3075-3078.

133. Prendergast, F. G., Meyer, M., Carlson, G. L., Iida, S., and Potter, J. D. (1983) Synthesis, spectral properties, and use of 6-acryloyl-2-dimethylaminonaphthalene (Acrylodan). A thiol-selective, polarity-sensitive fluorescent probe, *J. Biol. Chem. 258*, 7541-7544.

134. Zhu, P., Clamme, J., and Deniz, A. A. (2005) Fluorescence quenching by TEMPO: A sub-30 Å single-molecule ruler, *Biophys. J. 89*, L37-L39.

135. London, E., and Feigenson, G. W. (1981) Fluorescence quenching in model membranes: Characterization of quenching caused by a spin-labeled phospholipid, *Biochemistry 20*, 1935-1938.

136. Nagle, J. F., and Tristram-Nagle, S. (2000) *Curr. Opin. Struct. Biol. 10*, 474-480.

137. de Almeida, R. F., Fedorov, A., and Prieto, M. (2003) Sphingomyelin/phosphatidylcholine/cholesterol phase diagram: boundaries and composition of lipid rafts, *Biophys. J. 85*, 2406-2416.

138. Liu, M., Bagdade, J. D., and Subbaiah, P. V. (1995) Specificity of lecithin:cholesterol acyltransferase and atherogenic risk. Comparative studies on the plasma composition and in vitro synthesis of cholesteryl esters in 14 vertebrate species, *J. Lipid Res. 36*, 1813-1824.

139. Veatch, S. L., Gawrisch, K., and Keller, S. L. (2006) Closed-loop miscibility gap and quantitative tie-lines in ternary membranes containing diphytanoyl PC, *Biophys. J. 90*, 4428-4436.

140. Yin, Y., Liu, P., Anderson, R. G., and Sampson, N. S. (2002) Construction of a catalytically inactive cholesterol oxidase mutant: investigation of the interplay between active site-residues glutamate 361 and histidine 447, *Arch. Biochem. Biophys. 402*, 235-242.

141. Fenn, J. B., Mann, M., Meng, C. K., Wong, S. F., and Whitehouse, C. M. (1989) Electrospray ionization for mass spectrometry of large biomolecules, *Science 246*, 64-71.

142. Karas, M., and Hillenkamp, F. (1988) Laser desorption ionization of proteins with molecular masses exceeding 10,000 daltons, *Anal. Chem. 60*, 2299-2301.

143. Mann, M., Ronald, C., Hendrickson, R. C., and Pandey, A. (2001) Analysis of proteins and proteomes by mass spectrometry, *Annu. Rev. Biochem. 70*, 437-473.

144. Vasil'ev, Y. V., Khvostenko, O. G., Streletskii, A. V., Boltalina, O. V., Kotsiris, S. G., and Drewello, T. (2006) Electron transfer reactivity in matrix-assisted laser

desorption/Ionization (MALDI): ionization energy, electron affinity and performance of the DCTB matrix within the thermochemical framework *J. Phys. Chem. 110*, 5967 -5972.

145. Zenobi, R., and Knochenmuss, R. (1999) Ion formation in MALDI mass spectrometry, *Mass Spectrom. Rev. 17*, 337-366.

146. Knochenmuss, R., and Zenobi, R. (2003) MALDI ionization: the role of in-plume processes, *Chem. Rev. 103*, 441-452.

147. Gygi, S. P., Rist, B., Gerber, S. A., Turecek, F., Gelb, M. H., and Aebersold, R. (1999) Quantitative analysis of complex protein mixtures using isotope-coded affinity tags, *Nat. Biotechnol. 17*, 994-999.

148. Shiio, Y., and Aebersold, R. (2006) Quantitative proteome analysis using isotope-coded affinity tags and mass spectrometry, *Nat. Protoc. 1*, 139-145.

149. Wilkinson, J. M. (1986) Fragmentation of polypeptides by enzymatic methods, *Practical protein chemistry: A handbook. Darbre, A., ed., John Wiley and Sons, New York, NY*.

150. http://ca.expasy.org/tools/peptide-mass.html.

151. Ibanez, A. J., Muck, A., Halim, V., and Svatos, A. (2007) Trypsin-linked copolymer MALDI chips for fast protein identification, *J. Proteome Res. 6*, 1183-1189.

152. Leichert, L. I., and Jakob, U. (2006) Global methods to monitor the thiol–disulfide state of proteins in vivo, *Antioxidants & redox signaling 8*, 763-772.

153. Guo, Z., Chang, C. C. Y., Lu, X., Chen, J., Li, B., and Chang, T. (2005) The disulfide linkage and the free sulfhydryl accessibility of acyl-coenzyme A:cholesterol acyltransferase 1 as studied by using mPEG5000-maleimide, *Biochemistry 44*, 6537-6546.

154. Lu, J., and Deutsch, C. (2001) Pegylation: a method for assessing topological accessibilities in Kv1.3, *Biochemistry 40*, 13288-13301.

155. Pelis, R. M., Zhang, X., Dangprapai, Y., and Wright, S. H. (2006) Cysteine accessibility in the hydrophilic cleft of human organic cation transporter 2, *J. Biol. Chem. 281*, 35272-35280.

156. Tak, J. (1942) On bacteria decomposing cholesterol, *Antonie Leeuwenhoek 8*, 32-40.

157. Van der Geize, R., Yam, K., Heuser, T., Wilbrink, M. H., Hara, H., Anderton, M. C., Sim, E.,, and Dijkhuizen, L., Davies, J. E., Mohn, W. W., and Eltis, L. D. (2007) A gene cluster encoding cholesterol catabolism in a soil actinomycete provides insight into Mycobacterium tuberculosis survival in macrophages, *Proc. Natl. Acad. Sci. U. S. A. 104*, 1947-1952.

158. Fraaije, M. W., and Mattevi, A. (2000) Flavoenzymes: diverse catalysts with recurrent features, *Trends. Biochem. Sci. 25*, 126-132.

159. Kass, I. J., and Sampson, N. S. (1998) Evaluation of the role of His447 in the reaction catalyzed by cholesterol oxidase, *Biochemistry 37*, 17990-18000.

160. Lyubimov, A. Y. (2006) A Structural study of cholesterol oxidase at atomic and sub-atomic resolution, *Ph. D. Thesis, University of California, Santa Cruz*.

161. Hall, L. H., Bowers, M. L., and Durfor, C. N. (1987) Further consideration of flavin coenzyme biochemistry afforded by geometry-optimized molecular orbital calculations, *Biochemistry 26*, 7401-7409.

162. Walsh, J. D., and Miller, A. F. (2003) Flavin reduction potential tuning by substitution and bending, *Journal of Molecular Structure: THEOCHEM 623*, 185-195.

163. Hasford, J. J., Kemnitzer, W., and Rizzo, C. J. (1997) Conformational Effects on Flavin Redox Chemistry, *J. Org. Chem. 62*, 5244-5245.

164. Reibenspies, J. H., Guo, F., and Rizzo, C. J. (2000) X-ray Crystal Structures of Conformationally Biased Flavin Models, *Org. Lett. 2*, 903 -906.

165. Lennon, B. W., Williams, Jr. C. H., and Ludwig, M. L. . (1999) Crystal structure of reduced thioredoxin reductase from Escherichia coli: structural flexibility in the

isoalloxazine ring of the flavin adenine dinucleotide cofactor, *Protein Sci. 8*, 2366-2379.

166. Pellett, J., and Stankovich, M. (2002) Potentiometric measurements of proteins, in encylopedia of electrochemistry, *vol 9 Bioelectrochemistry Wiley-VCH: Weinheim, Germany*, 485-509.

167. Adam, W., Lazarus, M., Hoch, U., Korb, M. N., Saha-Möller, C. R., and Schreier, P. (1998) Horseradish peroxidase-catalyzed enantioselective reduction of racemic hydroperoxy homoallylic alcohols: a novel enzymatic method for the preparation of optically active, unsaturated diols and hydroperoxy alcohols, *J. Org. Chem. 63*, 6123-6127.

168. Svensson, S., Olin, A. C., Lärstad, M., Ljungkvist, G., and Torén, K. (2004) Determination of hydrogen peroxide in exhaled breath condensate by flow injection analysis with fluorescence detection, *J Chromatogr B Analyt Technol Biomed Life Sci. 2004 Oct 5;809(2):199-203. 809*, 199-203.

169. O'Neill, P., Stevens, D. L., and Garman, E. F. (2002) Physical and chemical considerations of damage induced in protein crystals by synchrotron radiation: a radiation chemical perspective, *J. Synchrotron Radiat. 9*, 329-332.

170. Davydov, R., Kuprin, S., Graeslund, A., and Ehrenberg, A. (1994) Electron paramagnetic resonance study of the mixed-valent diiron center in escherichia coli ribonucleotide reductase produced by reduction of radical-free protein R2 at 77 K, *J. Am. Chem. Soc. 116*, 11120-11128.

Supplement I: Strategies of plasmid construction of mutant cholesterol oxidases

1. Plasmid pCO270 (4CA in pET20b vector).

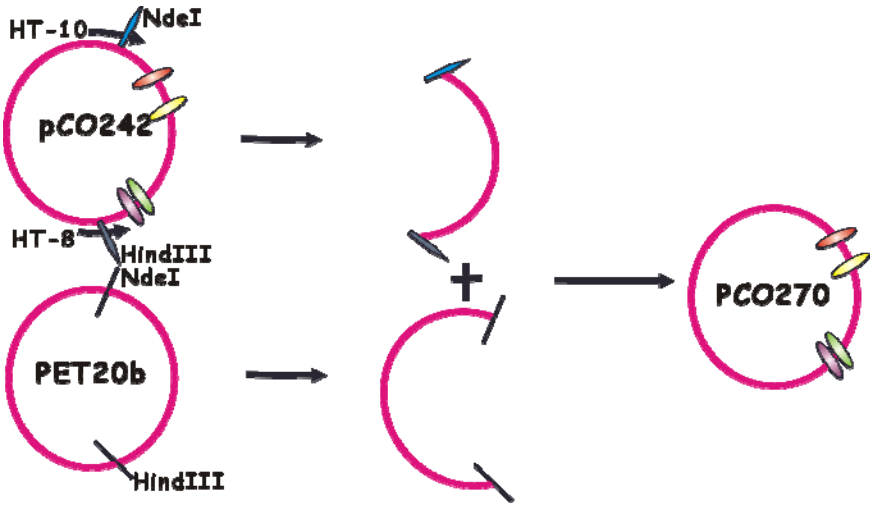

2. Plasmid pCO271 (I427C/4CA in pET20b vector).

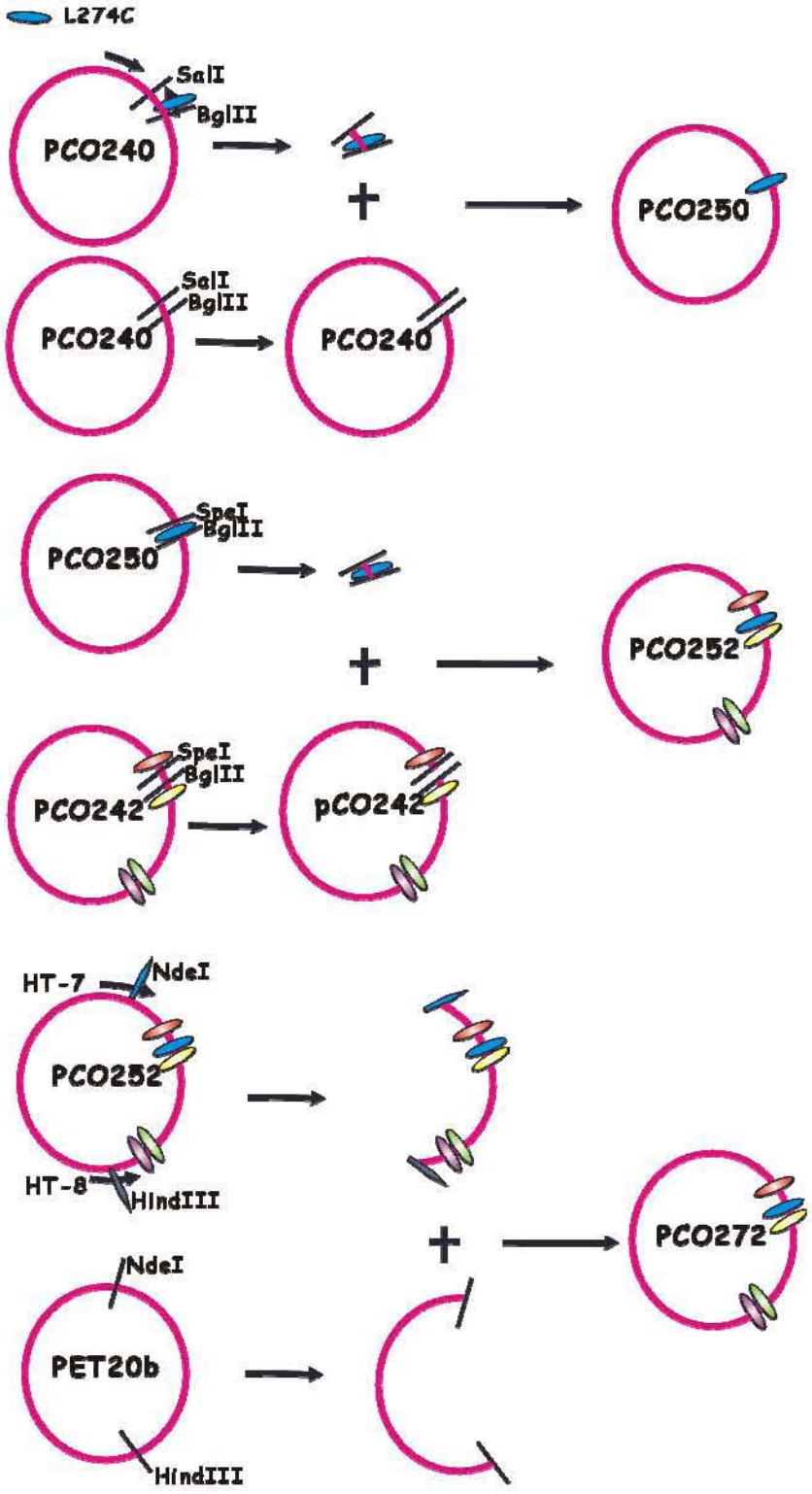

3. Plasmid pCO272 (L274C/4CA in pET20b vector).

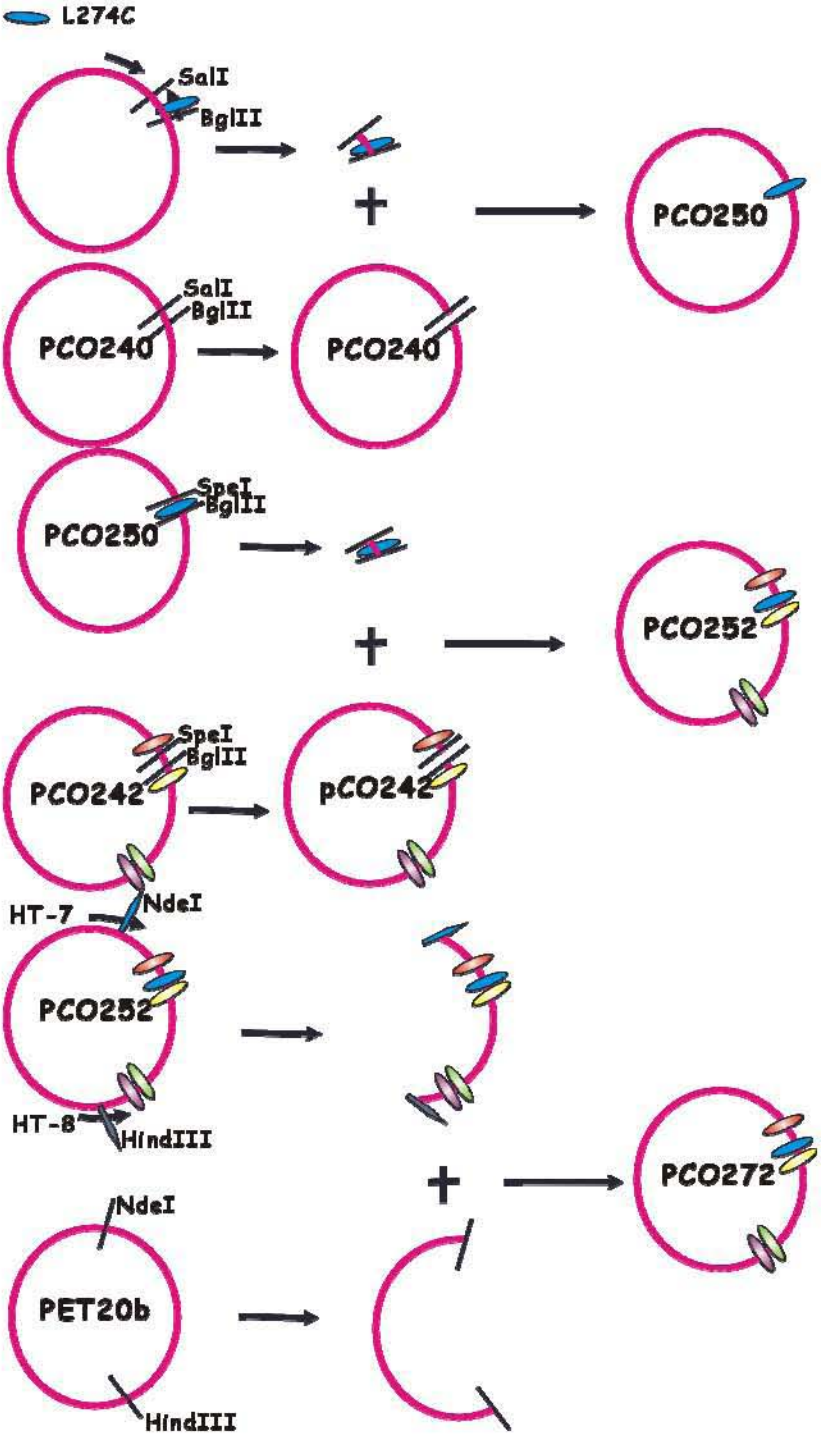

4. Plasmid pCO273 (L80C/4CA in pET20b vector).

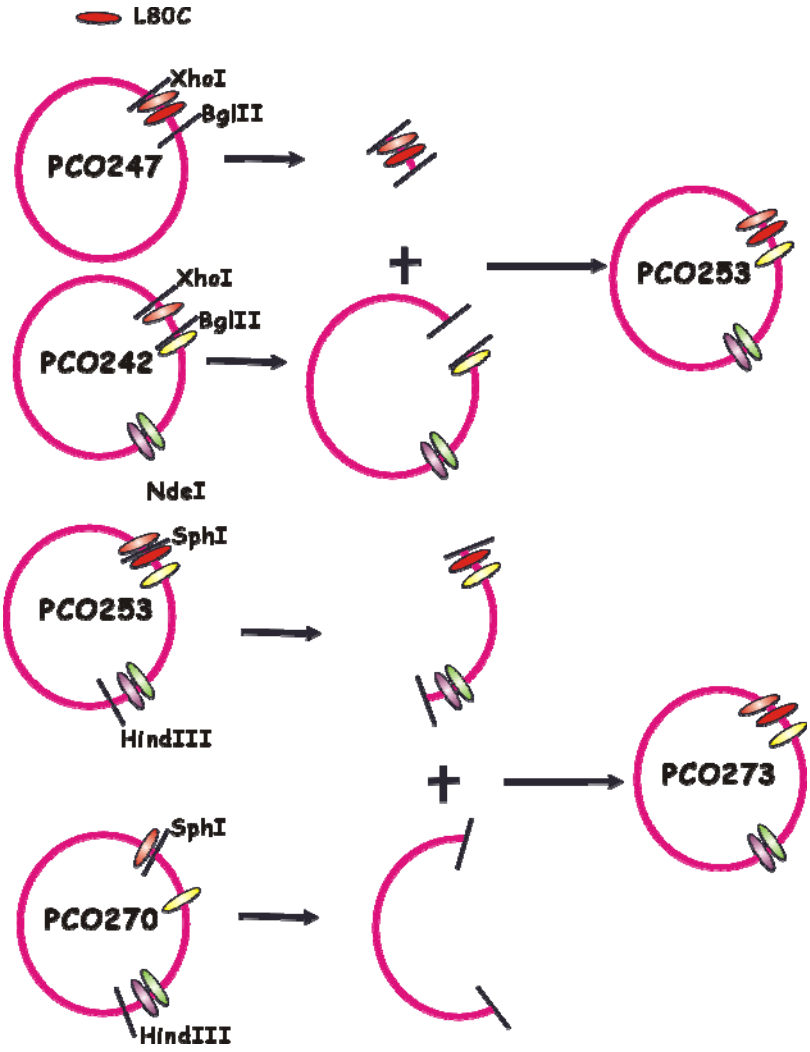

5. Plasmid pCO274 (M154C/4CA in pET20b vector).

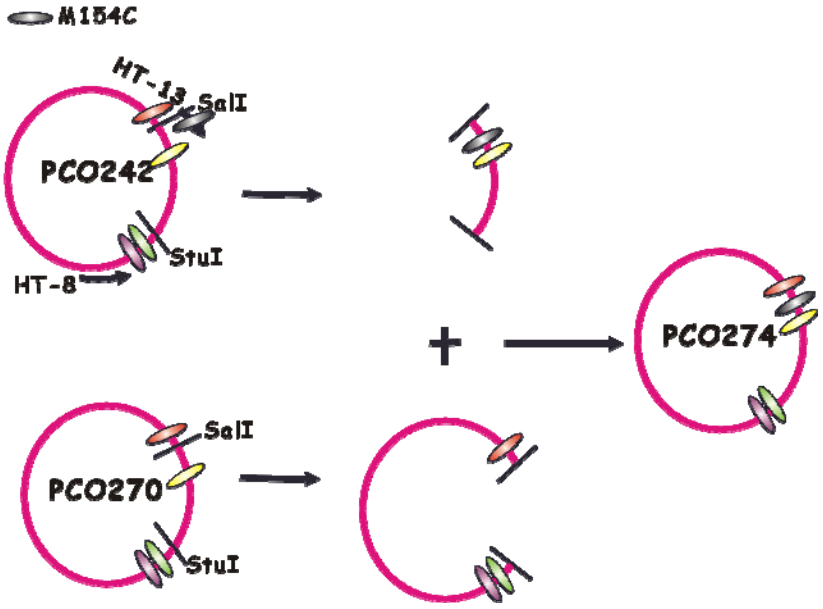

6. Plasmid pCO275 (A393C/4CA in pET20b vector).

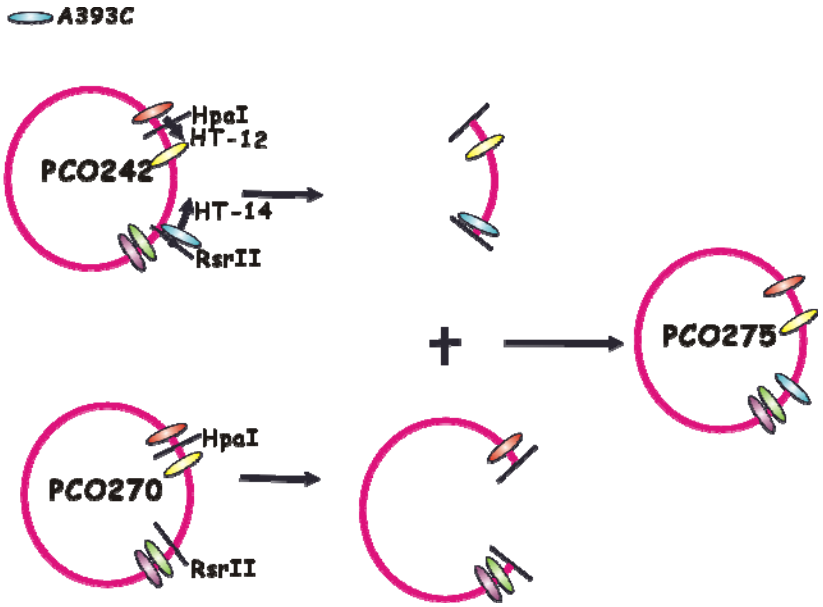

7. Plasmid pCO276 (V34C/4CA in pET20b vector).

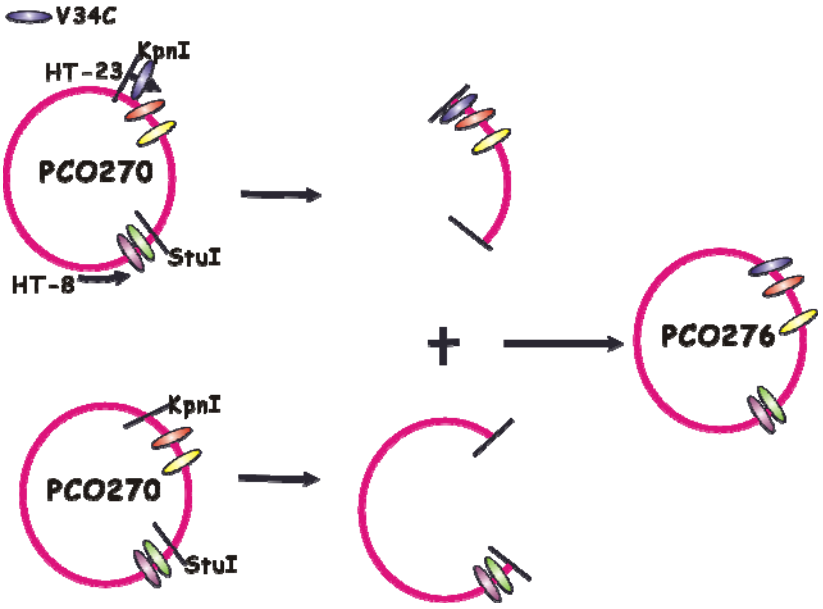

8. Plasmid pCO277 (N88C/4CA in pET20b vector).

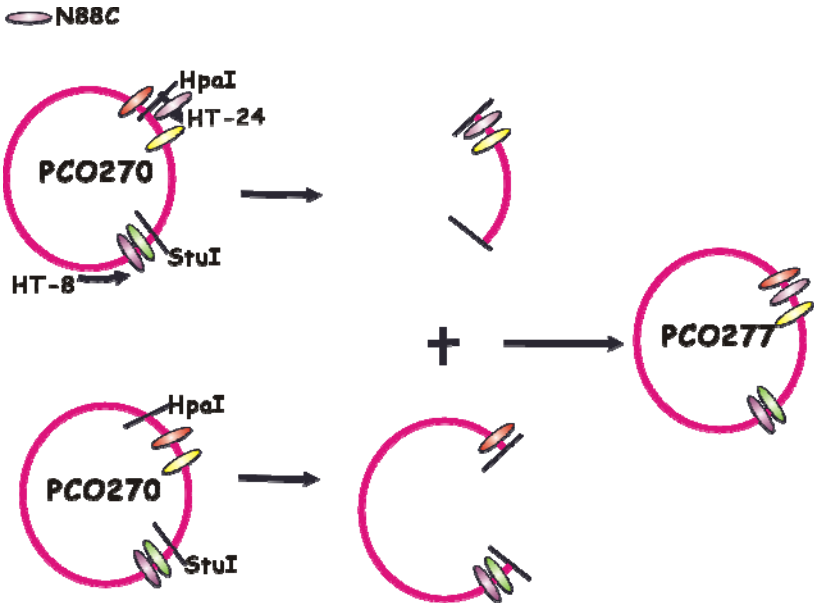

9. Plasmid pCO278 (W33C/4CA in pET20b vector).